Aus der
Berufsgenossenschaftlichen Unfallklinik
Klinik für Unfall- und Wiederherstellungschirurgie an der
Universität Tübingen

Diclofenac affects the bone and liver negatively: Establishment of an *in vitro* 3D liver-bone culture system

Inaugural -Dissertation
zur Erlangung des Doktorgrades
der Medizin

der Medizinischen Fakultät
der Eberhard Karls Universität
zu Tübingen

vorgelegt von

Chen, Guanqiao

2025

Dekan: Professor Dr. B. Pichler

1. Berichterstatter: Professor Dr. A. Nüssler
2. Berichterstatter: Privatdozent Dr. M. Schenk

Tag der Disputation: 17.07.2025

Table of contents

Index of figures and tables IV

List of figures.....VII
List of tables.....VIII
List of abbreviations.....IX

1. Introduction…….……1

1.1. Liver and Bone...…….....1
1.1.1. Liver function…….....1
1.1.2. Bone homeostasis…….....…….....2
1.1.3. Interaction between the liver and bone system.....4
1.2. Liver and bone disease…….....…….....6
1.2.1. Liver diseases…….....6
1.2.2. Impaired bone homeostasis……..…….....….....10
1.2.3. Hepatic osteodystrophy (HOD)…….....10
1.3. Non-steroidal anti-inflammatory drugs (NSAIDs)…….....12
1.3.1. Diclofenac …….....12
1.3.2. Diclofenac affect the liver and bone…….....12
1.4. Models for HOD studies…….……15
1.5. Aim of the study…….…17

2. Materials and Methods 19

2.1. Materials 19
2.1.1. Chemicals…….19
2.1.2. Solutions……..21
2.1.3. Consumables……..…...23
2.1.4. Equipment……..…...24
2.2. Methods 26
2.2.1. Manufacturing and sterilizing of hPRP scaffolds…...…….26
2.2.2. Manufacturing and sterilization of agarose plate and microwells……....27
2.2.3. Cell lines……..……..……...28
2.2.4. Cell seeding……..……..……...29
2.2.4.1. Bone cells co-culture……29
2.2.4.2. HepaRG cell culture…….……29
2.2.5. Testing the effects of supplements present in liver and bone media on 2D-cultured bone and liver cells, respectively……...……...30
2.2.6. Optimizing the medium for the 3D L-B system……...…31
2.2.7. Development of 3D liver-bone co-culture model…...……...…….31
2.2.8. Diclofenac exposure to the 3D L-B co-culture model……...…….....…….32
2.2.9. Exposure of the 3D bone co-culture model to 4'-hydroxydiclofenac……...32
2.2.10. IL-6 was exposed to the 3D bone co-culture model to evaluate its effects on cell

viability and function……..…..…….32
2.2.11. Resazurin conversion assay to measure mitochondrial activity…….32
2.2.12. CYPs activity assay using LC-HPLC/MS-based method (Phase I enzymes).33
2.2.13. Fluorescence-based method to detect CYP2C9 activity (Phase I enzyme) 34
2.2.14. Fluorescence-based method to measure UGT activity (Phase II enzyme) 34
2.2.15. AP activity was assessed using an absorbance-based assay…….…….35
2.2.16. CA II activity was assessed using an absorbance-based assay……..…….35
2.2.17. TRAP activity measurement using an absorbance-based method....…….36
2.2.18. Calcium deposition visualized by Alizarin red staining ……..…..…….36
2.2.19. Protein content measurement by sulforhodamine B (SRB) staining …….36
2.2.20. The process of DNA isolation and quantification from the samples…….37
2.2.21. The mineral composition of the bone scaffold was analyzed to determine its content…….....……..…..…..…..…..…..…….37
2.2.22. Stiffness of bone scaffold……..…..…..…..…..…..…….38
2.2.23. Detection of secreted protein by dot blot analysis…..…..…..…..…….38
2.2.24. Detection of reactive oxygen species by 2',7'-dichlorofluorescein-diacetate (DCFH-DA) assay ……..……..…..…..…..…..…..…….39
2.2.25. Detection of reduced glutathione (GSH) and oxidized glutathione (GSSG) by Ellman assay ……..…....…..…..…….39
2.2.26. Statistical analyses……..…..…..…..…..…..…….40

3. Results 41

3.1. The effects of osteogenic factors within bone differentiation medium on HepaRG cells..……..41
3.2. Effects of supplements in the HepaRG cell differentiation medium on SCP-1 and THP-1 cell co-cultures..…..……...43
3.3. HepaRG spheroids exposed to different proportions of liver-bone medium combinations……46
3.4. Bone 3D co-culture system exposed to various ratios of bone-liver medium combination……48
3.5. HepaRG spheroids maintain both viability and functionality for up to 21 days within the liver-bone co-culture system…….51
3.6. The 3D bone system maintains both viability and functionality for up to 21 days within the liver-bone co-culture system.…….……...……...52
3.7. Exposure to diclofenac three times weekly does not negatively affect the viability and function of liver spheroids or bone cells in the L-B system ……...53
3.8. Daily exposure to diclofenac does not negatively affect the HepaRG spheroids viability and function within the L-B co-culture system……56
3.9. Chronic daily exposure to diclofenac upregulates the osteoclast function in the L-B system……57
3.10. Daily treatment with diclofenac leads to a decrease in scaffold mineral density and stiffness, as well as an imbalance in the RANKL: OPG ratio within the L-B system...……...……....59

3.11. 4-OH diclofenac does not contribute to the enhanced osteoclast activity observed in the L-B system……...……61
3.12. Diclofenac exposure increased ROS and IL-6 levels, and decreased the GSH: GSSG ratio in the liver system ……62
3.13. IL-6 exposure upregulates the osteoclast cells' function in the bone co-culture system.……...……64

4. Discussion.....66

5. Summary.....76

6. Zusammenfassung.....78

7. Bibliography.....80

8. Declaration.....97

9. Publication.....98

10. Acknowledgement.....99

List of Figures

1.1. Types of liver cells and their functions…..……...……...2
1.2. The mechanisms of bone homeostasis……..……...……...4
1.3. The liver plays a crucial role in regulating bone homeostasis……...…...……6
1.4. The progression of liver disease…...……...……9
1.5. The effect of liver damage on bone homeostasis……....…….…11
1.6. The primary metabolic pathway of diclofenac in the liver...…….…...…….…14
1.7. Possible pathways of diclofenac affecting bone homeostasis…….…….…….15
2.1. Agarose microwell generation process and its characteristics.....…….28
2.2. Establishment of the liver-bone co-culture system.....…….31
3.1.1. Viability of HepaRG cells treated with osteogenic factors…….....……...…….42
3.1.2. Function of HepaRG cells treated with osteogenic factors…….....…….43
3.2.1. Viability of bone co-culture system treated with the supplements in HepaRG medium……...…...……...……...……...44
3.2.2. Function of bone co-culture system treated with the supplements in HepaRG medium……...……...……...……...……...45
3.3.1. Viability of HepaRG cells treated with different ratios of liver and bone medium……...……...…….47
3.3.2. Function of HepaRG cells treated with different ratios of liver and bone medium……...……...…….48
3.4.1. Viability of bone co-culture system treated with different ratios of bone and liver medium……...……...…….49
3.4.2. Function of bone co-culture system treated with different ratios of bone and liver medium ……...……...……50
3.5. Evaluation of HepaRG spheroids' viability and function in the liver-bone co-culture system……...……...……52
3.6. Evaluation of bone co-culture system's viability and function in the liver-bone co-culture system……...……53
3.7.1. Analysis of the influence of three times weekly exposure of diclofenac on HepaRG spheroids' viability and function…….…….……...…..…….54
3.7.2. Analysis of the influence of three times weekly exposure of diclofenac on bone co-culture system's viability and function…….……...……...…….56
3.8. Assessment of HepaRG spheroids' viability and function, with/without bone system, stimulated with daily exposure of diclofenac…...……...…….57
3.9. Assessment of bone system's viability and function, with/without HepaRG spheroids, stimulated with daily exposure of diclofenac.…….……59
3.10. Analysis of the changes of mineral content and stiffness of bone scaffolds and RANKL/OPG balance in the 3D liver-bone co-culture system impaired by diclofenac……...……...…….…….60
3.11. Analyze the influence of 4-OH diclofenac on bone co-culture system……..…62
3.12. Evaluation of ROS, GSH and IL-6 levels of HepaRG spheroids with the stimulation of diclofenac…….……...…….63

3.13. Assessment of bone system's viability, function, and RANKL/OPG balance following daily exposure to IL-6…….64

List of Tables

2.1.1. List of used chemicals…….19
2.1.2. List of solutions……...21
2.1.3. List of consumables…….23
2.1.4. List of used equipment……...24
2.2.1. List of LC-HPLC/MS-based method to determine CYPs activity……...34
2.2.2. List of used antibodies……...39

List of abbreviations

2D	Two dimensional
3D	Three dimensional
ALD	Alcoholic liver disease
AP	Alkaline phosphatase
ATP	Adenosine triphosphate
BMP-9	Bone morphogenetic protein 9
C/EBPα	CCAAT enhancer binding protein α
CA II	Carbonic anhydrase II
$CaCl_2$	Calcium chloride
COX	Cyclooxygenase
CT	Computer tomographic
CYP450	Cytochrome P450
DMSO	Dimethyl sulfoxide
EPHB4–EFNB2	Eph receptor B4– Ephrin B2
Ex/Em	Excitation/Emission
FASL–FAS	Fas ligand–Fas receptor
FCS	Fetal calf serum
GSH	Glutathione
GSSG	Oxidized glutathione
HGF	Hepatocyte growth factor
HOD	Hepatic osteodystrophy
hPRP	Human platelet-rich plasma
IGF-1	Insulin-like growth factor 1
IL-11	Interleukin 11
IL-6	Interleukin 6
L-B	Liver–bone
L-B medium	HepaRG cells and bone co-culture differentiation medium
LCAT	Lecithin-cholesterol acyltransferase
MAFLD	Metabolic associated fatty liver disease

MASH	Metabolic dysfunction-associated steatohepatitis
M-CSF	Macrophage colony stimulating factor
MEM α	Minimum Essential Medium Eagle alpha
miR-144	MicroRNA 144
NaCl	Sodium chloride
NAFLD	Non-alcoholic fatty liver disease
NaOH	Sodium hydroxide
Nrf2	Nuclear factor erythroid 2-related factor 2
NSAIDs	Non-steroidal anti-inflammatory drugs
OPG	Osteoprotegerin
PBS	Phosphate buffered saline
PDMS	Polydimethylsiloxane
PGE2	Prostaglandin E2
PMA	Phorbole-12-myristate-13-acetate
PPARγ	Peroxisome proliferator-activated receptor γ
PTH	Parathyroid hormone
RANKL	Receptor activator of nuclear factor-kappa B ligand
RAU	Relative absorbance units
RFU	Relative fluorescence units
ROS	Reactive oxygen species
SEM	Standard error of the mean
SEMA3A–NRP1	Semaphorin-3A– Neuropilin-1
SRB	Sulforhodamine B
TBS-T	TRIS-buffered saline/Tween-20
TEMED	Tetramethylethylenediamine
TGF-β	Transforming growth factor beta
TNF-α	Tumor necrosis factor alpha
TRAP	Tartrate-resistant acid phosphatase
UGT	UDP-glucuronosyltransferase

Chapter 1

1. Introduction

1.1 Liver and bone

1.1.1 Liver function

The liver is one of the largest and most complex internal organs in the human body. Its basic functional unit is the lobule, which is composed of numerous hepatocytes arranged in a plate-like structure surrounding a central vein (Ben-Moshe and Itzkovitz 2019). There are various cell types in the liver, including hepatocytes, hepatic stellate cells, endothelial cells, cholangiocytes, and Kupffer cells. These cells perform many important functions in the liver such as digestion, metabolism, detoxification, nutrient storage, and immune regulation, with hepatocytes' metabolic function being particularly critical (Trefts *et al.* 2017). In addition, the liver is the primary organ for drug metabolism in the body, many drugs metabolism processes take place through two classes of enzymatic reactions (Phase I and II reactions) and one excretion reaction (Phase III reactions). These enzymatic reactions transform drugs and other xenobiotics into more easily excreted forms, thereby reducing their toxicity and bioactivity. In Phase I reactions, the liver uses the Cytochrome P450 (CYP450) enzyme system to carry out oxidation, reduction, and hydrolysis reactions, in which includes introducing polar groups into drug molecules to increase their water solubility. These reactions include hydroxylation, dealkylation, and oxidative deamination, and the diversity of the CYP450 enzyme system allows it to metabolize a wide range of drugs and compounds. The UDP-glucuronosyltransferase (UGT) enzyme is essential for Phase II reactions in which the liver catalyzes conjugation reactions (such as glucuronidation, sulfation, acetylation, and glutathione conjugation) to bind drugs or their metabolites with endogenous water-soluble molecules, further increasing their solubilities and excretion rates. These enzymatic reactions occur in the endoplasmic reticulum and cytoplasm of hepatocytes and involve transforming drugs from lipophilic to hydrophilic forms, thus allowing their excretion through urine or bile. Phase III

reactions consist of the regular removal of drugs and/or metabolites from the body through the liver, kidney, lung, or stomach through the actions of transporters (Almazroo *et al.* 2017). The three phases of hepatic drug metabolism involve the coordinated work of different enzymes and transport proteins to ensure that drugs are efficiently metabolized and excreted.

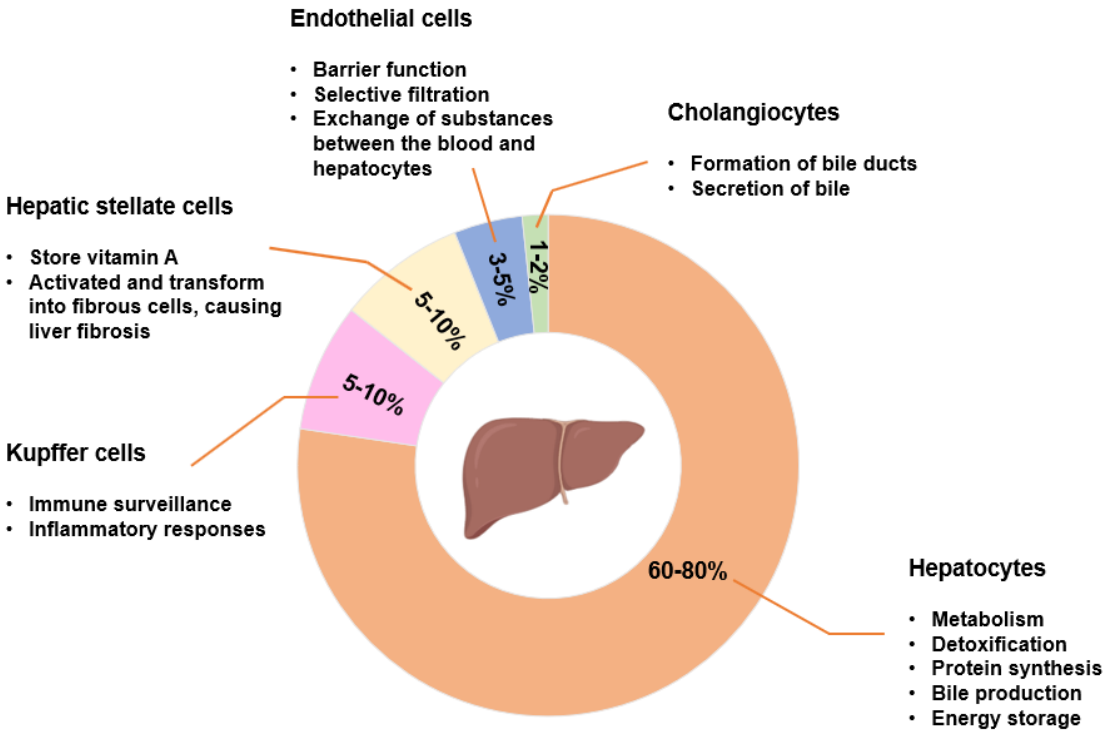

Figure 1.1 Types of liver cells and their functions. The various cell types in the liver work together to perform crucial functions, including metabolism, detoxification, nutrient storage, immune regulation, and bile production. Hepatocytes are not only the most numerous cell type in the liver but also its most important functional cells, responsible for various key physiological functions such as metabolism, detoxification, and protein synthesis. The image creation was supported by Biorender and Servier Medical Art.

1.1.2 Bone homeostasis

The bone system is among the most crucial structures in the human, providing essential functions such as support, the protection of internal organs, the facilitation of movement, and the production of blood (Boskey and Coleman 2010). Bone cells are the primary cellular constituents of bone tissue, and the predominantly types of bone cells are osteoblasts (osteocytes and osteoblast precursors) and osteoclasts. Osteoblasts, which

differentiate from mesenchymal stem cells, are the principal cells responsible for bone formation through synthesizing collagen and mineralizing the bone matrix to generate new bone tissue. Osteoblast precursors (stem cells and osteoprogenitor cells) mature into osteoblasts that maintain and repair the structure and function of bones (Khotib *et al.* 2023). Osteoclasts play a pivotal role in bone remodeling and repair by breaking down and resorbing bone tissue to regulate bone shape and density (Chen *et al.* 2018).

Bone cell homeostasis refers to the regulation of bone cell equilibrium within bone tissue, ensuring a dynamic balance between bone formation and resorption. This homeostasis is meticulously controlled by various cellular factors and signaling pathways to ensure the maintenance of bone structure and function. Osteoblast–-osteoclast contact is crucial for regulating bone remodeling to maintain bone homeostasis. These cells directly interact to control cell survival, proliferation, and differentiation *via* the Eph receptor B4– Ephrin B2 (EPHB4–EFNB2), Fas ligand–Fas receptor (FASL–FAS), and Semaphorin-3A–Neuropilin-1 (SEMA3A–NRP1) pathways (Kim *et al.* 2020). Transforming growth factor beta (TGF-β) and insulin-like growth factor 1 (IGF-1) are liberated from the bone matrix during the process of bone resorption mediated by osteoclasts, which subsequently leads to the production of bone by osteoblasts (Tang *et al.* 2009; Xian *et al.* 2012). Furthermore, osteoblasts synthesize osteoprotegerin (OPG) to inhibit osteoclast activity, while also secreting factors such as macrophage colony-stimulating factor (M-CSF) and receptor activator of nuclear factor κB ligand (RANKL), which promote the formation and differentiation of osteoclasts (Udagawa *et al.* 2021b). During bone formation, osteoblasts create new bone tissue by secreting collagen and a mineralized matrix, while their activity is modulated by osteogenic inhibitors such as angiogenesis inhibitors and inhibitors of macrophage inflammatory responses. Osteoclasts, on the other hand, participate in bone resorption through the secretion of enzymes such as acid phosphatase and extracellular matrix metalloproteinases. The disruption of bone cell homeostasis can lead to bone disorders such as osteoporosis and fractures (Hadjidakis and Androulakis 2006).

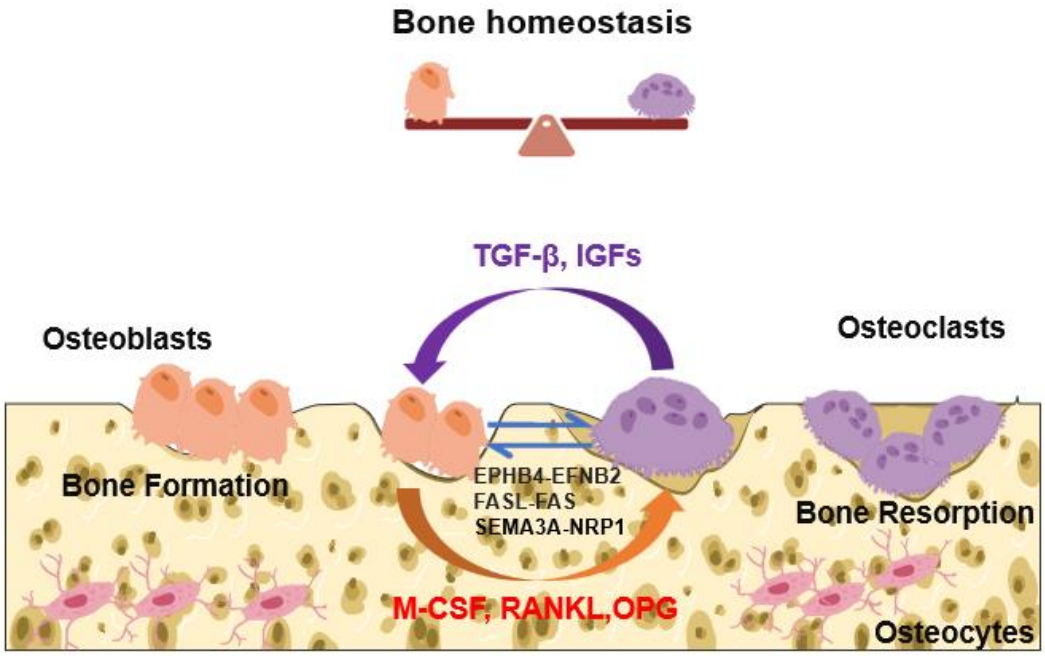

Figure 1.2 Bone homeostasis is maintained through a dynamic equilibrium involving the regulatory actions of three primary bone cells: osteoclasts, osteoblasts, and osteocytes. Osteoblasts and osteoclasts directly interact to control each survival, proliferation, and differentiation *via* the Eph receptor B4–Ephrin B2, Fas ligand–Fas receptor, and Semaphorin-3A–Neuropilin-1 pathways. Osteoblasts produce M-CSF, RANKL and OPG to regulate osteoclasts differentiation and function. TGF-β and IGF-1 are secreted from the bone matrix throughout the process of bone breakdown mediated by osteoclasts, subsequently influencing the differentiation and function of osteoblasts. EPHB4–EFNB2: Eph receptor B4–Ephrin B2; FASL–FAS: Fas ligand–Fas receptor; SEMA3A–NRP1: Semaphorin-3A–Neuropilin-1; TGF-β: Transforming growth factor beta; RANKL: Receptor activator of nuclear factor-kappa B ligand; M-CSF: Macrophage colony stimulating factor; IGFs: Insulin-like growth factors; OPG: Osteoprotegerin. The image creation was supported by Biorender and Servier Medical Art.

1.1.3 Interaction between the liver and the bone system

The liver and the bone system are closely interconnected through metabolic and physiological functions taking place within the human body (Barbu *et al.* 2017). As one of the largest metabolic organs, the liver regulates the metabolism of various nutrients such as sugars, fats, and proteins as well as maintaining metabolic balance through synthesis and secretion. In addition, it regulates vitamin D metabolism and synthesizes cytokines and other proteins that are essential for bone formation, including lecithin-cholesterol acyltransferase (LACT), TGF-β, IGFs and hepatocyte growth factor (HGF),

thereby directly or indirectly affecting the health and function of the bone system (Gatta *et al.* 2014). Bone tissue plays a crucial role in maintaining the balance of calcium and phosphorus by serving as the primary reservoir for these minerals (Taylor and Bushinsky 2009), which are closely linked to metabolic liver functions. Calcium and phosphorus are crucial for the production of adenosine triphosphate (ATP) (Tarasov *et al.* 2012), which provides energy for liver cells. Additionally, calcium plays a crucial role in modulating the function of enzymes that participate in lipid metabolism in the liver, contributing to the regulation of both lipogenesis and lipolysis (Chen *et al.* 2021). Similarly, studies indicate a significant correlation between serum levels of calcium and phosphorus and the prevalence of non-alcoholic fatty liver disease (NAFLD) (Shin *et al.* 2015).

Similarly, there is a reciprocal interaction between the liver and the skeletal system that influences immune regulation and inflammatory responses. The liver is essential for immune modulation. It synthesizes and secretes numerous immune-related proteins, such as albumin, globulins, and cytokines, thereby maintaining immune system stability (Jenne and Kubes 2013). These proteins are vital for blood and cellular transport functions; they also participate in regulating inflammatory responses and cellular signaling pathways by indirectly affecting the development and progression of inflammatory-related diseases within the bone system. Moreover, the connection between the liver and the bone system is evident in the realm of drug metabolism and toxicity regulation. The liver is the major organ for drug metabolism in the body, using enzymes such as the CYP450 and UGT system to convert drugs into metabolites to alter their potential toxicity to the bone system (Almazroo *et al.* 2017).

The relationship between the liver and the bone system constitutes a complex and multi-faceted network involving metabolic function, immune responses, and disease development.

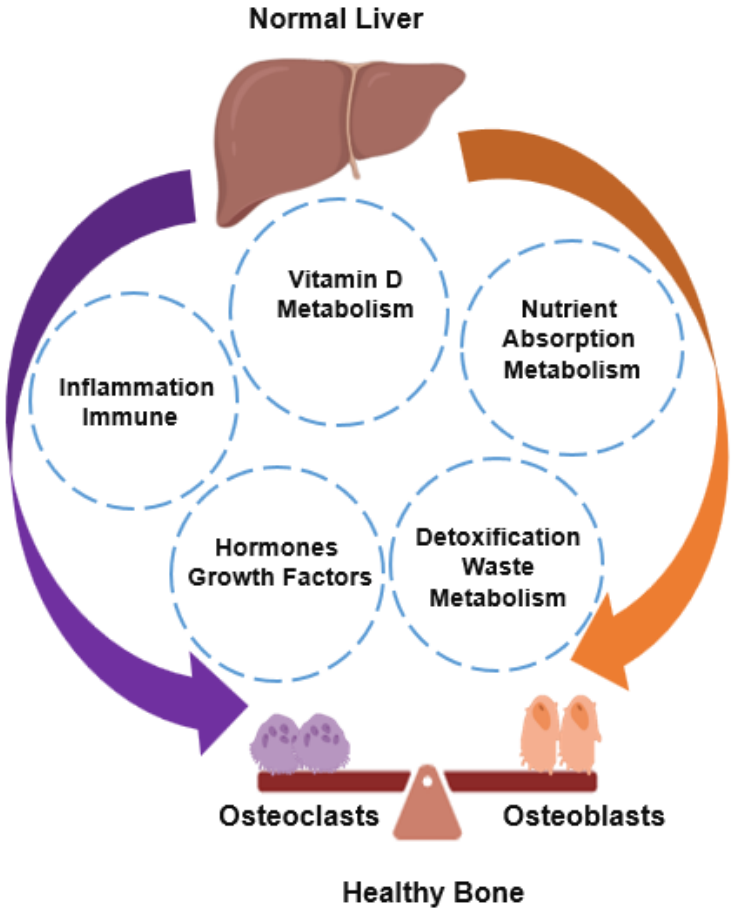

Figure 1.3 A healthy liver maintains bone homeostasis through various mechanisms and pathways (Nakchbandi and van der Merwe 2009; Saeki *et al.* 2024). The image creation was supported by Biorender and Servier Medical Art.

1.2 Liver and bone diseases

1.2.1 Liver diseases

Liver diseases encompass a broad spectrum of conditions that impact liver structure and function, varying in severity from mild to chronic and acute to progressive states. Acute and chronic liver injuries differ significantly in their causes, progression, and pathological characteristics. Acute liver injury—which can result in acute liver failure—is frequently brought on by medication toxicity, viral infections, or ischemia (Stravitz and Lee 2019). It is defined by the abrupt beginning of hepatocyte necrosis and an inflammatory response. Hepatocytes can promote cellular regeneration and repair after acute injury by secreting factors such as HGF (Chung *et al.* 2012). Chronic liver injury, on the other hand, is usually

caused by long-term viral infections (such as hepatitis B or C), chronic alcohol abuse, or NAFLD, or autoimmune hepatitis, which are characterized by persistent inflammation and fibrosis and eventually progresses to cirrhosis or liver cancer (Heidelbaugh and Bruderly 2006). During chronic injury, liver cell function gradually declines, and the levels of inflammatory cytokines (such as interleukin 6 (IL-6) and TNF-α) and fibrosis factors (such as TGF-β) remain elevated (Fabregat *et al.* 2016; Gong *et al.* 2022), leading to irreversible damage to the liver's structure and function.

One of the most common liver diseases is fatty liver disease, which comprises metabolic associated fatty liver disease (MAFLD) and its more severe form, metabolic dysfunction-associated steatohepatitis (MASH) (Moon *et al.* 2020). MAFLD is defined by the buildup of fat within the liver and is frequently linked to conditions such as obesity, diabetes, and metabolic syndrome. Without timely treatment, MAFLD can progress to MASH, which is characterized by liver inflammation and hepatocyte injury, ultimately leading to liver cirrhosis or liver cancer (Calzadilla Bertot and Adams 2016).

Alcoholic liver disease (ALD) results from long-term excessive alcohol consumption and encompasses a spectrum of liver damage. ALD is a major contributor to global liver-related mortality and morbidity rates. Alcohol is primarily metabolized in the liver by three enzymes: alcohol dehydrogenase, CYP2E1, and aldehyde dehydrogenase (Osna *et al.* 2017). During metabolism in the liver, alcohol produces acetaldehyde and reactive oxygen species (ROS), which are toxic substances that cause hepatocyte damage and oxidative stress. Alcohol also disrupts the oxidation of fatty acids—leading to their accumulation in the liver—and increases MASH levels, thereby inhibiting fatty acid oxidation and converting more fatty acids into triglycerides that are stored in the liver (Donohue 2007). Fatty degeneration of the liver is the earliest response to heavy drinking, and it can develop into steatohepatitis, liver fibrosis, or cirrhosis and ultimately lead to liver failure and liver cancer.

Viral hepatitis is another significant liver disease that is primarily caused by hepatitis

viruses, such as types A, B, C, D, and E. Hepatitis B and C are especially concerning because they can result in long-term infections, which may cause liver inflammation, fibrosis, cirrhosis, and a heightened possibility of developing liver cancer. Hepatitis A and E typically cause acute hepatitis and do not lead to chronic infection. The hepatitis virus directly infects liver cells, causing hepatocyte necrosis and inflammatory responses. Acute hepatitis may progress to chronic hepatitis, leading to liver fibrosis, cirrhosis, and eventually liver failure or cancer (Usuda *et al.* 2024).

Drug-induced liver injury refers to liver dysfunction or damage caused by medications or other external chemical substances. This category of liver injury ranges from a mild elevation of liver enzymes to severe liver failure (Fisher *et al.* 2015). Over a thousand drugs and herbal remedies have the potential to induce hepatotoxicity (Kuna *et al.* 2018). Several drugs have been withdrawn from the market due to their potential to cause hepatotoxicity, such as Troglitazone (for type 2 diabetes), Trovafloxacin (an antibiotic), and Nefazodone (an antidepressant) (Giustarini *et al.* 2018; Jaeschke 2007; Stewart 2002). The mechanisms behind drug-induced liver injury are diverse and include the direct toxicity of drugs or toxic metabolites that are produced during drug metabolism, or immune-mediated liver injury, in addition individual variations in drug metabolism and sensitivity (Fontana 2014; Gerussi *et al.* 2021). Drug-induced liver injury, which can cause both acute and chronic liver damage, is a prevalent and dangerous clinical issue. Acute liver injury usually results in severe hepatocyte necrosis and acute liver failure and is brought on by the short-term ingestion of high doses of medicines or the direct toxic effects of drug metabolites. However, some drug reactions are independent of dosage; these are known as idiosyncratic hepatotoxicity, which can be due to hypersensitivity or genetic variations in drug metabolism. Both acquired factors (such as sex, nutrition, pregnancy, alcohol abuse, and hepatic and extrahepatic diseases) and genetic factors influence an individual's susceptibility to drug-induced liver injury (Suriawinata and Thung 2006). No specific markers or tests are generally available for diagnosing this type of liver damage, which represents a significant challenge to ensuring safety in drug

development. On the other hand, chronic liver injury is brought on by long-term drug use and can also be induced by immune-mediated inflammatory reactions that persist, hepatocyte damage that occurs repeatedly, or incomplete healing. Chronic drug-induced hepatitis is often subtle, with clinical symptoms varying widely from the asymptomatic elevation of transaminase levels to cirrhosis. Drugs that have been reported to cause chronic hepatitis include Iproniazid, Diclofenac, Methyldopa and Trazodone (Suriawinata and Thung 2006). Chronic drug-induced hepatitis generally clinically and morphologically resembles chronic hepatitis that is caused by other factors. Comprehensive serological testing is required to exclude viral and autoimmune hepatitis, and obtaining a thorough drug-usage history is crucial. Up to now, diagnosing chronic drug-induced liver disease remains challenging.

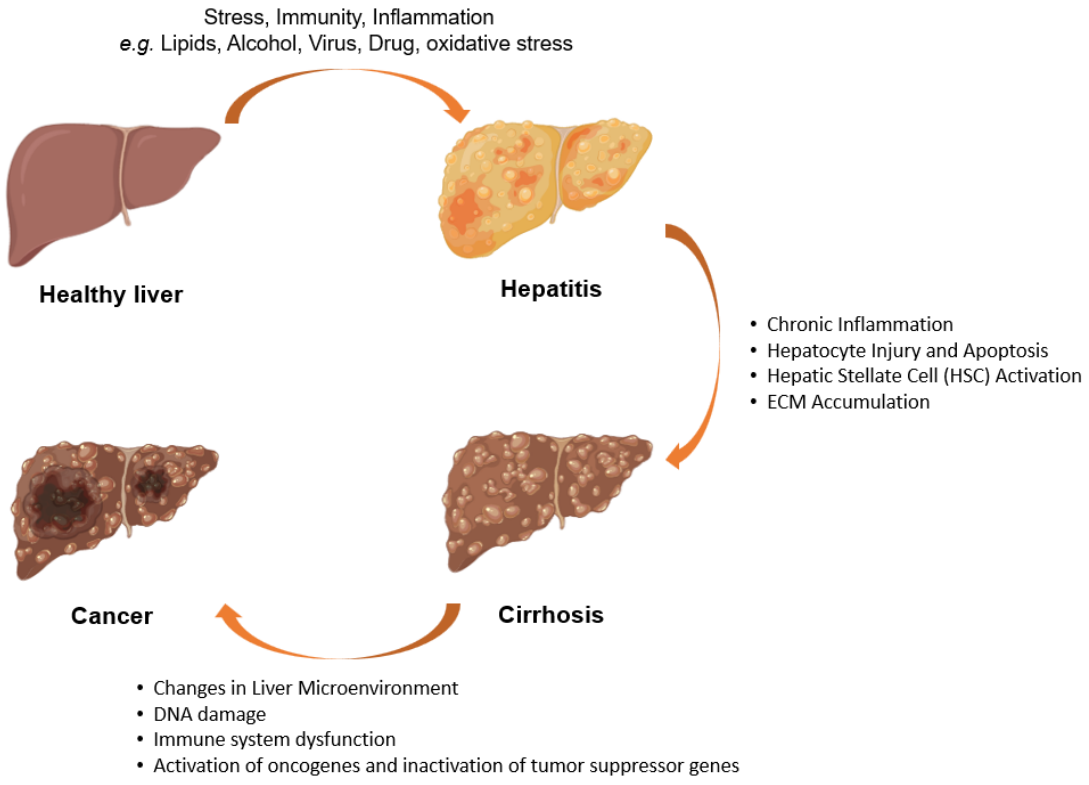

Figure 1.4 Liver disease is a progressive process involving three stages: inflammation, cirrhosis and eventually liver cancer (Levrero 2006). The image creation was supported by Biorender and Servier Medical Art.

1.2.2 Impaired bone homeostasis

Bone homeostasis imbalance refers to the disruption of the internal balance between bone formation and resorption that leads to issues such as decreased bone density, osteoporosis, and fracture. Under normal circumstances, bone cells (osteoblasts and osteoclasts) interact to maintain the stability of bone structure and function. However, when this balance is disrupted by conditions such as inflammation, oxidative stress, and altered potential of hydrogen, it results in bone homeostasis imbalance (Arnett 2008; Callaway and Jiang 2015; Hardy and Cooper 2009). The dysregulation of these two processes can lead to osteoporosis, which is characterized by reduced bone density and weakened bones that are more prone to fractures (Hadjidakis and Androulakis 2006).

1.2.3 Hepatic osteodystrophy (HOD)

HOD is a medical condition that affects the bones of individuals with liver disease. The condition is marked by a reduction in bone mineral density, heightened bone fragility, and changes in bone metabolism, which can result in a greater risk of fractures. More than 844 million people are affected by HOD worldwide (Shergill *et al.* 2018), and almost 75% of patients with chronic liver disease also have osteopenia or osteoporosis (Ehnert *et al.* 2019). HOD involves the complex interplay of physiological and metabolic processes. Firstly, impaired synthesis and activation of vitamin D in the liver lead to vitamin D synthesis disorders (Stokes *et al.* 2013). Vitamin D is essential for maintaining healthy bone, and a lack of it influences the absorption and usage of calcium and phosphate, which in turn impairs the mineralization and strength of bone, worsening conditions like osteoporosis and fragility (Bikle 2012). Secondly, Vitamin D deficiency and hypocalcemia stimulate the parathyroid glands to secrete parathyroid hormone (PTH). Elevated PTH levels promote bone resorption, leading to decreased bone mass and osteoporosis (Khundmiri *et al.* 2016).

Hepatic osteodystrophy also involves the dysregulation of cytokines, such as HGF and IGF-1; changes in these cytokines can inhibit osteoblast activity and proliferation and/or

promote osteoclast activity, leading to bone loss and reduced bone quality (Liu *et al.* 2018; Zhen *et al.* 2018). In chronic liver disease, injured liver cells and activated hepatic inflammation trigger the release of various inflammatory mediators, including cytokines like TNF-α and IL-6. These inflammatory mediators not only directly affect bone cell metabolism and function but also potentially exacerbate bone inflammation and damage by influencing bone cell differentiation, proliferation, and apoptotic processes (Marahleh *et al.* 2019; Wu *et al.* 2017a). Moreover, recent research showed that chronic liver disease downregulated the secretion of lecithin-cholesterol acyltransferase (LCAT) in liver, causing HOD and worsening liver fibrosis (Lu *et al.* 2022).

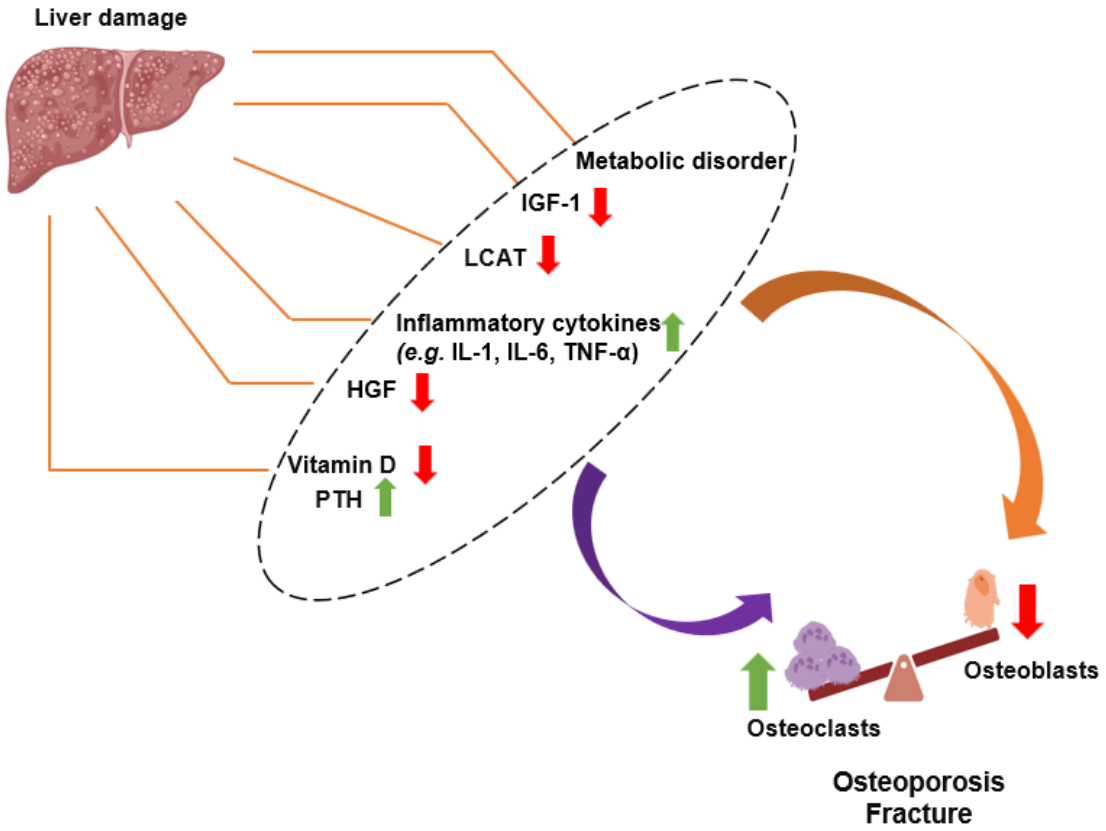

Figure 1.5 Changes in cytokines caused by liver damage can enhance bone resorption and inhibit bone formation, leading to osteoporosis and increased risk of fractures (Ehnert *et al.* 2019; Nakchbandi and van der Merwe 2009). IGF-1: Insulin-like growth factor 1; LCAT: Lecithin-cholesterol acyltransferase; IL-1: Interleukin 1; IL-6: Interleukin 6; TNF-α: Tumor necrosis factor-alpha; HGF: Hepatocyte growth factor; PTH: Parathyroid Hormone. The image creation

was supported by Biorender and Servier Medical Art.

1.3 Non-steroidal anti-inflammatory drugs (NSAIDs)

NSAIDs are a class of medications commonly used for their anti-inflammatory, pain-relieving, and fever-reducing properties; they are often prescribed for headaches, arthritis, and muscle pain (Díaz-González and Sánchez-Madrid 2015). NSAIDs work by inhibiting the cyclooxygenase (COX) enzymes, which reduces the production of prostaglandins to alleviate inflammation and pain. These drugs can be classified into non-selective NSAIDs (such as ibuprofen and diclofenac)—which inhibit both COX-1 and COX-2—and selective COX-2 inhibitors (such as meloxicam and celecoxib), which primarily target COX-2 to reduce gastrointestinal side effects (Arfeen *et al.* 2024). Although NSAIDs are widely used due to their excellent anti-inflammatory and analgesic effects, there are also reports of long-term use of NSAIDs potentially delaying bone fracture healing (Geusens *et al.* 2013; Wheatley *et al.* 2019) and are therefore controversial

1.3.1 Diclofenac

Diclofenac is an NSAID with anti-inflammatory, analgesic, and antipyretic properties. It works by inhibiting the synthesis of prostaglandins, thereby reducing pain and fever caused by inflammatory reactions. Diclofenac is widely used to treat various inflammatory conditions such as rheumatoid arthritis, osteoarthritis, and ankylosing spondylitis, as well as providing non-inflammatory pain relief for conditions such as headaches, dental pain, and musculoskeletal pain. Diclofenac is administered orally or topically and is still extensively used in clinical practice (Gan 2010).

1.3.2 Diclofenac affects the liver and bone

Diclofenac is commonly prescribed for orthopedic conditions associated with various inflammatory conditions. Following oral intake, nearly 40% of the drug is metabolized in the liver. This process is primarily facilitated by CYP450 and UGT enzymes in hepatocytes. Among these, CYP2C9 plays a key role by hydroxylating diclofenac, leading to the formation of its primary metabolite, 4′-hydroxydiclofenac (4-OH diclofenac). Other

enzymes such as CYP3A4 may play a role in the hydroxylation of diclofenac to 5′-hydroxydiclofenac (5-OH diclofenac), a less stable metabolite (Dorado *et al.* 2003; Tateishi *et al.* 2020). After the formation of hydroxylated metabolites, a part of metabolites is catalyzed by the UGT2B7 enzyme, which adds a glucuronic acid molecule to the hydroxylated metabolites, making them more soluble in water, which increases their ability to be excreted *via* the kidney. Apart from glucuronidation, some diclofenac metabolites undergo sulfation or glutathione conjugation. Glutathione conjugation helps to neutralize any reactive intermediates, thus preventing potential cellular damage (Dean and Kane 2012; Tateishi *et al.* 2020; Todd and Sorkin 1988). Despite its significant effectiveness in relieving inflammation and pain, long-term or high-dose usage of diclofenac may lead to hepatocyte injury. Research reported that diclofenac-induced liver injury is characterized by a progressive insult that builds up over time and eventually reaches a threshold rather than by an acute toxic response, and it is primarily caused by damage to the hepatobiliary excretory system (Boelsterli 2003). The specific mechanisms through which diclofenac causes hepatocyte damage remain incompletely understood, but this damage likely results from the toxicity of its metabolites, oxidative stress, and the induction of hepatocyte apoptosis (Gomez-Lechon *et al.* 2003; Thai *et al.* 2023).

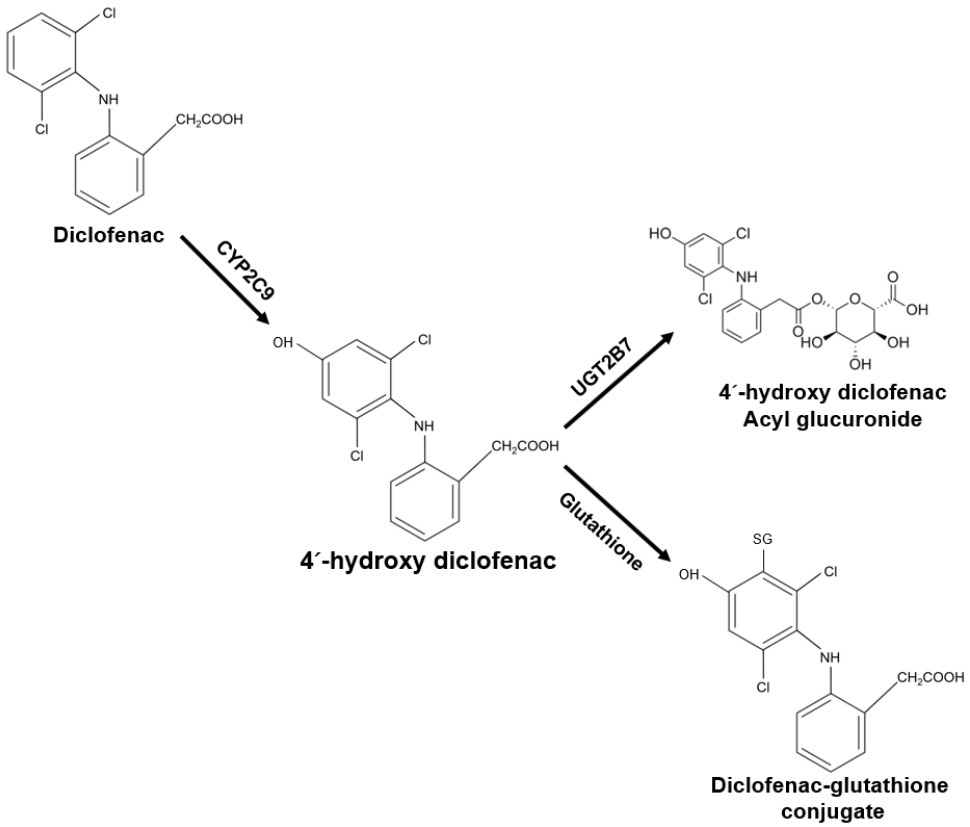

Figure 1.6 The primary metabolic pathway of diclofenac in the liver. The image creation was supported by Biorender and Servier Medical Art.

Regarding diclofenac usage and the bone system, preclinical and animal studies have identified adverse effects such as the disruption of bone homeostasis and delayed fracture healing that are associated with diclofenac use (Krischak *et al.* 2007b; Menger *et al.* 2023). Possible pathophysiological mechanisms could involve the inhibition of prostaglandins and COX-2, which are crucial mediators during the inflammatory phase of fracture healing (Gerstenfeld *et al.* 2003; Maruyama *et al.* 2020), as well as impaired communication between osteoclasts and osteoblasts through the imbalance of OPG and RANKL (Jurado *et al.* 2010). As figure 1.7 shows, in addition to potentially having a direct effect on bone homeostasis, diclofenac and its metabolites may also have an indirect effect on liver function, which may lead to the development of hepatic osteodystrophy (Gomez-Lechon *et al.* 2003; Karanikola *et al.* 2022; Menger *et al.* 2023). However, the mechanisms by which diclofenac affects bone homeostasis remains unknown.

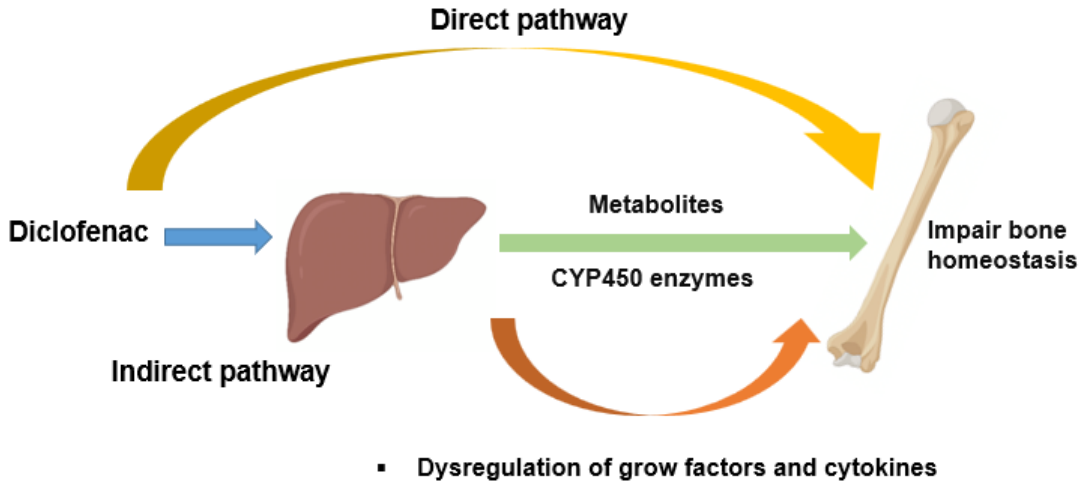

Figure 1.7 Diclofenac may impair bone homeostasis through several potential pathways (Gomez-Lechon *et al.* 2003; Karanikola *et al.* 2022; Menger *et al.* 2023). The image creation was supported by Biorender and Servier Medical Art.

1.4 Models for hepatic osteodystrophy studies

To date, several studies has used animal models to investigate the mechanisms underlying hepatic osteodystrophy (Hochrath *et al.* 2013; Lu *et al.* 2022; Nussler *et al.* 2014). Animal models serve as critical tools in investigative toxicology, with over 100 million animals utilized in experimental research annually (Doke and Dhawale 2015; Park *et al.* 2024). The main purposes to perform animal experiments are: the development of drugs and vaccines, toxicity testing of pharmaceuticals and chemicals, environmental research, as well as studies on biological behavior and training (Taylor and Alvarez 2019). However, animal experiments have several limits that must be recognized. Despite their value, animal experiments are costly, time-intensive, and raise ethical concerns. Additionally, replicability can be challenging, particularly in complex experimental conditions. Moreover, differences in drug metabolism and mechanical stress responses between humans and animals limit the direct applicability of animal-derived results to human contexts (McGonigle and Ruggeri 2014). Researchers have long sought to establish *in vitro* liver and bone models using two-dimensional (2D) cell culture. However, 2D models fail to precisely mimic the intricate three-dimensional (3D) structure and cell-cell relationship *in vivo*, limiting their forecasting abilities in drug discovery and development

(Foglietta *et al.* 2020; Jensen and Teng 2020). However, there is no established 3D *in vitro* model that effectively shows the relationship between the two systems.

Thus, an *in vitro* 3D L-B co-culture model with long-term stability is essential to closely imitate the *in vivo* situation and elucidate the mechanisms underlying hepatic osteodystrophy in humans. For the liver part, several hepatic cell lines are widely used as alternatives to primary human hepatocytes for human drug metabolism studies, such as HepG2, Huh-7, HCC-T, and HCC-M. These cell lines are easily accessible, inexpensive to maintain, and produce highly reproducible results. However, compared with human hepatocytes, the metabolic activity of these cells is much reduced (phases I and II drug-metabolizing enzymes), which limits their usefulness as an alternative model for drug toxicity screening (Lin *et al.* 2012). However, the HepaRG cell line has been widely adopted for hepatotoxicity studies, demonstrating a metabolic capacity that could appropriately imitate primary human hepatocytes (Hammour *et al.* 2022; Lubberstedt *et al.* 2011; Ruoß *et al.* 2020; Zahmatkesh *et al.* 2022). In this research, 3D HepaRG spheroids were developed to enhance the metabolic performance of the liver *in vitro* model and represent the liver's functional metabolic environment.

Regarding the bone tissue, early bone cell *in vitro* research primarily utilized monolayer cultures of osteoblasts that had been isolated from bone tissue. This method is simple and easy to operate; however, monolayer cell models cannot adequately simulate the complex 3D structure of bone tissue (Yuste *et al.* 2021). To better replicate physiological conditions, researchers are increasingly transitioning toward 3D culture models. These models utilize biomaterials such as scaffolds or hydrogels that allow bone cells to grow and differentiate in a 3D space (Häussling *et al.* 2019; Sun *et al.* 2021; Weng *et al.* 2020). In recent years, researchers have developed multicellular co-culture models that include not only osteoblasts but also osteoclasts and osteocytes. These models simulate the interactions between different bone cells, particularly focusing on their roles in the bone remodeling and resorption processes (Borciani *et al.* 2020; Lambertini *et al.* 2021). A cryogel-based scaffold was developed to incorporate human platelet-rich plasma (hPRP) as an organic

element of the bone matrix (Häussling *et al.* 2019) (Raina *et al.* 2016). The scaffold's apposite pore size and stiffness make it well-suited for its intended applications while reducing reliance on animal-derived materials and experimental animal use (Weng *et al.* 2020).

As osteoblasts and osteoclasts are bone resorbing–forming progenitor cells, the most common method for isolating these primary cells is to extract them from the bone tissues of animals—such as rats, mice, or rabbits - or from humans. Although these isolated cells perform similar functions *in vitro* to those they perform *in vivo*, the isolation methods are complex and yield limited numbers of cells with significant high batch-to-batch variability (Piwocka *et al.* 2024). In contrast, bone cell lines offer advantages such as stability, reproducibility, and ease of handling that make them widely used in laboratory experiments. Commonly used cell lines in osteoblast research include the MC3T3-E1, MG-63, SaOS-2, and SCP-1 lines (Aspera-Werz *et al.* 2018; Czekanska *et al.* 2014; Weng *et al.* 2023). Among these cell lines, SCP-1 cell was chosen for the research because they are human bone marrow-derived immortalized human mesenchymal stem cells that exhibit strong osteoblast-like characteristics (Weng *et al.* 2020). Furthermore, human monocytic-like cells (THP-1 cells) can be induced to differentiate into macrophage-like cells by treatment with phorbole-12-myristate-13-acetate (PMA). Due to their ease of differentiation, biological characteristics that are very similar to those of osteoclast precursors, and high reproducibility, we have chosen THP-1 cells as a model for osteoclasts (Weng *et al.* 2021).

1.5 Aim of the study

The primary objective of this dissertation was to develop an *in vitro* co-culture model using human liver and bone cell lines to mimic L-B interactions observed *in vivo*. This model serves as a platform for assessing diclofenac's negative effects on bone cells, facilitating a deeper understanding of underlying mechanisms and interactions within the L-B axis. The study focused on the following aspects:

1. Establishing and optimizing a 3D *in vitro* co-culture model of liver and bone
    a. Establishing separate 3D *in vitro* models of liver and bone
    b. Combining the liver and bone models together on an agarose plate and optimizing a suitable medium for the liver–bone system
    c. Culturing the 3D *in vitro* system for up to 21 days and testing the viability and function of both liver and bone models over this time period
2. Testing the effects of different concentrations and frequencies of diclofenac treatment on the 3D *in vitro* liver and bone co-cultures.
    a. Testing low-frequency (three times weekly) diclofenac exposure in the liver–bone system for 21 days and testing the viability and function of the liver and the bone system.
    b. Testing high-frequency (every day) diclofenac exposure in the liver–bone system for 21 days and testing the viability and function of the liver and the bone system.
3. Investigating how diclofenac exposure results in negative effects on bone homeostasis.
    a. Testing whether diclofenac directly influences bone homeostasis.
    b. Testing whether 4-OH diclofenac affects bone homeostasis.
    c. Testing whether diclofenac could cause oxidative stress in the liver part and increase the release of inflammatory factors.
    d. Testing whether the inflammatory factors affect bone homeostasis.

Chapter 2

2. Materials and Methods

Some of the experimental designs and methods employed in this dissertation are based on my previously published articles (Aspera-Werz *et al.* 2024; Chen *et al.* 2024).

2.1. Material

2.1.1 Chemicals

Table 2.1.1 List of used chemicals.

Substance	Company	Article No.
2-Hydroxyethylmethacrylat	Sigma-Aldrich KGaA-Aldrich	128635
3,3′-Methylene-bis(4-hydroxycoumarin)	Sigma-Aldrich KGaA-Aldrich	M1390
4′-Hydroxydiclofenac	Sigma-Aldrich KGaA-Aldrich	32412
4-Methylumbelliferone	Sigma-Aldrich KGaA-Aldrich	M1381
4-Nitrophenyl acetate	Sigma-Aldrich KGaA-Aldrich	N8130
4-Nitrophenyl-phosphate disodium salt hexahydrate	Carl Roth GmbH + Co.KG	4165.1
Acetic acid	VWR International LLC	20104.298
Agarose	Genaxxon bioscience GmbH	M3044.1000
Alizarin Red solution	Carl Roth GmbH + Co.KG	0348.2
Ammonium Persulfate	Sigma-Aldrich KGaA	A3678-25G
Bis-Acrylamide	Carl Roth GmbH + Co.KG	3039.1
Bufuralol Hydrochloride	Toronto Research Chemicals Inc.	B689540
Bupropion Hydrochloride	Toronto Research Chemicals Inc.	B689625
Calcein AM	Sigma-Aldrich KGaA	17783
Calcium chloride ($CaCl_2$)	Carl Roth GmbH + Co.KG	CN93.2
Cetylpyridinium chloride solution	Carl Roth GmbH + Co.KG	CN27.1
Cholecalciferol ($VitD_3$)	Sigma-Aldrich KGaA	95230
Dibenzylfluoresceine	Sigma-Aldrich KGaA	D7191
Diclofenac sodium salt	Sigma-Aldrich KGaA	D6899
Dimethyl sulfoxide (DMSO)	Carl Roth GmbH + Co.KG	4720.2

Di-Sodium hydrogen phosphate buffer	Carl Roth GmbH + Co.KG	T876.1
Di-sodium tartrate	Carl Roth GmbH + Co.KG	0254.1
Fetal calf serum	Life Technologies Corporation	10270-106
Glutamine	Sigma-Aldrich KGaA	M11-006
Glutaraldehyde	Carl Roth GmbH + Co.KG	3778.1
Glycine	Carl Roth GmbH + Co.KG	3908.2
HEPES	Carl Roth GmbH + Co.KG	HN78.2
Hoechst 33342	Sigma-Aldrich KGaA	14533
Hydrocortison	Pfizer Inc.	
Hydrogen peroxide (H_2O_2)	Carl Roth GmbH + Co.KG	CP26.5
Insulin	Novo Nordisk A/S	
Interleukin 6	Peprotech Inc.	200-06
L-Ascorbic acid 2-phosphate	Sigma-Aldrich KGaA	A8960-5G
Luminol	Carl Roth GmbH + Co.KG	4203.1
Magnesium chloride ($MgCl_2$)	Carl Roth GmbH + Co.KG	KK36.2
Methanol	Honeywell international Inc.	32213
Minimum Essential Medium Eagle Alpha	Sigma-Aldrich KGaA	M4655
P-Coumaric acid	Carl Roth GmbH + Co.KG	9908.1
Penicillin/Streptomycin	Sigma-Aldrich KGaA	P0781
Phenacetin	Sigma-Aldrich KGaA	77440
Phorbol 12-myristate 13-acetate	Abcam plc	ab120297
Phosphate-buffered saline	Merck KGaA	L182-50
Resazurin sodium salt	Sigma-Aldrich KGaA	199303
RPMI 1640	Sigma-Aldrich KGaA	R8758
S-Mephenytoin	Toronto Research Chemicals Inc.	M225000
Sodium acetate	Carl Roth GmbH + Co.KG	X891.2
Testosterone	Sigma-Aldrich KGaA	T1500

Tetramethylethylenediamine (TEMED)	Carl Roth GmbH + Co.KG	2367.3
TRIS	Sigma-Aldrich KGaA	T1503
Tween-20	Carl Roth GmbH + Co.KG	9127.1
William's E medium	Sigma-Aldrich KGaA	W1878
β-Glycerophosphate disodium salt hydrate	Sigma-Aldrich KGaA	G9422

2.1.2 Solutions

Table 2.1.2 List of used solutions.

Buffers/Medium/Solutions	Compounds and handing
4′-Hydroxydiclofenac stock solution (10 mM)	1 mg 4'-Hydroxydiclofenac 320 µl Methanol
4-MU stock solution (25 mM)	44.05 mg 4-Methylumbelliferone 10 ml DMSO
4-MU working solution for UGT activity	4 µl 4-Methylumbelliferone stock solution 1 ml William's E medium
Acetic acid solution (1%)	500 µl Acetic acid 49.5 ml ddH20
Agarose working solution (2%)	4 mg Agarose Adjust volume to 200 ml ddH_2O
Alizarin Red Staining Solution (0.5%)	200 mg Alizarin Red S Adjust volume to 40 ml with ddH_2O Adjust pH to 4.0
AP activity assay buffer	3.75 g Glycine 12.11 g Tris-Base 95.21 mg $MgCl_2$ Adjust volume to 900 ml with ddH_20 Adjust pH to 10.5 with NaOH Adjust volume to 1 L with ddH_20
AP substrate solution	1.3 mg 4-Nitrophenyl phosphate disodium salt hexahydrate (pNPP) 1 ml AP Activity Assay Buffer (pH 10.5)
APS solution (10%)	2 g Ammonium Persulfate 20 ml ddH_20
CA II activity solution	54.3 mg 4-Nitrophenyl acetate 1.5 ml Ethanol (99%)
CA II substrate buffer	75.7 mg TRIS 219.2 mg NaCl Adjust pH to 7.5 Adjust volume to 50 ml with ddH_20
Calcein AM stock solution	502 µl DMSO

	1 mg Calcein AM
Calcium chloride substrate solution (1M)	11.09g Calcium chloride Adjust volume to 100 ml with ddH_2O
Cetylpyridium chloride Solution (10%)	10 g Cetylpyridium chlorid monohydrate Adjust volume to 40 ml with tap water Heat in the water bath for dissolving the chemical
Cholecalciferol stock solution	2 mg Cholecalciferol 10 ml DMSO
DBF stock solution (2.5 mM)	5 mg Dibenzylfluoresceine Adjust volume to 3910 µl with DMSO
DBF working solution for CYP2C9 activity	2 µl DBF stock solution 1 µl Dicumarol stock solution 1 ml William's E medium
Diclofenac sodium stock solution (10 mM)	0.0318 g Diclofenac sodium salt 10 ml Methanol
Dicumarol stock solution (10 mM)	33.6 mg 3,3'-Methylene-bis(4-hydroxycoumarin) 10 ml DMSO
Di-Sodium hydrogen phosphate substrate solution (1M)	7.1 g Di-Sodium hydrogen phosphate Adjust volume to 50 ml with ddH_2O
HepaRG cell differentiation medium medium	100 ml HepaRG cell growing medium 1.7 ml DMSO
HepaRG cell growing medium	500 ml William's E medium 5 ml Penicillin/Streptomycin 50 ml Fetal calf Serum 5 ml L-Glutamine 800 µl Insulin 200 µl Hydrocortisone
Hoechst stock solution	10 mg Hoechst 33342 5 ml DMSO
Human platelet-rich plasma (hPRP) scaffold	1320 µl pHEMA (97%) 1320 µl Bis-Acrylamid (2%) 800 µl Human platelet-rich plasma (2.4 g/L) 1952 µl ddH_2O Incubate for 30 mins on ice 2400 µl Na_2HPO_4 (1M) 160 µl APS (10%) 16 µl TEMED (99%) 32 µl Glutaraldehyde (25%)

Interleukin 6 stock solution (10 µg/ml)	5 µg Interleukin 6 50 µl ddH_2O 450 µl 0.1% bovine serum albumin
NaOH solution for DNA quantification (50 mM)	1.25 ml 2 M NaOH solution 48.75 ml ddH20
Osteogenic differentiation medium for SCP-1/THP-1 co-culture System	250 ml RPMI 1640 medium 250 ml MEM α medium 29 mg L-Ascorbic acid 2-phosphate 0.54 g β-Glycerophosphate 2.98 g HEPES 83 mg Calcium chloride 50 µl Cholecalciferol stock solution 10 ml Fetal calf serum
PMA stock solution (200 µM)	1 mg Phorbole- 12-myristate-13-acetate 8.1 ml DMSO
Resazurin stock solution (11 X)	12.5 mg Resazurin sodium salt 50 ml PBS
Resazurin working solution (1 X)	100 µl Resazurin stock solution (11X) 1 ml PBS or plain medium
SCP-1 cell growing medium	500 ml MEM α medium 25 ml Fetal calf serum
Sulforhodamine B solution (0.4%)	0.2 g Sulforhodamine B Adjust volume to 50 ml with 1% acetic acid
THP-1 cell growing medium	500 ml RPMI 1640 medium 25 ml Fetal calf serum
TRAP activity assay buffer	8.2 g Na-Acetate 11.5 g Na_2-Tartrate Adjust volume to 900 ml with ddH_2O Adjust pH to 5.5 with HCl Adjust volume to 1 L with ddH_2O
TRAP reaction stop solution	10 ml 2M NaOH 10 ml ddH_2O
TRAP substrate solution	1.3 mg 4-Nitrophenyl phosphate disodium salt hexahydrate (pNPP) 1 ml TRAP Activity Assay Buffer (pH 5.5)
TRIS solution for DNA quantification (1M)	6.06 g TRIS Adjust volume to 40 ml with ddH_20 Adjust pH to 8.0 with HCl Adjust volume to 50 mL with ddH_20
Trypan blue solution	62.5 mg Trypan blue 50 ml PBS

Unbuffered TRIS Solution for SRB staining (10 mM)	1.2 g TRIS Adjust volume to 1 L with ddH_20

2.1.3 Consumables

Table 2.1.3 List of used consumables.

Consumable	Manufacturer	Type	Serial number
Cell culture flasks	Greiner bio-one GmbH	75 CM^2	658175
Cell culture flasks	Greiner bio-one GmbH	175 CM^2	660175
Cell culture plates	Greiner bio-one GmbH	96-well, flat bottom	655180
Cell culture plates	Greiner bio-one GmbH	96-well, V bottom	651101
Cell culture plates	Greiner bio-one GmbH	48-well, flat bottom	677102
Cell culture plates	Coming Inc.	6-well, flat bottom	353046
Cell culture tubes	Greiner bio-one GmbH	50 ml	227261
Cell culture tubes	Greiner bio-one GmbH	15 ml	188271
Eppendorf tubes	SARSTEDT AG	0.5 ml, white	72.699
Eppendorf tubes	Carl Roth GmbH + Co.KG	1.5 ml, white	4182.1
Eppendorf tubes	Eppendorf SE	2.0 ml, white	2549
Pipette	Greiner bio-one GmbH	5 ml	606160
Pipette	Greiner bio-one GmbH	10 ml	607160
Pipette	Greiner bio-one GmbH	25 ml	760160
Pipette tips	Greiner bio-one GmbH	0.1-10 µl	772350
Pipette tips	Greiner bio-one GmbH	2-200 µl	775350
Pipette tips	Greiner bio-one GmbH	100-1000 µl	777350

2.1.4 Equipment

Table 2.1.4 List of used equipment.

Equipment	Manufacturer	Type	Serial nummer
Agitator, magnetic stirrer	IKA-Werke GmbH	RH B2	06.050357
Agitator, magnetic stirrer	Heidolph Instruments GmbH	MR Hei-Mix L	040700340
Centrifuge	Dako Deutschland GmbH	Stat Spin	620E50000693
Centrifuge	Thermo Fisher Scientific Inc.	Megafuge 40 R	41307652
Centrifuge	Scientific Industries Inc.	SI DD 58	DD58-1001
Centrifuge (Mirco)	Labnet International Inc.	BN 08060235	C1301B
Centrifuge (Mirco)	HERAEUS Med GmbH	Fresco 17	41250019

CT scanner	Siemens Healthineers AG	SOMATOM Definition Edge	
Electrophoresis power supplies	Bio-Rad Laboratories GmbH	Power Pac 200	285BR05538
Freezer -20°C	BSH GmbH	IQ500	GS51NYW41 (01)
Freezer -20°C	Liebherr AG	Med Line	LGex3410-21K 001
Freezer -80 °C	Thermo Fisher Scientific Inc.	905	827860-2521
Fridge +4 °C	Liebherr AG	Comfort	3523-21L
Fridge +4 °C	Cool Compact Kühlgeräte GmbH	HKMT 040-01	CC00412514
Ice maker	Scotsmen Inc.	AF 80	DD 8837 11 X
Incubator	Thermo Fisher Scientific Inc.	Heratherm OMS 60	41296334
Incubator	Binder GmbH	9040-0078	11-22649
Incubator	Binder GmbH	9040-0081	11-22190
Laboratory pump (Bench)	Carl Roth GmbH + Co.KG	Cyclo 2	1109-065
Microscope	Peqlab Biotechnologie GmbH	EVOS-fl	91-AF-4301
Mixer	Corning Inc.	Vortex Mixer	804995
Mixer	Labinco B.V.	LD-76	76000
Multichannel Pipette	Corning Inc.	5-50 µl	151620022
Multichannel Pipette	Corning Inc.	20-200 µl	551630277
Multichannel Pipette	Thermo Fisher Scientific Inc.	0.5-10 µl	CH98998 4510
Multichannel Pipette	Corning Inc.	50-300 µl	151640033
PCR thermal cyclers	Thermo Fisher Scientific Inc.	Arktik	10040953
PCR thermal cyclers	Applied Biosystems GmbH	Forschungslabor	50132
pH meter	Mettler-Toledo GmbH	Five Easy FE 20	1232315296
pH meter	Mettler-Toledo GmbH	Five Easy F 20	30266626
Pipette controller	Integra GmbH	Pipetboyacu	629619
Pipette controller	Heathrow Scientific LLC	Rota-Filler 3000	HSA05119
Refrigerator	Cool Compact Kühlgeräte GmbH	HKMT 040-01	CC 00412516

Refrigerator	Cool Compact Kühlgeräte GmbH	HKMN 062-01	CC 00412513
Safety workbench	Thermo Fisher Scientific Inc.	Maxisave S20201.8	41293949
Safety workbench	Thermo Fisher Scientific Inc.	Maxisave S20201.8	41293948
Scale	Kern & Sohn GmbH	ABJ 120-4M	WB 1140084
Shaker, laboratory	Peqlab Biotechnologie GmbH	ES-20	010111-1107-0119
Shaker, laboratory	LTF Labortechnik GmbH	DRS 12	11DE243
Shaker, laboratory	LTF Labortechnik GmbH	DRS 12	11DE090
Shaker, laboratory	Corning Inc.	LSE Vortex Mixer	1101260
Single-channel Pipette	Corning Inc.	100-1000 µl	058261237
Single-channel Pipette	Corning Inc.	20-200 µl	158250088
Single-channel Pipette	Corning Inc.	10-100 µl	158240031
Single-channel Pipette	Eppendorf SE	0.1-2.5 µl	P35434B
Single-channel Pipette	Corning Inc.	0.5-10 µl	158220060
Single-channel Pipette	Corning Inc.	2-20 µl	158230441
Spectrophotometer	BMG Labtech GmbH	Fluostar Omega	415-1264
Water-bath	Lauder Dr. R. Wobser GmbH	A1 25	LCB 0727-11-0094
Water-bath	Lauder Dr. R. Wobser GmbH	ECO ET 20	LY 06.1
ZwickiLine	Zwick GmbH & Co. KG	2.5 TN	059003

2.2 Methods

2.2.1. Manufacturing and sterilizing of hPRP scaffolds

A human platelet-rich plasma (hPRP) scaffold was created as described in a prior publication (Haussling *et al.* 2019). Blood samples were collected from healthy individuals into EDTA tubes, which were centrifuged for 10 min at 1000 × g to separate the PRP. Next, an aqueous mixture comprising 16.0% 2-hydroxyethylmethacrylate, 0.25 g/L PRP, and 0.3% bis-acrylamide was combined. This combination was then mixed well and cooled on ice. After 30 minutes, disodium hydrogen phosphate buffer was added to the mixture. The next stage involved mixing 0.1% glutaraldehyde, 0.2% TEMED, and

0.2% ammonium persulfate. The final mixture was poured into casting molds made of polystyrene, with 2 mL added to each mold. The molds were then promptly frozen for at least 12 hours at –18 °C. The temperature and rate of freezing each affect the pores' shape and size in the scaffolds (Adnan Memic and Joseph Steingold 2019). To facilitate slicing, the matrix was frozen at −80 °C for one hour. The resulting scaffolds, measuring 6 mm in width and 4 mm in height, were immediately immersed in a 1 M $CaCl_2$ solution to facilitate the hydroxyapatite formation. After 24 hours, the scaffolds were thoroughly rinsed with PBS for 15 minutes to eliminate residual $CaCl_2$. Subsequently, the scaffolds were submerged in 70% ethanol and agitated for a minimum of 12 hours to remove any unreacted chemicals and ensure sterilization. Following this, the scaffolds were washed four times in sterile PBS every 30 minutes until the ethanol was completely removed. Finally, the scaffolds were cultured in THP-1 cell growth medium for 48 hours in the incubator (5% CO_2, 37 °C). This pretreatment procedure ensures sterility.

2.2.2. Manufacturing and sterilization of agarose plates and microwells

As previously mentioned, a mold-replication technique was used to generate non-adherent agarose microwell plates (Ghezelayagh *et al.* 2022). To create the micro-well plates, a PDMS insert (generously provided by Dr. Massoud Vosough) was used to create 300 pyramidal micro-wells (800 µm diameter/well), in a 6-well plate (Zahmatkesh *et al.* 2022). After adding 3 mL of molten 2% agarose to each well, the insert was carefully removed once the agarose had solidified, leaving behind a patterned agarose surface with an inverted mirror image (Figure 2.2.1). Before being used, the plate was sterilized by exposure to ultraviolet radiation for one hour (Zahmatkesh *et al.* 2022).

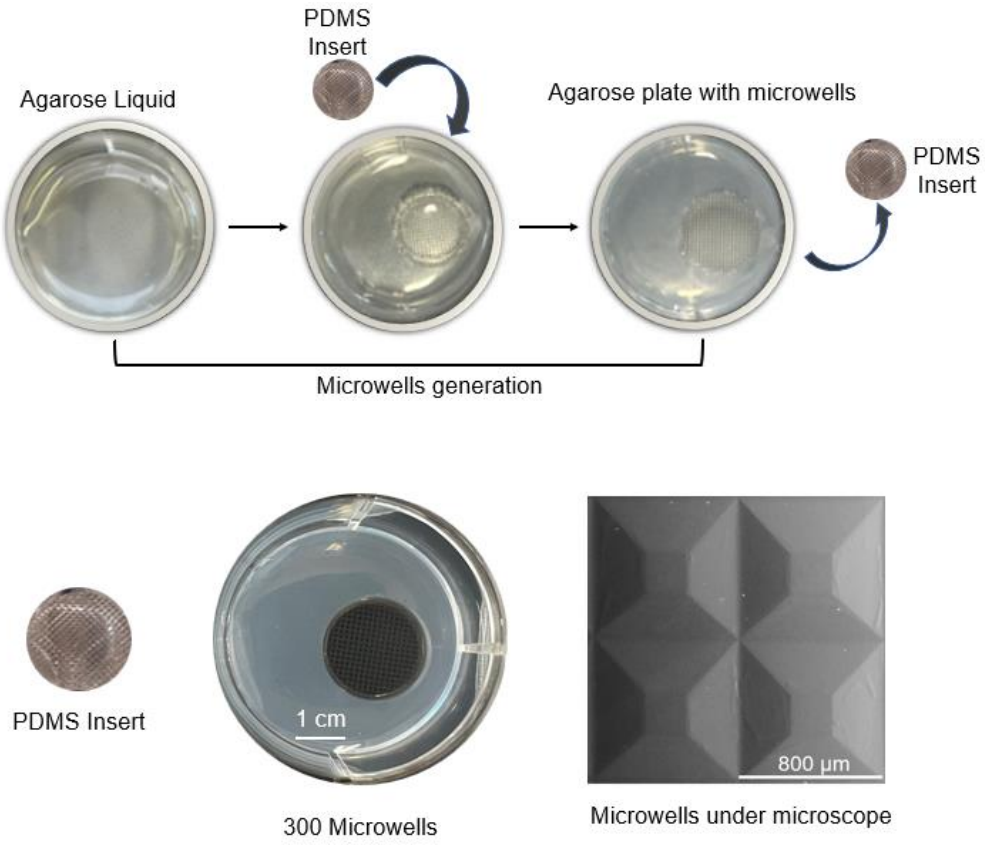

Figure 2.2.1 The process of generating an agarose microwell plate and its characteristics.

2.2.3. Cell lines

The HepaRG human immortalized hepatic cell line (Biopredic International, Saint Grégoire, France) was maintained in William's E medium supplemented with 10% FCS, 2 mM glutamine, 5 µg/mL insulin, 1% Penicillin/Streptomycin, and 50 µM hydrocortisone for two weeks to facilitate cell proliferation. The cells were cultured in a humidified incubator (37 °C, 5% CO_2), and the medium was changed three times per week. Differentiation was triggered by adding 1.7% DMSO to the culture (Hammour *et al.* 2022; Ruoß *et al.* 2020).

Osteoprogenitor cells, SCP-1 cells—a mesenchymal stem cell line (Bocker *et al.* 2008)—were maintained in MEM α medium containing 5% FCS in a humidified incubator (37 °C, 5% CO_2), with the medium changed twice per week.

To provide osteoclastic progenitor cells (ACC16, DSMZ), the THP-1 human leukemia

monocytic cell line was used. The cells were maintained in suspension using RPMI 1640 medium added with 5% FCS in a humidified incubator (37 °C, 5% CO_2). The medium was changed twice per week (Weng *et al.* 2021).

2.2.4. Cell seeding

2.2.4.1. Bone co-culture system

For the 2D bone cell co-culture model, 2.4×10^4 THP-1 cells within 100 µL of growth medium were plated into a single well of a 96-well plate, and then treated with 200 nM PMA. After 24 hours, the THP-1 growth medium was replaced, and 0.3×10^4 SCP-1 cells were added to with 100 µL of osteogenic differentiation medium (Table 2.2.1). The THP-1 and SCP-1 co-culture system was maintained in a humidified environment (37 °C, 5% CO_2), and the medium was refreshed twice per week (Weng *et al.* 2021).

Regarding the 3D osteoblast-osteoclast co-culture model, the scaffold's medium was removed after the sterile control in a 48-well plate. Scaffold was positioned in the middle of each well. As a published protocol, 8×10^4 THP-1 cells in 15 µL of THP-1 growth medium were plated onto the scaffold, and then treated with 200 nM PMA. After 4-hour incubation, 500 µL of medium containing 200 nM PMA was gently added. To ensure proper cell attachment, the scaffolds were incubated for an additional 24 hours under the same conditions. The next day, the medium was discarded, and 1×10^4 SCP-1 cells in 15 µL bone differentiation medium were plated onto the same scaffold. After a 4-hour incubation, each scaffold was given 500 µL of differentiation medium. The co-culture scaffolds were maintained in a humidified environment (37 °C, 5% CO_2). The bone differentiation medium was replaced twice per week (Weng *et al.* 2020).

2.2.4.2. HepaRG cell culture

For the 2D liver model, each well of a 96-well plate was filled with 100 µL of HepaRG cell culture medium and seeded with 0.9×10^4 HepaRG cells. Before the experiment, the cells were cultured for two weeks for proliferation and then were cultured for a further two weeks with the treatment of 1.7% DMSO to induce cell differentiation. The cells were maintained in a humidified environment (37 °C, 5% CO_2). In addition, the

HepaRG differentiation medium was refreshed three times weekly.

Regarding the liver spheroid model, 2ml of HepaRG growth medium was added into agarose well. And then 30×10^4 cells/mL/well HepaRG cells (1000 cells/microwell) in 1 mL of HepaRG culture medium were plated into each well to make spheroid formation. To achieve uniform cell distribution within the microwells, the plate was promptly centrifuged at 1200 rpm for 3 minutes. Light microscopy was used to check the distribution of HepaRG cells in the microwells. The following day, 1.7% DMSO was used to induce cell differentiation. The spheroids were incubated in a humidified environment (37 °C, 5% CO_2). The culture medium for HepaRG cells, supplemented with 1.7% DMSO, was refreshed three times weekly (Hammour *et al.* 2022).

2.2.5. Testing the effects of supplements present in liver and bone media on 2D-cultured bone and liver cells, respectively

To assess the impact of bone differentiation medium's supplements on HepaRG cells, the cells were maintained in 96-well plates and treated with 1.5 mM calcium chloride, 5 mM β-glycerophosphate, 25 mM HEPES, 20 ng/mL cholecalciferol (Vitamin D3), and 200 µM L-ascorbic acid 2-phosphate. The medium was refreshed, and stimulation was conducted three times a week. The viability and function of HepaRG cells were assessed every 7 days (7, 14, 21 days).

To evaluate the impact of HepaRG differentiation medium's factors on osteoblast–osteoclast co-culture system, the bone cells were treated with 1.7% DMSO, 5 µg/ml insulin, 2 mM L-glutamine, and 50 µM hydrocortisone. Medium change was performed three times a week. The viability and function of osteoblasts–osteoclasts were assessed every 7 days (7, 14, 21 days).

2.2.6. Optimizing the medium for the 3D L-B system

In order to identify an optimal medium ratio capable of sustaining both the functionality and viability of liver and bone cells, various proportions of liver differentiation medium plus bone differentiation medium (referred to as L-B medium or B-L medium,

respectively) were evaluated independently for their impact on the function and viability of liver and bone cells. We independently cultured HepaRG spheroids and bone scaffolds using medium mixtures with ratios of 100:0, 75:25, 50:50, and 25:75 of L-B medium to B-L medium. The cells' viability and functionality were assessed on 7, 14, and 21 days.

2.2.7. Development of a 3D liver–bone co-culture model

After the spheroids were created, the cell-free agarose was hollowed out to create pockets for the bone scaffolds. Each cell-attached scaffold was placed in an agarose pocket. The ratio of HepaRG spheroids to bone scaffolds was 300:2. The co-culture system was maintained for 21 days using a L-B differentiation medium following the combining of the HepaRG spheroids and bone scaffolds (Figure 2.2). The medium was meticulously refreshed every two days. The L-B system was maintained in a humidified environment (37 °C, 5% CO_2).

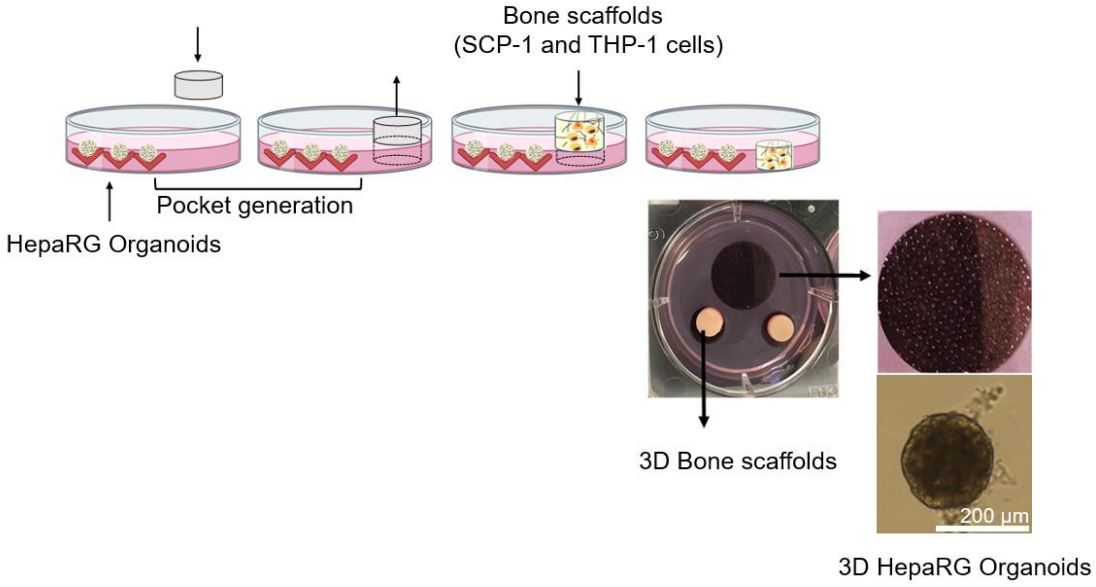

Figure 2.2 Establishment of the L-B co-culture system. Once the formation of HepaRG spheroids, we utilized the insert to create spaces on the agarose for bone scaffolds. The two cell-attached scaffolds were transferred into the agarose pocket and indirectly cultured with liver spheroids to develop the 3D L-B system.

2.2.8. Diclofenac exposure to the 3D L-B co-culture model

The 10 mM stock solution of diclofenac was prepared by dissolving it in 99%

formaldehyde and then stored at –20 °C for refrigeration. The *in vitro* L-B model was exposed to daily doses of 3–6 µM diclofenac, determined according to findings from a clinical study; these diclofenac concentrations correspond to the human plasma levels of diclofenac following treatment (50 mg oral intake) (Cuklev *et al.* 2011; Miyatake *et al.* 2009; Scallion and Moore 2009).

2.2.9. Exposure of the 3D bone co-culture model to 4'-hydroxydiclofenac

99% formaldehyde was used to dissolve 4'-hydroxydiclofenac to get the 10 mM stock solution and then refrigerated at –20 °C. Concentrations of 75, 300, and 600 nM 4'-hydroxydiclofenac were added daily to the 3D bone model to replicate the human plasma concentration of 4-OH diclofenac following diclofenac administration (Degen et al. 1988; Yasar et al. 2001).

2.2.10. IL-6 was exposed to the 3D bone co-culture model to evaluate its effects on cell viability and function

A 10 µg/ml stock solution was prepared by dissolving 5 µg of IL-6 in 50 µl of double-distilled water (ddH_2O), followed by the addition of 450 µl of 0.1% bovine serum albumin. The stock solution was frozen at –80 °C before use. Based on previous researches, IL-6 (5–10 pg/ml) was administered daily to the 3D bone model to simulate an inflammatory environment similar to that observed in humans (Bakker et al. 2014; Singh et al. 2015).

2.2.11. Resazurin conversion assay to measure mitochondrial activity

Cell mitochondrial activity was assessed using a resazurin conversion assay. For the bone part of the model, bone scaffolds were placed to a new 48-well plate after PBS washing. Subsequently, 500 µL of resazurin working solution (Table 2.1.2) was immediately added to the scaffolds. The cell-free scaffold was used as background control. Following a 2-hour incubation, 3 × 100 µL aliquots of each scaffold sample were transferred to a 96-well plate for fluorescence assessment. The fluorescence intensity of resorufin was measured using the microplate reader, with excitation and emission (ex/em) wavelengths set at 544 nm and 590–10 nm, respectively (Haussling *et al.* 2019).

Regarding the liver spheroids, they were gently harvested from agarose microwells. After collection, HepaRG plain medium was utilized to wash the spheroids three times. After that, 200 µL of resazurin working solution (Table 2.1.2) was immediately added to each sample. Two aliquots of 100 µL each were moved to a 96-well plate. Additionally, 100 µL of the cell-free resazurin working solution was utilized to present background value (McMillian *et al.* 2002). Using the microplate reader, the fluorescence emitted by resorufin was measured at ex/em wavelengths of 544 nm/590–10 nm after incubation periods of 30 mins, 60 mins, 90 mins, and 120 minutes. The rate of resazurin conversion to resorufin was calculated to assess mitochondrial activity.

2.2.12. CYP activity assay using LC-HPLC/MS-based (Phase I enzymes).

As previously mentioned (Hoffmann *et al.* 2012; Ruoss *et al.* 2019), we tested CYP activities by quantifying CYP-isoform-specific metabolites of several medications using LC-HPLC/MS detection. The substrates selected, along with their respective incubation times, working concentrations, and the metabolites measured, are outlined in Table 2.2.1. For use as substrates for cocktail C1, stock solutions of 10 mM phenacetin, 10 mM testosterone, 10 mM bupropion hydrochloride, and 10 mM diclofenac were mixed with HepaRG plain medium in a 1:1000 dilution. For cocktail C2, stock solutions of 10 mM S-mephenytoin and 10 mM bufuralol hydrochloride were mixed with HepaRG plain medium in a 1:1000 dilution. HepaRG spheroids were then cultured with 100 µL solution for either C1 or C2, following the culture times specified in Table 2.2.1. After that, the supernatants were kept cold at –80 °C. The samples from three separate tests were pooled together, and metabolites was assessed by an LC-HPLC/MS-based technique by Pharmacelsus (Saarbrücken, Germany). Data were normalized using the DNA content of the liver spheroids.

Table 2.2.1. LC-HPLC/MS-based method to determine CYPs activity (Phase I enzymes). Conditions, Substrates, concentrations, and measured reactions (Chen *et al*. 2024)

Enzyme	Incubation time	(µM) Substrate → Metabolites
CYP1A2	1.5 h	(28 µM) Phenacetin → Phenacetin-deethylation
CYP3A4	1.5 h	(55 µM) Testosterone → Testosterone-6b-hydroxylation
CYP2B6	1.5 h	(111 µM) Bupropion → Bupropion-hydroxylation
CYP2C9	1.5 h	(10 µM) Diclofenac → Diclofenac-4'-hydroxylation
CYP2C19	3 h	(22 µM) S-Mephenytoin → Mephenytoin-4-hydroxylation
CYP2D6	3 h	(10 µM) Bufuralol Hydrochloride→Bufuralol-1-hydroxylation

2.2.13. Fluorescence-based method to detect CYP2C9 activity (Phase I enzyme).

Based on the previously published technique, CYP2C9 enzyme activity was assessed using the microplate reader (Donato *et al.* 2015). First, the liver spheroids were carefully harvested and washed using plain HepaRG medium. Next, a 200 µL freshly prepared DBF working solution (as described in Table 2.1.2) was added to each HepaRG spheroid sample. After mixing, a 100 µL DBF working solution with liver spheroids was moved in duplicate to the 96-well plate wells. To control the background, a 100 µL DBF working solution without liver spheroids was placed into a well. Every 30 mins of incubation, the fluorescence from fluorescein production was detected using a microplate reader, which ex/em wavelengths set to 485 nm and 520 nm. The activity of the CYP2C9 was determined based on the rate at which dibenzyl-fluorescein is converted into fluorescein. Data normalization was performed using DNA content from the liver spheroids.

2.2.14. Fluorescence-based method to measure UGT activity (Phase II enzyme).

Based on the previously described method, UGT activity was measured by Omega Plate Reader (Hammour *et al.* 2022). First, the HepaRG spheroids were carefully harvested and washed using plain HepaRG medium. Next, 200 µL of a freshly prepared 4-MU working solution (as described in Table 2.1.2) was utilized to each HepaRG spheroids sample. After mixing, the 100 µL samples consisting of spheroids in the solution were moved in duplicate to the wells of a 96-well plate; A 100 µL cell-free 4-MU working solution was

added to an empty well as a background control. Every 30 minutes, the activity of the UGT enzyme was detected by the consumption rate of 4-methylumbelliferone to fluorescein using a microplate reader, which ex/em wavelengths set to ex/em 355 nm/460 nm. Data normalization was performed using DNA levels from the liver spheroids.

2.2.15. AP activity was assessed using an absorbance-based assay

As a marker of osteogenic differentiation, AP activity was measured using a microplate reader (Aspera-Werz *et al.* 2018). Following three washes with PBS, the scaffolds were incubated at 37 °C with 500 µL AP reaction buffer (as described in Table 2.1.2) for 2 hours to facilitate the reaction process. The transformation of 4-nitrophenyl phosphate into 4-nitrophenol was photometrically quantified at a wavelength of 405 nm. The experimental results were corrected by subtracting the background control values, which were derived from a cell-free scaffold (Guo *et al.* 2022a). Subsequently, measurements normalization was performed using DNA content from the bone cells.

2.2.16. CA II activity was assessed using an absorbance-based assay

CA II is the osteoclast differentiation early marker, and it was measured to observe the osteoclast differentiation situation (Zhu *et al.* 2020). After three times washing with PBS, 100 µl or 500 µL CA II reaction buffer (Table 2.1.2) was immediately added to 2D cells or each scaffold for a 15 min incubation at 37 °C. The rate at which 4-nitrophenyl acetate was converted to 4-nitrophenol served as a measure of CA II activity. The amount of 4-nitrophenol produced was measured using a photometer at a wavelength of 405 nm. The experimental data were normalized by subtracting the background control values, which were obtained from a scaffold without cells. Data normalization was performed using DNA levels from the bone cells.

2.2.17. TRAP activity measurement using an absorbance-based method

TRAP, a late-stage indicator of osteoclast activity, was detected to evaluate the osteoclasts function (Zhu *et al.* 2020). 90 µL TRAP substrate working solution (as described in Table 2.1.2) and 30 µL supernatant were mixed and incubated for 6 hours at 37 °C to facilitate reaction. After that, 90 µL of NaOH (1 M) was transferred to each sample to halt any

further reaction. 4-nitrophenol, as the reaction product, was measured using a photometer at a wavelength of 405 nm. The experimental values were corrected by subtracting the background, which was derived from a cell-free scaffold. Data normalization was performed using DNA content from the bone cells.

2.2.18. Calcium deposition visualized by Alizarin red staining

To evaluate matrix mineralization, we firstly used 100% ethanol fixed cells overnight at −20 °C. The following day, tap water was utilized to wash the cells to remove ethanol residues. Subsequently, the samples were treated with 50 µL Alizarin Red staining solution (as described in Table 2.1.2). The staining process was carried out at room temperature for 30 minutes in the dark. Following incubation, solution was discarded and the cells were gently washed with faucet water to eliminate any unbound Alizarin Red staining solution. As previously described, for quantitative analysis, the Alizarin Red bound to the mineralized matrix was solubilized using a 10% w/v cetylpyridinium chloride solution. The absorbance of the dissolved Alizarin Red was then measured photometrically at a wavelength of 562 nm using a microplate reader (Zhu *et al.* 2020).

2.2.19. Protein content measurement by sulforhodamine B (SRB) staining

Based on the previous publication (Ehnert *et al.* 2018), we used SRB staining to quantify the total protein content in the 2D cell culture samples. Following a PBS wash, the samples were fixed directly with ethanol for a minimum of 60 minutes at −20 °C. Subsequently, the samples were treated with the working solution and incubated for half an hour in the absence of light. After binding, SRB was released by dissolving it in an unbuffered Tris solution. The absorbance at 565 nm was then measured using a microplate reader to evaluate the staining results.

2.2.20. The process of DNA isolation and quantification from the samples

According to the previous publication, DNA analysis was carried out to determine cell viability and for data normalization (Haussling *et al.* 2019). The liver spheroids were first gently harvested from the microwells and washed using PBS. They were then treated with 100 µL of 50 mM NaOH, preheated to 98 °C, for a duration of 5 minutes.

Following vortexing, the spheroids in NaOH solution were stored at –20 °C for freezing. On the next day, 110 µL of 0.1 M Tris buffer (pH 8.0) was loaded to the thawed sample. The solution was thoroughly mixed, collected, and then centrifuged for 10 minutes at 20,000 × g. Scaffolds were gently collected, and then they were treated with 250 µL of 50 mM NaOH, preheated to 98 °C, for 5 minutes. After that, the scaffolds were stored at –20 °C for freezing. On the next day, 275 µL of 0.1 M Tris buffer (pH 8.0) was added to the thawed sample. The solution was thoroughly mixed, collected, and then centrifuged for 10 minutes at 20,000 × g. To determine the DNA concentration, samples were analyzed using the BMG Labtech LVIS Plate in two stages. In the first stage, 2 µL DNA isolation solution (50 mM NaOH mixed with 0.1 M Tris (pH 8.0)) was measured as a blank. After that, a 2 µL DNA sample from each specimen was tested in duplicate. The DNA concentrations were determined at a wavelength of 260 nm using the Omega MARS analysis software.

2.2.21. The mineral composition of the bone scaffold was analyzed to determine its content

Quantitative CT scans were performed on a clinical CT scanner to measure the scaffold's mineral content. The scanning was carried out using the following parameters: a tube voltage of 80 kV, an effective tube current of 500 mA, a pitch value of 0.4, and a 16 × 0.3 mm acquisition with 0.4 mm slice thickness. The images were then reconstructed using a high-resolution V80u kernel and iterative image reconstruction technology at level 5 was applied for bone visualization. The axial field of view, in a rectangular shape, covered an area of approximately 10 cm by 10 cm, with an image resolution of 512 pixels by 512 pixels. The DICOM images obtained from the scan were imported into ImageJ software for processing. The image stack was then adjusted to focus on the area of interest. To quantify the scaffold, its mean integrated density was determined and subsequently normalized using the reference block as a baseline (Weng *et al.* 2020).

2.2.22. Stiffness of bone scaffold

The Young's modulus method was utilized to calculate the stiffness of scaffold (Weng *et*

al. 2020). The scaffolds were uniaxially compressed four times by 10% of their original height (speed = 5 mm/min) using a ZwickiLine Z 2.5TN material testing machine. An X-force HP 5N sensor was used to measure the load exerted in real-time. The load-deformation data were converted into a stress-strain curve using the uncompressed scaffold's height and area. Young's modulus for the linear elastic deformation region was computed using the formula provided below:

$$\text{Young's modulus [MPa]} = \frac{applied\ force\ [N]\ \times initial\ scaffold\ height\ [mm]}{area\ of\ the\ scaffold\ [mm^2]\ \times change\ in\ height\ [mm]}$$

2.2.23. Detection of secreted protein by dot blot analysis

To detect the protein that was released in the culture supernatant, a dot blot analysis was performed. Either 100 or 60 µL of the sample was carefully added to the pre-wet nitrocellulose membrane. A vacuum pump was employed in conjunction with a 96-well dot blot apparatus to facilitate efficient transfer during this process. Ponceau S staining was used to visualize and confirm the transfer of proteins onto the membrane. Following a 1-hour blocking step using 5% BSA in TBS-T, the membrane was incubated overnight at 4 °C with the primary antibodies. On the following day, the membrane was thoroughly washed with TBS-T and then exposed to the appropriate secondary antibody for 2 hours. The specific details of the antibodies used are provided in Table 2.2.2. Signal detection was carried out using chemiluminescence involving a reagent solution containing 100 mM Tris, 1.25 mM Luminol, 0.2 mM p-coumaric acid, and 0.03%H_2O_2, and the data were analyzed using ImageJ software for further processing and quantification (Guo *et al.* 2022a).

Table 2.2.2. The antibodies used for dot blot (Chen *et al*. 2024).

Antibodies	Order#	Company	Dilution
Osteocalcin (OCN)	sc-365797	Santa Cruz Biotechnology, Heidelberg, Germany	1:1000
Soluble receptor activator of nuclear factor kappa-B ligand (sRANKL)	500-m46	PeproTech, Hamburg, Germany	1:1000
Osteoprotegerin (OPG)	500-p149	PeproTech, Hamburg, Germany	1:1000
Interleukin-6 (IL-6)	500-m06	PeproTech, Hamburg, Germany	1:1000
Mouse anti-rabbit IgG-HRP	sc-2357	Santa Cruz Biotechnology, Heidelberg, Germany	1:10000
Anti-Mouse IgG HRP-linked Antibody	7076	Cell Signaling Technology, Massachusetts, USA	1:10000

2.2.24. ROS were detected using the 2',7'-dichlorofluorescein-diacetate (DCFH-DA) assay

Before measurement, plain medium was utilized to wash the HepaRG spheroids to remove any residual components. A 100 µL DCFH-DA (10 µM) solution was then added to the spheroids. Following half an hour of incubation at 37°C, PBS was utilized to wash the spheroids to eliminate excess working solution. The spheroids were exposed to diclofenac as per the experimental design, meanwhile, 0.03% hydrogen peroxide was utilized as a positive control in the experiment. The production of the 2'7'-dichlorofluorescein was constantly monitored every 2 minutes from 0 to 10 minutes using a microplate reader and the fluorescence was measured at ex/em wavelengths of 485 nm/520 nm (Aspera-Werz *et al.* 2018).

2.2.25. Reduced glutathione (GSH) and oxidized glutathione (GSSG) were detected using Ellman assay

Liver spheroids were treated with diclofenac (3–6 µM) for 1 hour. After exposure, the

spheroids were gently harvested and washed with cold PBS. To precipitate the proteins, cells were treated with 3% m-phosphoric acid. Re-neutralization of the samples was performed with EDTA (5 mM) in a potassium phosphate buffer (0.1 M). Following this, the samples were centrifuged for 10 minutes at 3000 × g, and the supernatant was transferred to a new tube for the determination of GSH and total GSH levels. Regarding GSH detection, 20 µL supernatant was combined with 120 µL 5,5′-dithiobis-(2-nitrobenzoic acid) (DTNB; 0.56 mM) dissolved in potassium phosphate buffer (0.1 M). For the measurement of total GSH, a 20 µL supernatant was cultured for 30s with 120 µL 1:1 mixture, which consisted of glutathione reductase (2.5 U/mL) and DTNB (1.68 mM) in potassium phosphate buffer. Subsequently, 60 µL of NADPH (0.8 mM) was added, and the absorbance was detected at a wavelength of 412 nm. The GSSG level was calculated by subtracting the GSH value from the total GSH value (Aspera-Werz *et al.* 2018).

2.2.26. Statistical analyses

Either box plots showing the median, interquartile range, minimum, and maximum were used to present the data. Every experiment was conducted a minimum of three rounds, with 2-4 technical replicates per round. Statistical analyses were performed with GraphPad Prism software (GraphPad Software 9.0, La Jolla, CA, USA). Comparisons between two groups were made using the Mann–Whitney test. The data from multiple experimental groups were statistically analyzed using the non-parametric Kruskal–Wallis test to evaluate overall differences. This was followed by Dunn's multiple comparison test to identify specific pairwise differences between groups. When comparing two independent variables across different groups, a two-way analysis of variance (ANOVA) was conducted, followed by Dunnett's multiple comparisons test for detailed statistical evaluation. The thesis’s statistical method was discussed and adapted according to the advice of Dr. Johann Jacoby, affiliated with the Institute of Clinical Epidemiology and Applied Biometry at the University of Tübingen.

Chapter 3

3. Results

3.1. The effects of osteogenic factors within bone differentiation medium on HepaRG cells

HepaRG cells were exposed to various supplements of bone medium (Calcium chloride, Cholecalciferol-VitD3, L-ascorbic acid 2-phosphate, β-glycerophosphate, and HEPES) to assess their effects on cell differentiation. The HepaRG cells' viability and function were assessed every 7 days (7, 14 and 21 days) of exposure. On day 21, mitochondrial activity decreased considerably in the mixture group ($p < 0.01$; Figure 3.1.1a). None of the osteogenic substances tested individually had a significant impact on the mitochondrial activity of HepaRG cells. When β-glycerophosphate or calcium chloride were added to HepaRG cell cultures, there was a tendency for metabolic activity to increase. The total protein levels of HepaRG cells verified that the group treated with ascorbic Acid and a mix of osteogenic components had less viability than the control group at all time points (Figure 3.1.1b). *The data from day 21 has already been published in the article* (Chen *et al.* 2024).

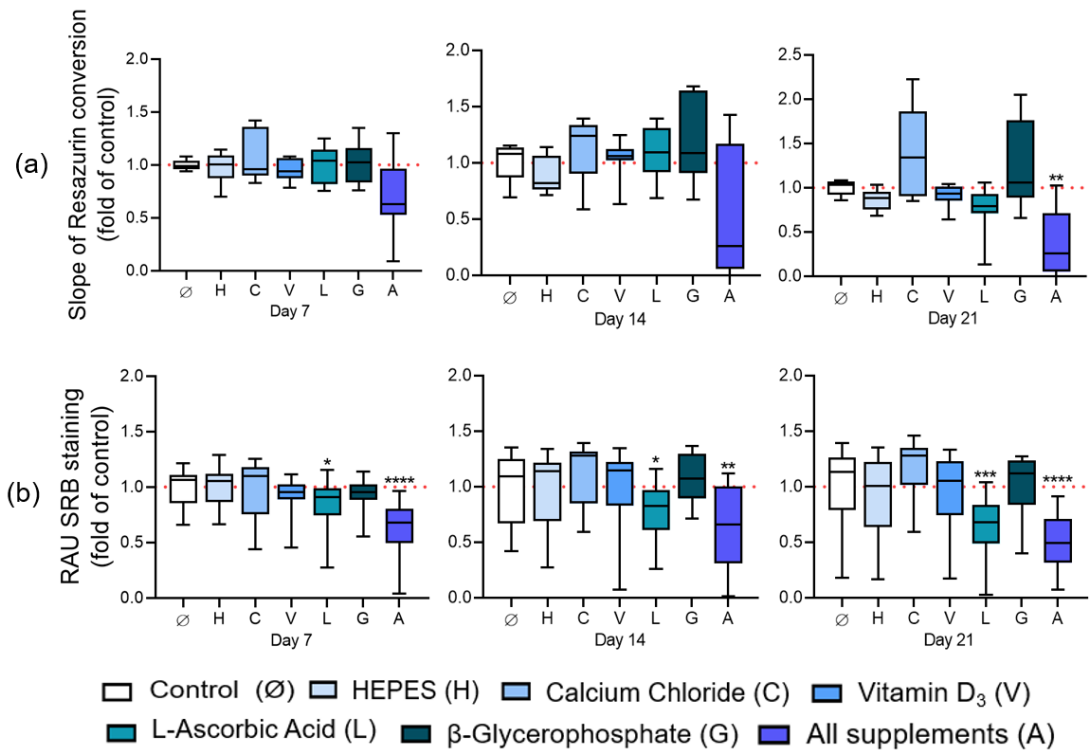

Figure 3.1.1 The impact of the bone differentiation medium supplements on HepaRG cell viability was investigated. HepaRG cells were cultured and exposed to HEPES (25 mM), calcium chloride (1.5 mM), cholecalciferol-VitD3 (20 ng/mL), L-ascorbic acid 2-phosphate (200 µM), and β-glycerophosphate (5 mM) alone or mixed for 21 days. To assess cell viability, (a) mitochondrial activity was measured by resazurin conversion on 7 days, 14 days, and 21 days, with results expressed as relative fluorescence units (RFU). (b) Total protein content was determined using SRB staining on 7 days, 14 days, and 21 days and expressed as relative absorbance units (RAU). To assess statistical differences, the Kruskal–Wallis test was applied, followed by Dunn's test for multiple comparisons. The data are presented using box plots, illustrating the median, minimum, maximum, and interquartile range (25^{th} to 75^{th} percentile). Significance levels are shown as * $p < 0.05$, ** $p < 0.01$, *** $p < 0.001$, and **** $p < 0.0001$ relative to the control group. $N = 3$, $n \geq 3$.

CYP2C9 transcripts in HepaRG cells has been shown to reach levels comparable to those found in human hepatocytes (Lubberstedt *et al.* 2011), and it is the main enzyme responsible for diclofenac metabolism. CYP2C9 activity was selected to assess whether osteogenic supplements affect the drug-metabolizing ability of HepaRG cells (Aninat *et al.* 2006). Although treatment with the supplement mixture led to a significant reduction in CYP2C9 activity on 14 days and 21 days, exposure to one of the bone differentiation medium supplements had no effect on CYP2C9 activity (Figure 3.2.1a). Similarly, in

HepaRG cells, UGT activity was reduced when mixed osteogenic supplements were present compared to the control group (Figure 3.2.1b). Furthermore, after being exposed for 21 days, UGT activity was markedly decreased in the 5 mM β-glycerophosphate and 200 µM L-ascorbic acid group ($p = 0.006$ and $p = 0.033$; Figure 3.2.1b).

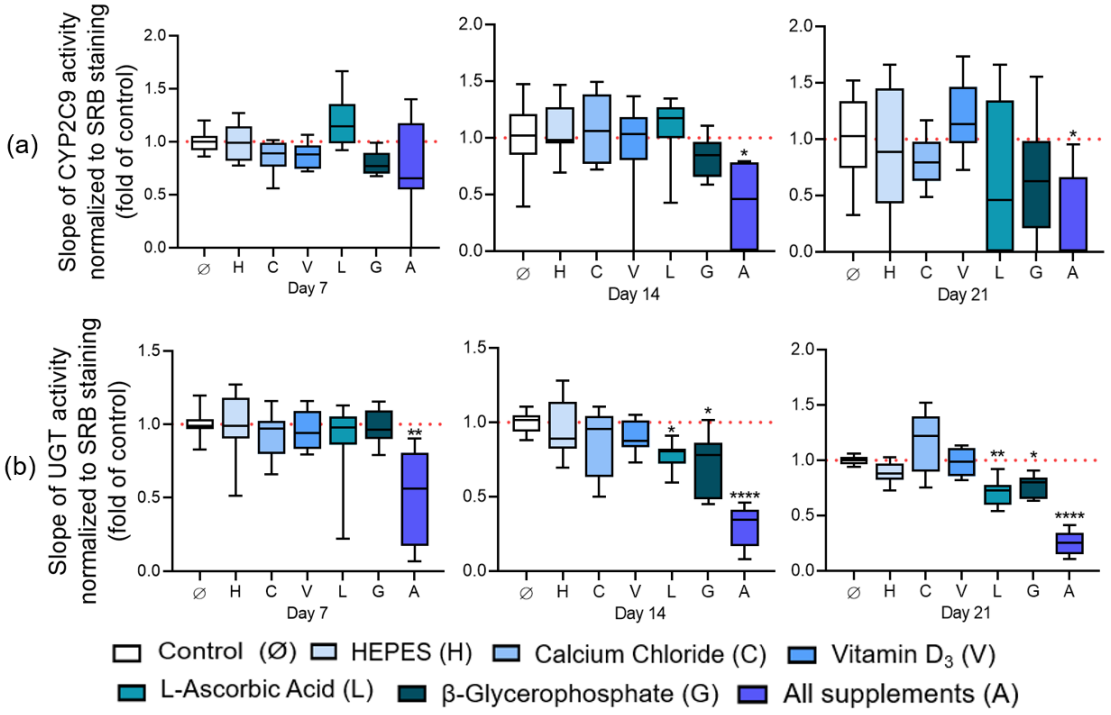

Figure 3.1.2 The impact of the bone differentiation medium supplements on the function of HepaRG cell was investigated. HepaRG cells were incubated with HEPES [25 mM], calcium chloride [1.5 mM], cholecalciferol-VitD3 [20 ng/ml], L-ascorbic acid 2-phosphate [200 µM], and β-glycerophosphate [5 mM], either individually or in combination, for 21 days. To assess HepaRG cell function, the enzymatic activities of liver-specific markers CYP2C9 (a) and UGT (b) were measured and relative to those of untreated cells on 7 days, 14 days, and 21 days. To assess statistical differences, the Kruskal–Wallis test was applied, followed by Dunn's test for multiple comparisons. The data are presented using box plots, illustrating the median, minimum, maximum, and interquartile range (25^{th} to 75^{th} percentile). Significance levels are shown as * $p < 0.05$, ** $p < 0.01$, and **** $p < 0.0001$ relative to the control group. $N = 3$, $n \geq 3$.

3.2. The impact of the HepaRG differentiation medium supplements on the function of osteoblast osteoclast co-culture system was investigated

The osteoblast-osteoclast co-culture system was treated with L-glutamine [2 mM], hydrocortisone [50 mM], insulin [5 µg/ml], and DMSO [1.7%] to assess the impact of various factors included in the HepaRG differentiation medium on bone cells.

Our findings demonstrated that, both 1.7% DMSO group and the mixture of supplements group markedly suppressed mitochondrial function in bone cells on 14 days and 21 days (Figure 3.2a), while also decreasing total protein levels at each time point (Figure 3.2b), in contrast to untreated controls. These results indicate that DMSO negatively affects the vitality of bone cells. *The data from day 21 has already been published in the article* (Chen *et al.* 2024).

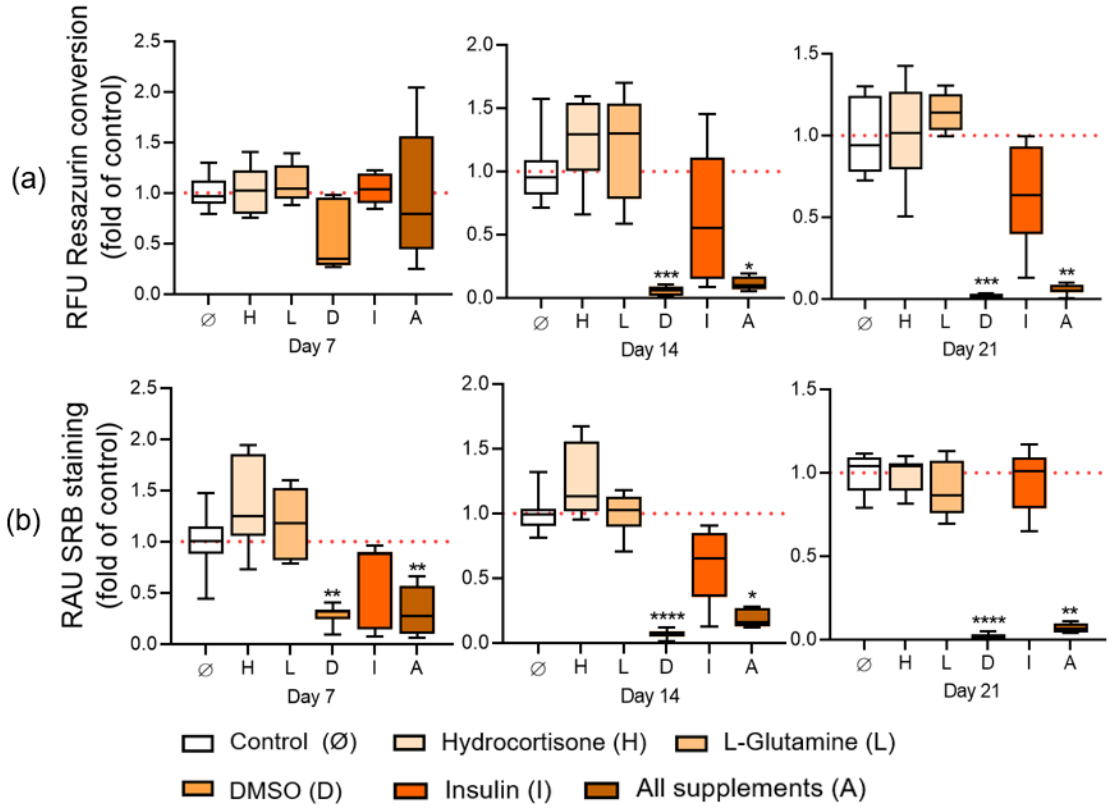

Figure 3.2.1 The impact of HepaRG cell differentiation medium supplements on the viability of the osteoblast-osteoclast co-culture system was investigated. The osteoblast-osteoclast co-culture system was exposed to hydrocortisone [50 µM], L-glutamine [2 mM], dimethyl sulfoxide [1.7%], and insulin [5 µg/ml], either individually or in combination, for 21 days. On 7 days, 14 days, and 21 days, (a) mitochondrial activity, assessed *via* resazurin conversion, was detected and expressed as RFU, and (b) the total protein of cells was detected using SRB staining and presented as RAU. To assess statistical differences, the Kruskal–Wallis test was applied, followed by Dunn's test for multiple comparisons. The data are presented using box plots, illustrating the median, minimum, maximum, and interquartile range (25^{th} to 75^{th} percentile). Significance levels are shown as * $p < 0.05$, ** $p < 0.01$, *** $p < 0.001$, and **** $p < 0.0001$ relative to the control group. N = 3, n = 3.

The function of bone cells was assessed, focusing on osteoblast-like and osteoclast-like

activities. AP activity, as an indicator of osteoblast activity, remained unaffected by supplementation. Notably, hydrocortisone clearly promoted AP activity in the osteoblast-osteoclast co-culture system on days 14 and 21 (Figure 3.2.2b). CA II activity, as an indicator of osteoclast activity, was elevated with the addition of DMSO and mixed group in the osteoblast-osteoclast co-culture system at different time points (Figure 3.2.2a). Moreover, calcium staining analysis showed an increase in the activity of osteoclasts in DMSO-treated bone co-cultures at each time point, as well as in the mixed supplement-treated group on 21 days (Figure 3.2.2c).

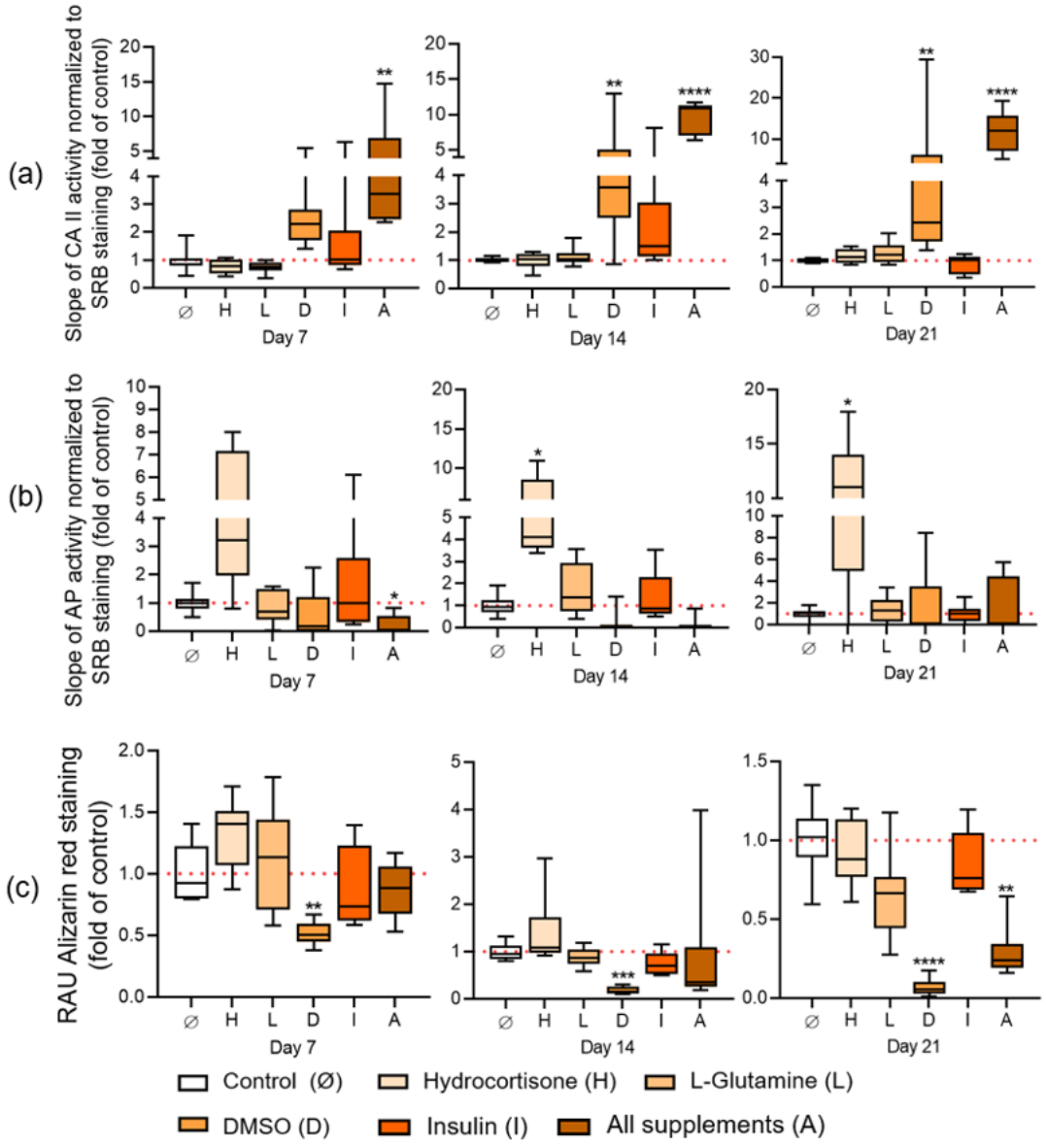

Figure 3.2.2 The impact of factors in the HepaRG differentiation medium on a osteoblast-osteoclast co-culture system' function was investigated. The osteoblast-osteoclast co-culture system was exposed to hydrocortisone [50 μM], L-glutamine [2 mM], dimethyl sulfoxide [1.7%], and insulin [5 μg/ml], separately or in combination, for 21 days. On 7 days, 14 days, and 21 days, (a) CA II activity, a marker for osteoclast function, (b) AP activity, an indicator of osteoblast function, (c) calcium staining analysis of bone cells were detected and expressed as relative absorbance units (RAU). To assess statistical differences, the Kruskal–Wallis test was applied, followed by Dunn's test for multiple comparisons. The data are presented using box plots, illustrating the median, minimum, maximum, and interquartile range (25^{th} to 75^{th} percentile). Significance levels are shown as * $p < 0.05$, ** $p < 0.01$, *** $p < 0.001$, and **** $p < 0.0001$ relative to the control group. N = 3, n = 3.

3.3. HepaRG spheroids exposed to different proportions of liver-bone medium combinations

To determine the ideal medium for maintaining liver and bone cell viability and function over 21 days, HepaRG spheroids were incubated with varying proportions of liver differentiation medium and bone co-culture medium mixture (L-B medium). The ratios tested were 100:0, 75:25, 50:50, and 25:75. Mitochondrial activity (Figure 3.3.1a), DNA content (Figure 3.3.1b), CYP2C9 enzyme activity (Figure 3.3.2a), and UGT enzyme activity (Figure 3.3.2b) were evaluated on 7 days, 14 days, and 21 days, with comparisons made to the 100% HepaRG differentiation medium. The findings demonstrated a notable increase in mitochondrial activity was observed in the 50:50 L-B medium group on day 7 vs. the control group ($p = 0.005$; Figure 3.3.1a). DNA content analysis revealed that HepaRG cell proliferation was significantly enhanced in the 75:25 and 50:50 L-B medium groups on 7 days and 14 days vs. the control group. By day 21, however, only the 75:25 L-B medium significantly elevated DNA content in HepaRG spheroids (Figure 3.3.1b). Notably, mitochondrial activity significantly increased in the 50:50 L-B medium group on day 7 compared to the control ($p = 0.005$; Figure 3.3.1a). In contrast, cultures with a 25:75 L-B medium ratio exhibited reduced mitochondrial activity after 21 days, relative to the control HepaRG spheroids (0.42 ± 0.704; Figure 3.3.1a). *The data has already been published in the article* (Chen *et al.* 2024).

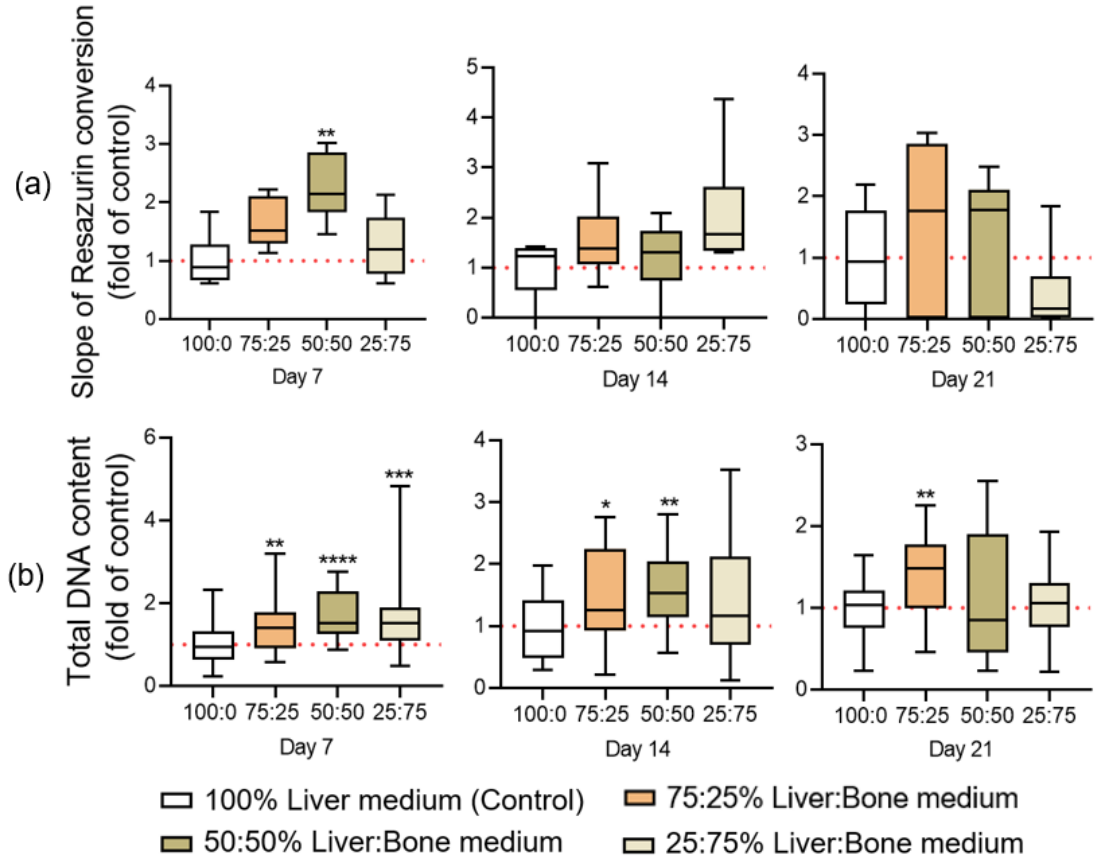

Figure 3.3.1 Assessment of HepaRG spheroids viability treated with L-B medium mixtures. Spheroids were exposed to 100:0, 75:25, 50:50, and 25:75 ratios of L-B medium for 21 days. The spheroid's viability was evaluated on 7 days, 14 days, and 21 days *via* (a) mitochondrial activity, and (b) total DNA levels. To assess statistical differences, the Kruskal–Wallis test was applied, followed by Dunn's test for multiple comparisons. The data are presented using box plots, illustrating the median, minimum, maximum, and interquartile range (25^{th} to 75^{th} percentile). Significance levels are shown as * $p < 0.05$, ** $p < 0.01$, *** $p < 0.001$, and **** $p < 0.0001$ relative to the control group. $N = 3$, $n \geq 2$.

Regarding cellular function, none of the medium mixtures adversely affected HepaRG spheroid performance regarding CYP2C9 and UGT activities (Figure 3.3.2a-b). These results indicate that all L-B medium mixtures, with the exception of the 25:75 ratio, are capable of maintaining HepaRG spheroid functionality.

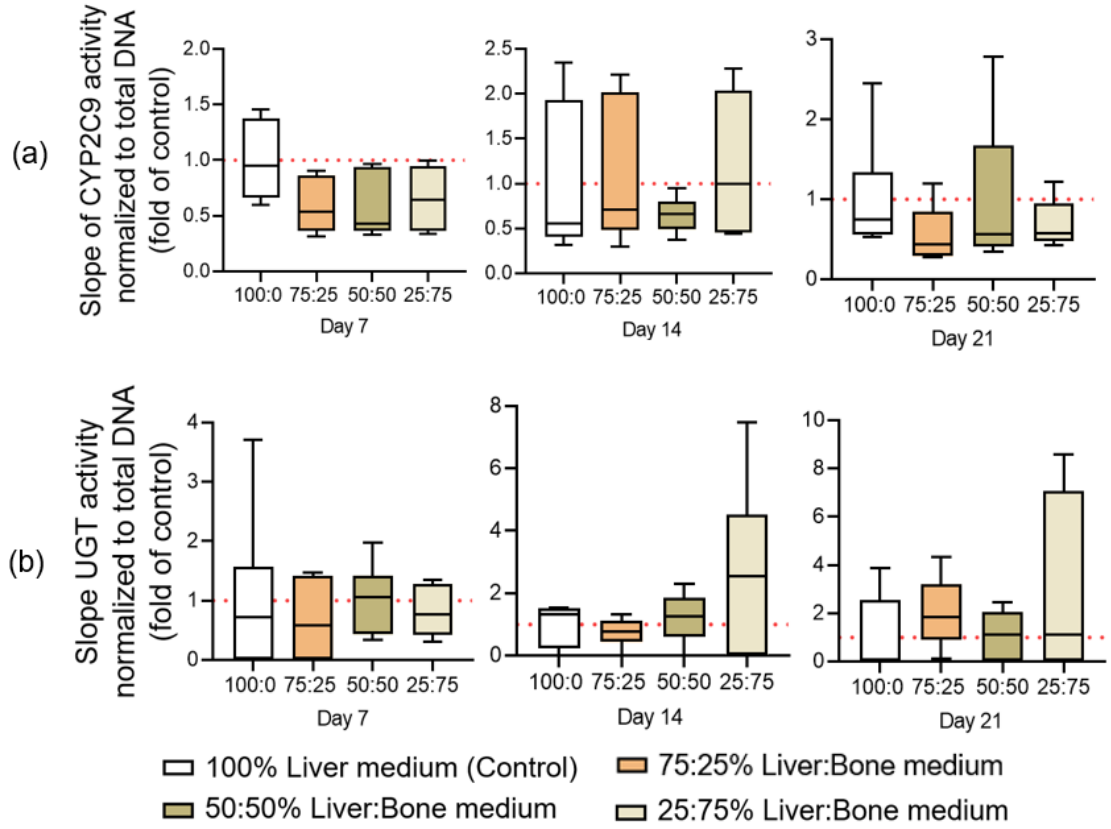

Figure 3.3.2 Assessment of HepaRG spheroids function treated with L-B medium mixtures. Enzymatic functions of phase I and phase II metabolism were evaluated on 7 days, 14 days, and 21 days. Specifically, (a) CYP2C9 activity was quantified and normalized to DNA content to assess phase I metabolism, while (b) UGT activity served as a representative indicator of phase II metabolic function. The data are presented using box plots, illustrating the median, minimum, maximum, and interquartile range (25^{th} to 75^{th} percentile). Statistical differences were determined using the Kruskal–Wallis and Dunn's multiple comparisons tests. N = 3, n = 2.

3.4. Osteoblast-osteoclast 3D co-culture model exposed to different proportions of bone-liver medium combinations

Osteoblast-osteoclast co-culture system was cultured with various proportions of bone co-culture and liver differentiation medium (B-L medium), specifically 100:0, 75:25, 50:50, and 25:75. To evaluate cellular viability, both mitochondrial activity (Figure 3.4.1a) and DNA content (Figure 3.4.1b) were assessed on 7 days, 14 days, and 21 days. The obtained results were compared to those from cultures maintained in 100% bone differentiation medium, which served as the control. Notably, a substantial decline in

mitochondrial activity was observed in the 25:75 and 50:50 B-L medium on 21 days, indicating a reduced bone cell viability trend in these conditions (Figure 3.4.1a). DNA content also significantly decreased in a dose-dependent manner with the B-L medium mixtures relative to the control at day 21 (Figure 3.4.1b). *The data has already been published in the article* (Chen *et al.* 2024).

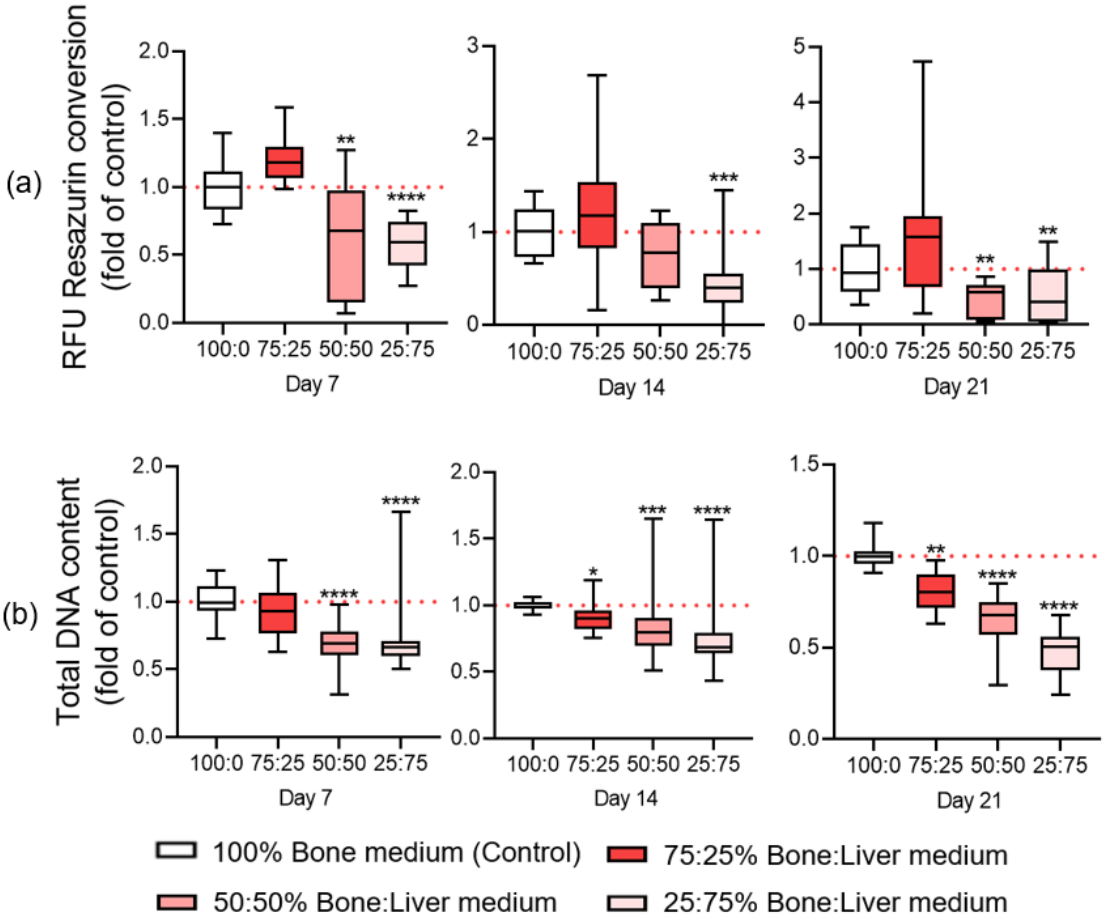

Figure 3.4.1 Assessment of bone cells viability treated with B-L medium mixtures. (a) Mitochondrial activity, assessed *via* resazurin conversion, was measured on 7 days, 14 days, and 21 days and expressed as RFU. Meanwhile, (b) DNA content was quantified on 7 days, 14 days, and 21 days. To assess statistical differences, the Kruskal–Wallis test was applied, followed by Dunn's test for multiple comparisons. The data are presented using box plots, illustrating the median, minimum, maximum, and interquartile range (25^{th} to 75^{th} percentile). Significance levels are shown as * $p < 0.05$, ** $p < 0.01$, *** $p < 0.001$, and **** $p < 0.0001$ relative to the control group. $N = 3$, $n \geq 3$.

To assess osteoclast functionality, TRAP activity—an indicator of late-stage differentiation—was measured at three time points: 7 days, 14 days, and 21 days (Figure

3.4.2a). Osteoblast functionality was assessed by detecting osteocalcin, a protein involved in bone mineralization, through dot blots on days 7, 14, and 21 (Figure 3.4.2b). TRAP activity in osteoclasts was significantly reduced in the 25:75 B-L group at day 21 ($p = 0.0038$; Figure 3.4.2a). Osteocalcin levels secreted by osteoblasts declined with 75:25, 50:50, and 25:75 B-L medium ratios at day 21. Nevertheless, no statistically significant variations were observed (Figure 3.4.2b). In summary, these findings indicate that, with the exception of the 25:75 B-L, all tested combinations preserved both the viability and function of bone cells.

Based on the overall findings from both liver spheroids and osteoblast-osteoclast co-cultures, the 50:50 medium group is optimal for co-culturing liver and bone cells to maximize the maintenance of their viability and function.

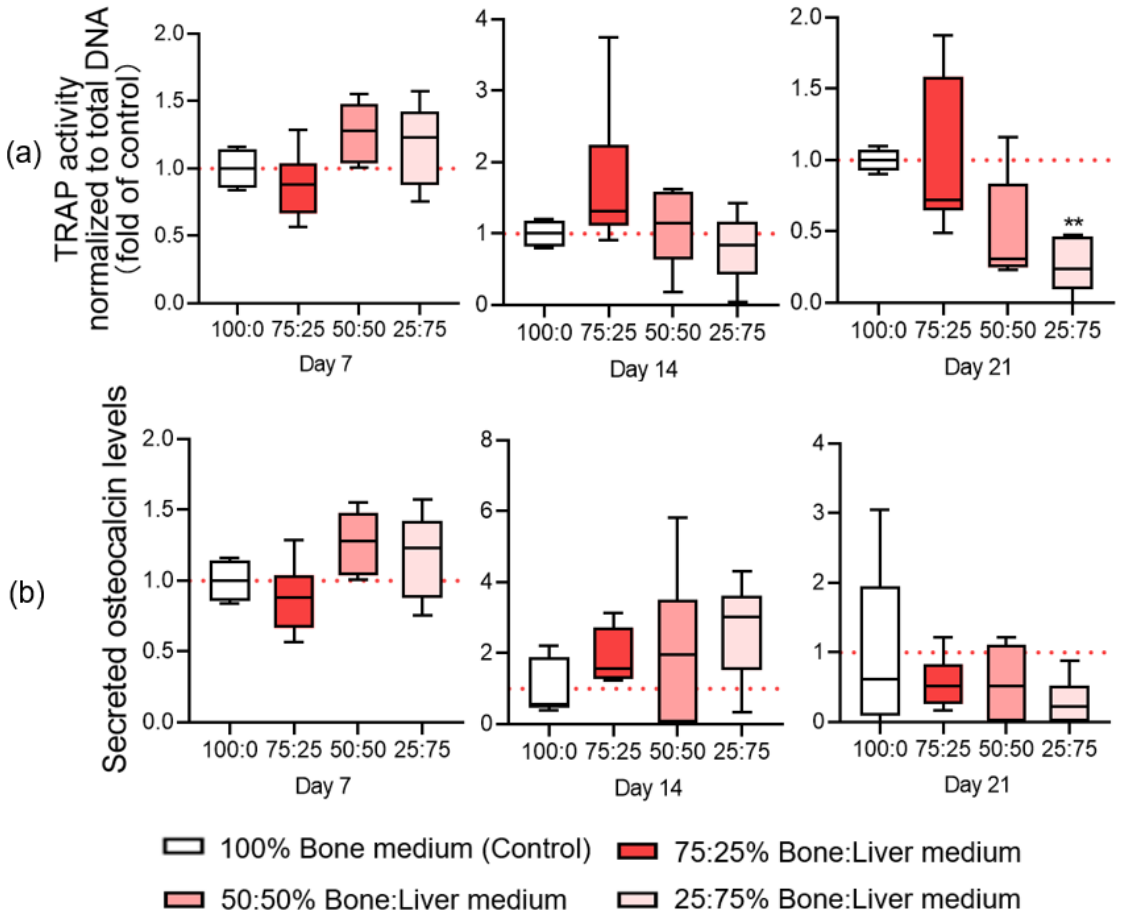

Figure 3.4.2 Assessment of bone cells function treated with B-L medium mixtures. (a) Osteoclast function was assessed by measuring TRAP activity, which was normalized to DNA content, at

three time points: 7 days, 14 days, and 21 days. (b) To evaluate osteoblast activity, the concentration of secreted osteocalcin was quantified at the same time intervals. To assess statistical differences, the Kruskal–Wallis test was applied, followed by Dunn's test for multiple comparisons. The data are presented using box plots, illustrating the median, minimum, maximum, and interquartile range (25^{th} to 75^{th} percentile). Significance levels are shown as ** $p < 0.01$ relative to the control group. N = 3, n = 2.

3.5. The L-B co-culture system effectively sustains HepaRG spheroids, preserving both cellular viability and metabolic activity for a period of up to 21 days

Following the optimization analysis of the L-B medium (refer to Sections 3.3 and 3.4), a 50:50 ratio of L-B medium was identified as optimal for maintaining both liver and bone *in vitro* models, maximally preserving their viability and functional integrity for a period of up to 21 days. This optimized medium composition was subsequently applied in further experimental studies. Next, the stability of the L-B model was investigated. On 7 days, 14 days, and 21 days, the viability of HepaRG spheroids in the L-B co-culture system was assessed through measurements of mitochondrial activity and DNA content. The results indicated no obvious variations in mitochondrial activity or DNA content across these time points (Figure 3.5a-b). Using LC-MS/MS method, we quantified the activities of cytochrome P450 enzymes, specifically CYP3A4, CYP1A2, CYP2C9, CYP2B6, CYP2D6, and CYP2C19. The data revealed a time-dependent increase in all CYP activities (Figure 3.5d-i). Over time, the activity of the phase II enzyme UGT exhibited a continuous increase (Figure 3.5c). These findings demonstrate that liver spheroids, when co-cultured with scaffolds in a 50:50 L-B medium, remain viable and sustain their drug metabolism potential for as long as 21 days. *The data has already been published in the article* (Chen *et al.* 2024).

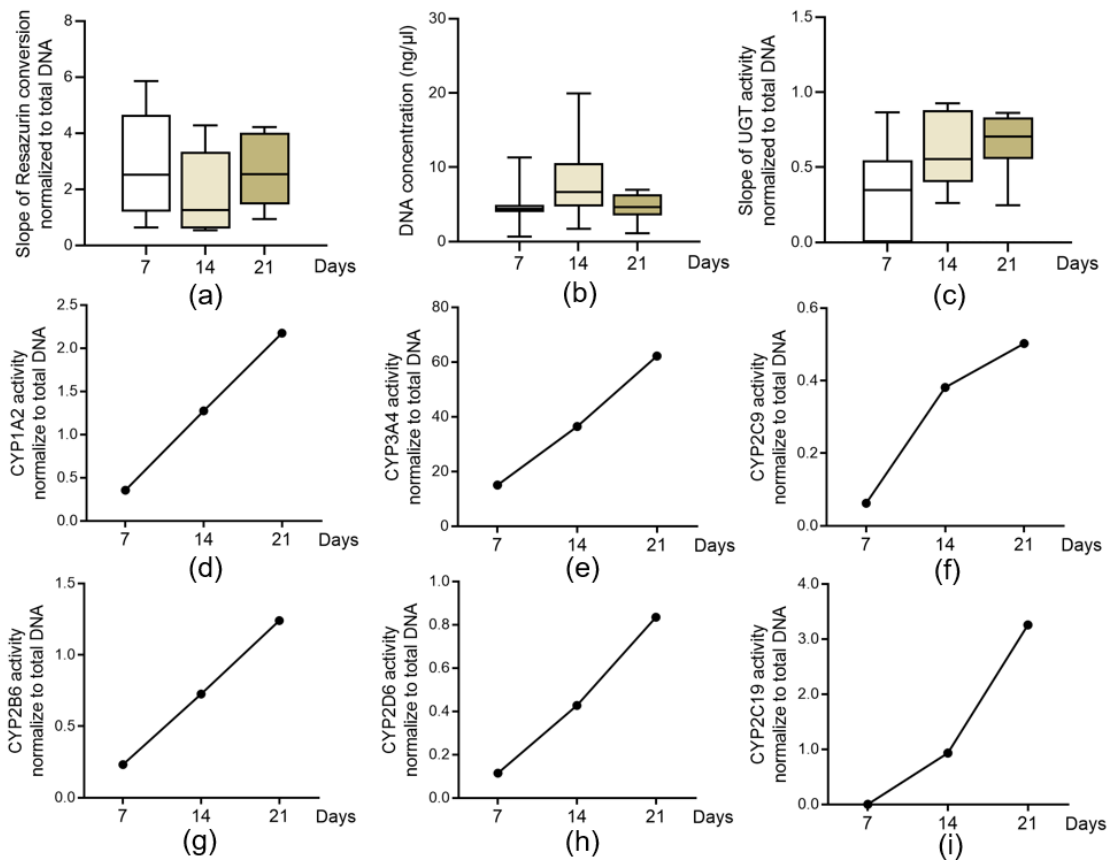

Figure 3.5 The assessment of HepaRG spheroids' viability and metabolic function in the L-B system was performed every 7 days (7 days, 14 days, and 21 days). The evaluation included: (a) mitochondrial function determined by resazurin reduction, (b) DNA content, and (c) UGT activity, an indicator of phase II metabolism, normalized to DNA content. To assess statistical differences, the Kruskal–Wallis test was applied, followed by Dunn's test for multiple comparisons. The data are presented using box plots, illustrating the median, minimum, maximum, and interquartile range (25^{th} to 75^{th} percentile). $N = 4$, $n \geq 2$. (d) CYP1A2, (e) CYP3A4, (f) CYP2C9, (g) CYP2B6, (h) CYP2D6, and (i) CYP2C19 were analyzed as indicators of phase I enzymatic activity. Data were obtained from three separate experiments using pooled samples, with values normalized to DNA content.

3.6. The osteoblast-osteoclast co-culture system maintains both cellular viability and functional activity for at least 21 days in the L-B system

The viability and DNA quantity of osteoblast and osteoclast cells were analyzed at three time points—7 days, 14 days, and 21 days—to determine their survival within the L-B co-culture environment. The data revealed that neither mitochondrial activity nor DNA quantity of osteoblast and osteoclast cells was adversely affected by the presence of spheroids, showing bone cells remained viable for at least 21 days in the L-B system

(Figure 3.6a-b). Bone-resorbing cell activity, as indicated by TRAP activity, showed an increase after 14 and 21 days compared to day 7, although these changes were not statistically significant across the three time points (Figure 3.6c). In addition, bone-forming cell function, measured by AP activity, exhibited a significant increase over time ($p = 0.044$, $p = 0.0002$; Figure 3.6d). These findings confirm that both bone-forming and bone-resorbing viability was maintained in the L-B system for at least 21 days and bone cells properly differentiated into functional osteoblast and osteoclast-like cells. *The data has already been published in the article* (Chen *et al.* 2024).

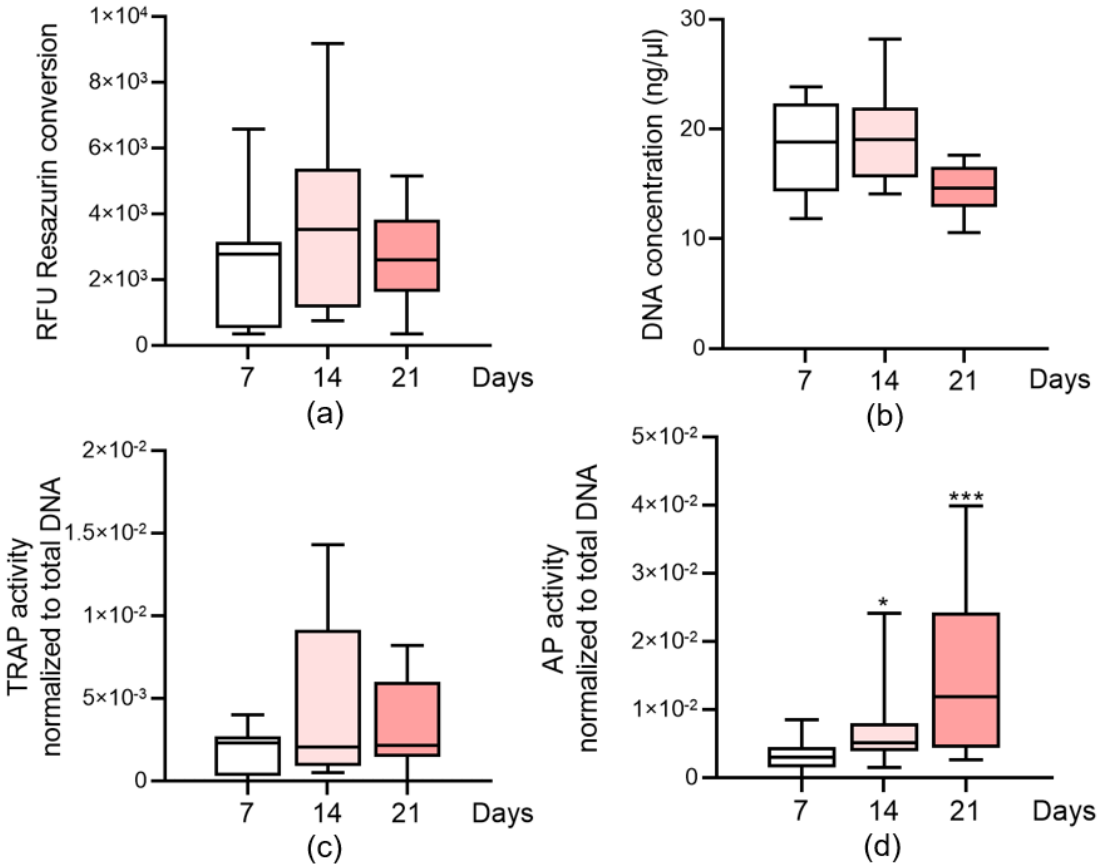

Figure 3.6 The assessment of bone cell viability and function in L-B model. At three time points, 7 days, 14 days, and 21 days, (a) Mitochondrial activity, measured *via* resazurin conversion, with results expressed as RFU, and (b) DNA content was detected. To assess osteoclast activity, TRAP activity was normalized to DNA content and measured on the same days. Similarly, osteoblast function was assessed by measuring AP activity, also normalized to DNA content, at the same time points. To assess statistical differences, the Kruskal–Wallis test was applied, followed by Dunn's test for multiple comparisons. The data are presented using box plots, illustrating the median, minimum, maximum, and interquartile range (25^{th} to 75^{th} percentile), with significance levels indicated as * $p < 0.05$ and *** $p < 0{,}001$ vs. the day 7 group. $N = 4$, $n \geq 2$.

3.7. Exposure to diclofenac three times weekly does not negatively affect the viability and function of liver spheroids or bone cells in the L-B system

According to the overall findings, we established a HepaRG spheroids co-culture with the osteoblast-osteoclast system that maintains both liver and bone cellular viability and function for at least 21 days. First, we explored the effects of low-frequency diclofenac exposure for 21 days. The L-B system was exposed to 3 µM diclofenac (a concentration reflective of human plasma levels following a single 50 mg oral dose) three times per week for 21 days. At day 21, the results showed diclofenac did not affect liver cell viability (Figure 3.7.1a-b). Meanwhile, the activities of the two key enzymes involved in diclofenac metabolism, CYP2C9 and UGT, were not affected by stimulation with 3 µM diclofenac three times a week for 21 days (Figure 3.7.1c-d).

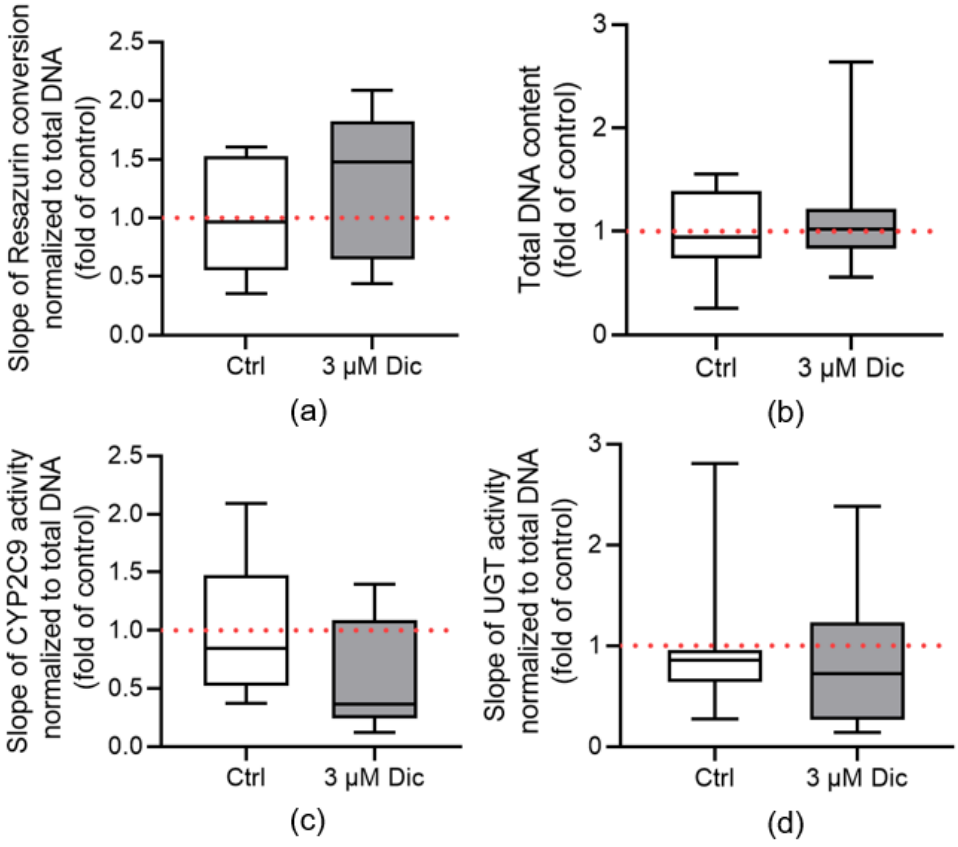

Figure 3.7.1 On day 21, the viability and function of HepaRG spheroids in the liver-bone system, which had been stimulated with diclofenac three times a week, were assessed. The impact of diclofenac on HepaRG spheroids was measured by assessing bone cell viability *via* (a) resazurin conversion (mitochondrial activity) and (b) DNA content. (c) CYP2C9 activity, normalization by DNA content, was assessed as an indicator of phase I enzyme function. Similarly, (d) UGT activity, also normalization by DNA content, was measured on the same day to assess phase II enzyme

function. Statistical differences were determined using the Mann-Whitney test. The data are presented using box plots, illustrating the median, minimum, maximum, and interquartile range (25^{th} to 75^{th} percentile). N = 4, n ≥ 2.

For the bone part, on day 21, mitochondrial activity in the diclofenac group showed a remarkable elevation when vs. the control (Figure 3.7.2a). DNA content analysis revealed that diclofenac enhanced bone cells viability compared to the control on day 21 (Figure 3.7.2b). For osteoblast function, AP activity did not show any changes between control and diclofenac group (Figure 3.7.2c). However, a decline trend of osteoclast function (TRAP activity) was detected in diclofenac group on day 21 (Figure 3.7.2d).

These results indicate that three times a week exposure to diclofenac does not affect liver cells and bone homeostasis viability in our liver-bone system. The function of osteoclasts was reduced in the diclofenac group; however, the difference did not reach statistical significance.

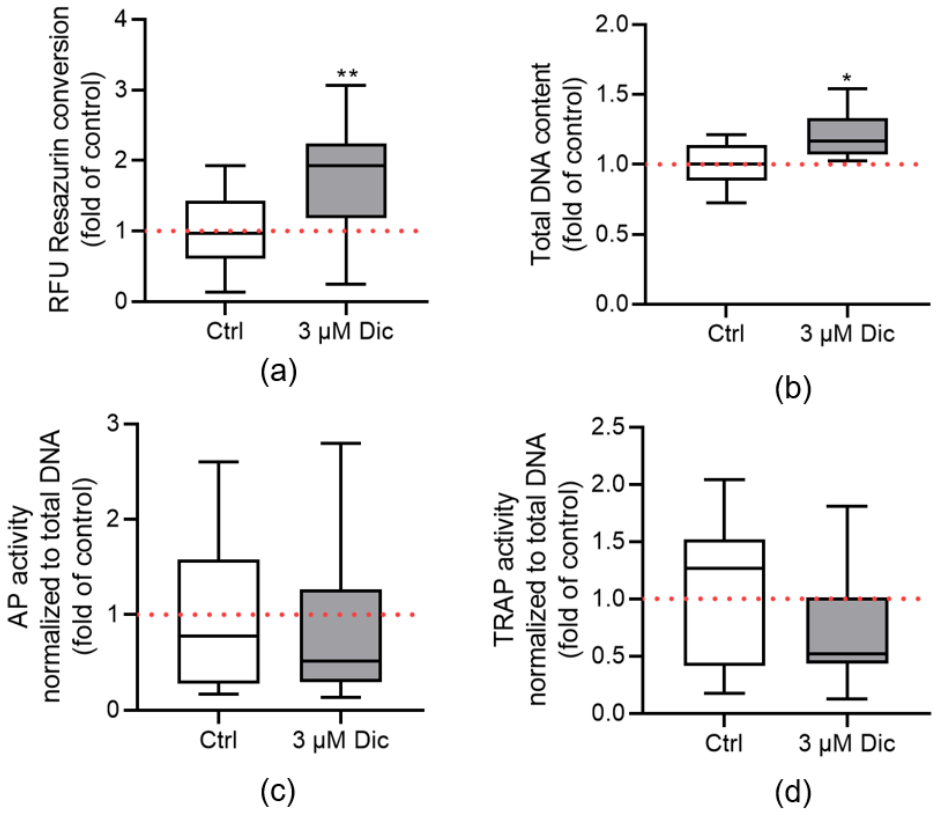

Figure 3.7.2 Liver-bone systems were treated with diclofenac at a concentration of 3 µM,

administered three times a week for 21 days. The impact of diclofenac on bone cells was evaluated by assessing bone cell viability *via* (a) resazurin conversion (mitochondrial activity) and (b) DNA content on day 21. Osteoblast function was evaluated *via* AP activity (c), while osteoclast function was assessed using TRAP activity (d) on day 21. Statistical differences were determined using the Mann-Whitney test. The data are presented using box plots, illustrating the median, minimum, maximum, and interquartile range (25^{th} to 75^{th} percentile). Significance levels are shown as * $p < 0.05$ and ** $p < 0.01$ relative to the control group. $N = 4$, $n \geq 2$.

3.8. Daily exposure to diclofenac does not negatively affect the HepaRG spheroids viability and function within the L-B co-culture system

Since three times weekly exposure to diclofenac did not significantly affect the viability and function of the system, we increased the frequency and concentration of diclofenac exposure to better represent daily diclofenac intake in orthopedic patients. The liver-bone system was exposed daily to either 3 µM or 6 µM diclofenac (human plasma concentration after a single oral dose of 50 mg diclofenac is 1.4–6.6 µM about (Yasar *et al.* 2001)) for 21 days. As a control, HepaRG spheroids were treated alone with diclofenac. Exposure to diclofenac did not show any toxicity to HepaRG spheroids, whether cultured alone or with bone scaffolds (Figure 3.8a-b). Furthermore, on day 21, the activity of CYP2C9 and UGT enzymes remained unchanged compared to unstimulated conditions in both HepaRG spheroids alone and in co-culture with bone scaffolds (Figure 3.8c-d). These results indicate that diclofenac metabolism in HepaRG spheroids is unaffected by daily diclofenac exposure in the co-culture system. *The data has already been published in the article* (Chen *et al.* 2024).

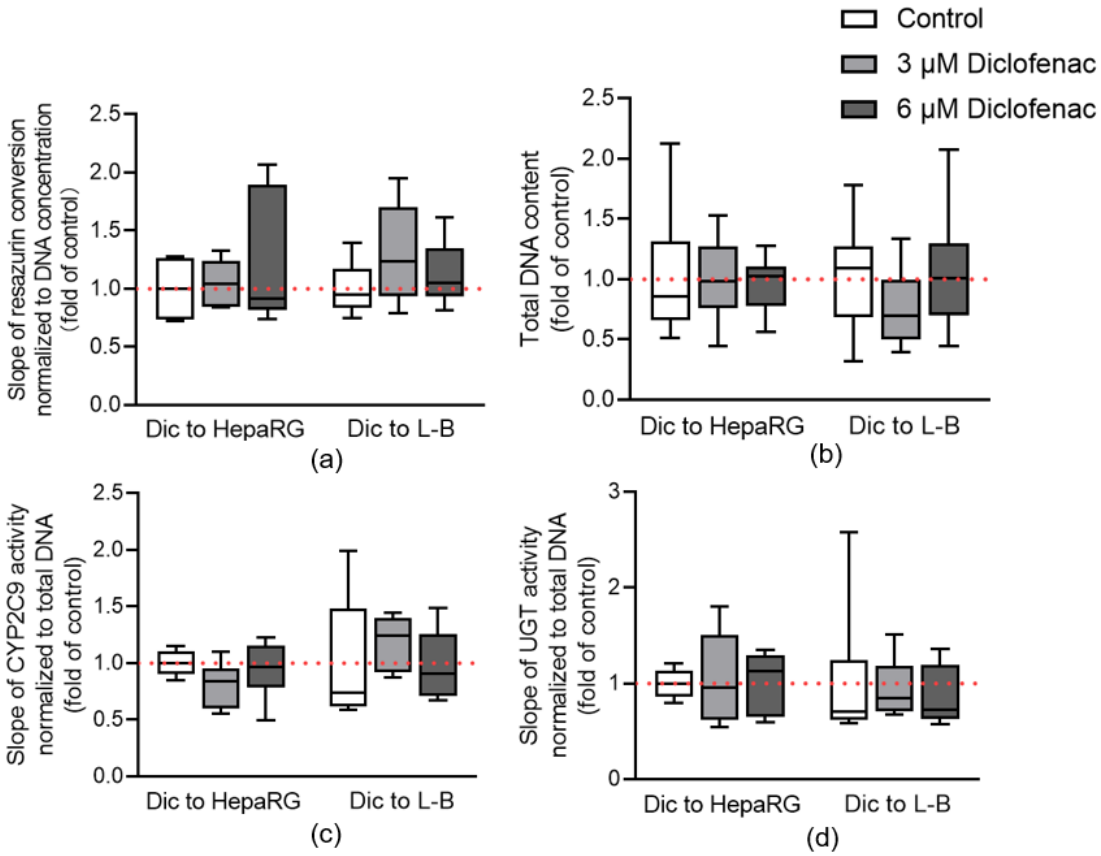

Figure 3.8 HepaRG spheroids or L-B system were stimulated with 3-6 µM diclofenac daily for 21 days. The impact of diclofenac on liver spheroids, both without or with bone cells, was evaluated by assessing hepatocyte viability through (a) mitochondrial activity and (b) DNA content on day 21. Hepatocyte function was assessed by measuring (c) CYP2C9 and (d) UGT at the same day. Statistical differences were assessed using a two-way ANOVA followed by Dunnett's multiple comparisons test. The data are presented using box plots, illustrating the median, minimum, maximum, and interquartile range (25^{th} to 75^{th} percentile). N = 3, n ≥ 2.

3.9. Chronic daily exposure to diclofenac upregulates the osteoclast function in the L-B system

The L-B system was administered 3-6 µM diclofenac daily for 21 days to investigate its effects on bone cells. As a control, bone scaffolds also were treated alone with diclofenac. The results demonstrated that daily diclofenac stimulation did not influence bone cell viability, either without or with HepaRG spheroids (Figure 3.9a-b). Beyond the viability, the effects of daily diclofenac treatment on the functional markers of osteoclasts (TRAP activity) and osteoblasts (AP activity) in bone cells within the L-B system were also determined. Our findings indicate that, diclofenac did not markedly affect AP activity in

both bone scaffolds alone or the bone scaffolds in L-B co-culture system (Figure 3.9c). Notably, after 21 days of diclofenac treatment, a marked increase in TRAP activity was detected in the L-B system (Figure 3.9d). However, Diclofenac did not elevate TRAP activity in bone scaffolds in the absence of the liver system (Figure 3.9d), indicating that its impact on osteoclast function requires interaction with a functional liver compartment. These findings indicate that diclofenac is metabolized by liver and then influences bone-resorbing cells activity. *The data has already been published in the article* (Chen *et al.* 2024).

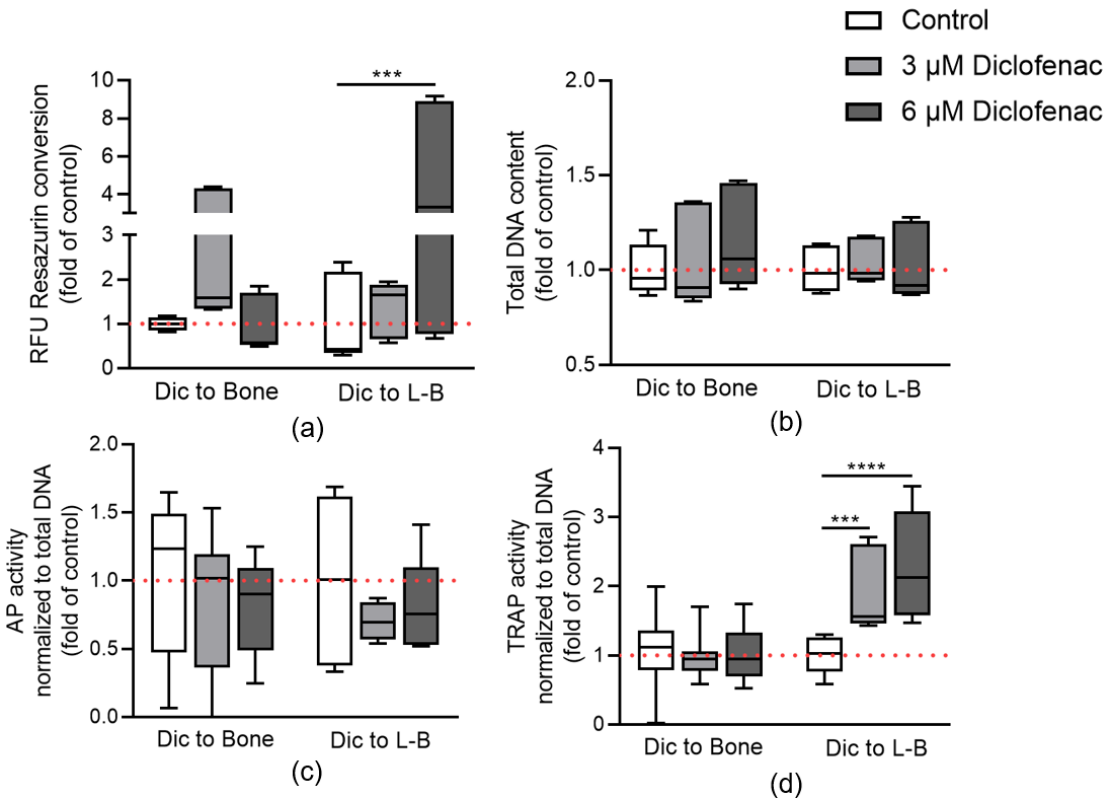

Figure 3.9 Daily administration of diclofenac at 3 μM and 6 μM concentrations was applied to bone scaffolds and the L-B system for 21 days. On day 21, bone cell viability was assessed in scaffolds co-culture with or without liver spheroids using (a) mitochondrial activity and (b) DNA content. Osteoblasts function was evaluated *via* AP activity (c), while osteoclasts function was assessed using TRAP activity (d) on day 21. Statistical differences were evaluate using a two-way ANOVA followed by Dunnett's multiple comparisons test. The data are presented using box plots, illustrating the median, minimum, maximum, and interquartile range (25^{th} to 75^{th} percentile). Significance levels are shown as *** $p < 0.001$ and **** $p < 0.0001$ relative to the control group. $N = 3$, $n \geq 3$.

3.10. Daily treatment with diclofenac leads to a decrease in scaffold mineral density and stiffness, as well as an imbalance in the RANKL: OPG ratio within the L-B system

On day 28, we measured bone scaffolds' stiffness and mineral content in the L-B system, which were subjected to daily treatment with 3 μM or 6 μM diclofenac. The findings revealed that daily exposure to diclofenac led to a significant reduction in bone scaffolds' mineral content and stiffness in the L-B system, in addition to increasing osteoclast activity (Figure 3.10a-c). Moreover, the diclofenac-treated group showed a significant upregulation in the secretion of RANKL protein on day 7, detected by dot blot (Figure 3.10d). While OPG protein levels also went up, this rise was not as marked as that of RANKL (Figure 3.10e). As a result, the RANKL: OPG ratio was elevated in the diclofenac group relative to the control (Figure 3. 10f). The data has already been published in the article (Chen *et al.* 2024).

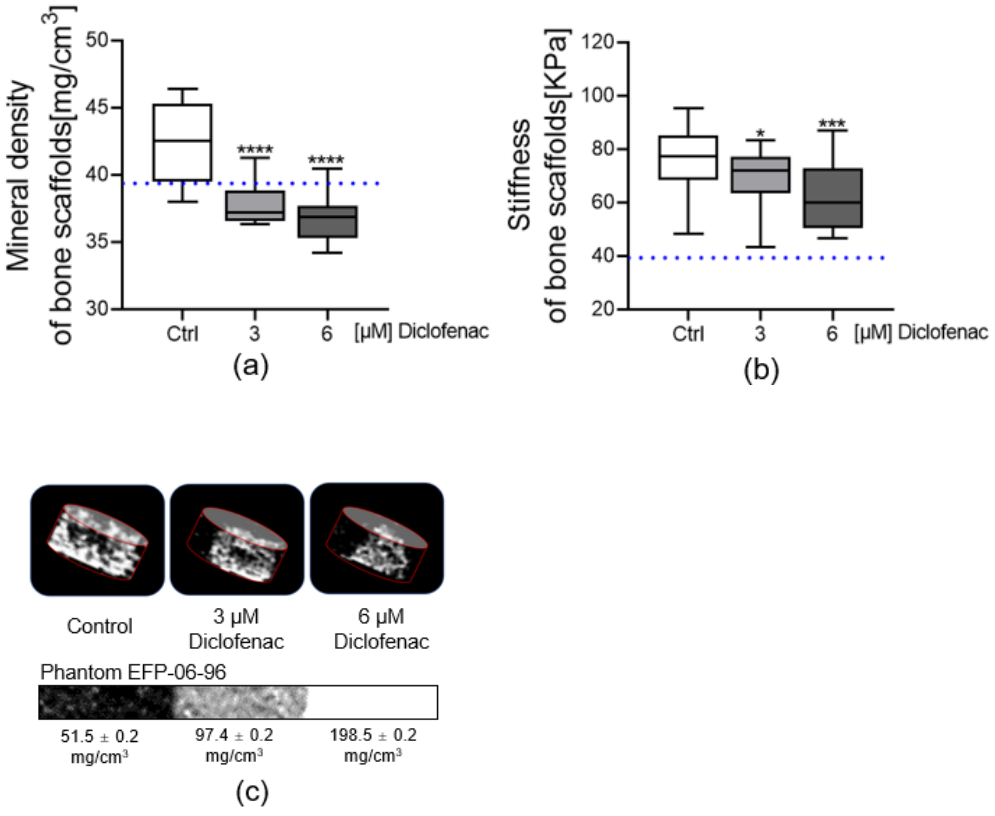

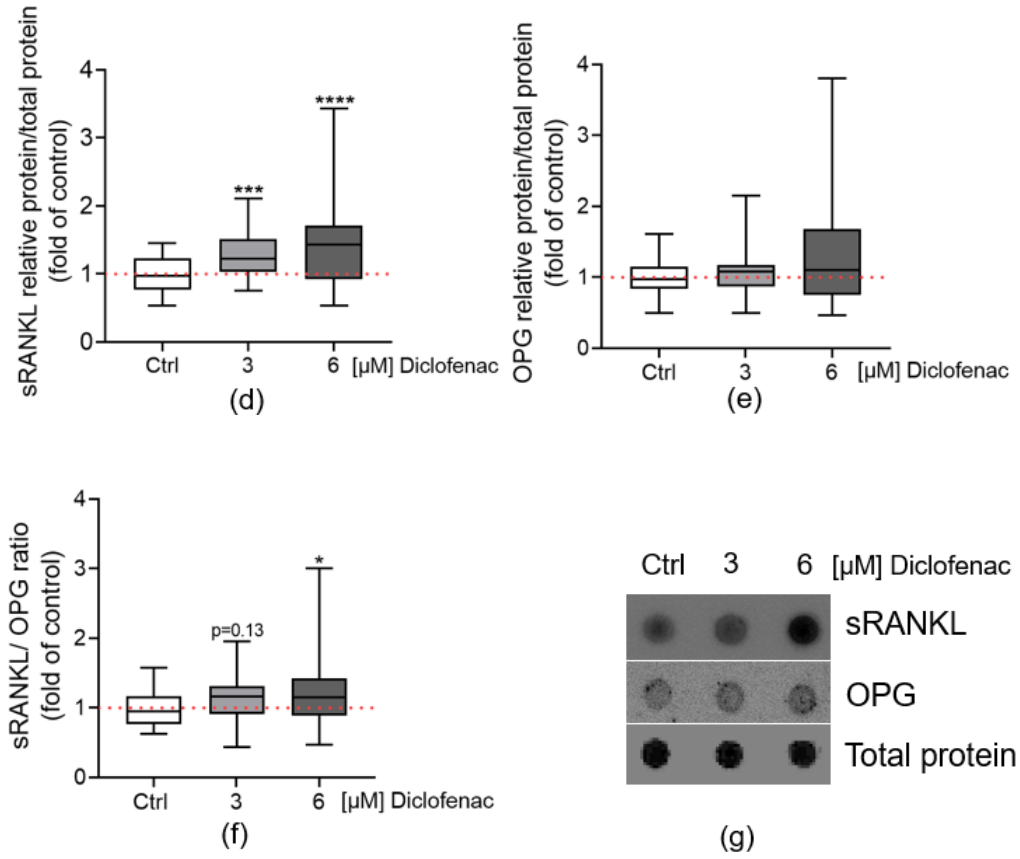

Figure 3.10 On day 28, (a) CT analysis was performed to assess the scaffold's mineral content within the L-B system, and (b) scaffold's stiffness was evaluated using a ZwickiLine machine. The blue line indicated the mineral content and stiffness of cell-free scaffold. (c) Representative 3D scaffold reconstructions generated obtained from CT scans. Statistical differences were assessed using the Kruskal-Wallis test and Dunn's multiple comparison test. On day 7, (d) detection of sRANKL protein in the supernatant after continuous exposure to 3–6 µM diclofenac. (e) Detection of OPG protein in the supernatant after continuous exposure to 3–6 µM diclofenac. (f) The sRANKL to OPG ratio was analyzed in the L-B system. (g) The image presents representative results of secreted protein levels (sRANKL, OPG, and total protein) in the supernatant, detected using dot blot analysis. The data are presented using box plots, illustrating the median, minimum, maximum, and interquartile range (25^{th} to 75^{th} percentile). Significance levels are shown as * $p < 0.05$, *** $p < 0.001$, and **** $p < 0.0001$ relative to the control group. $N \geq 3$, $n \geq 3$.

3.11. 4-OH diclofenac does not contribute to the enhanced osteoclast activity observed in the L-B system

4-OH diclofenac, the primary metabolite of diclofenac generated by the liver (Tateishi *et al.* 2020), was investigated for its potential role in the elevated osteoclastic function observed in the diclofenac-treated L-B system. To test this, scaffolds were exposed to 4-OH diclofenac every day. Previous studies have established that 4-OH diclofenac circulates in human plasma at about 13%–30% of diclofenac level (Degen *et al.* 1988; Yasar *et al.* 2001). To model these physiological levels, we chose 75, 300, and 600 nM of 4-OH diclofenac into the bone system. After 21 days of stimulation, no detectable toxicity to bone cells was observed (Figure 3.11a-b). Moreover, exposure to 4-OH diclofenac for 21 days did not enhance osteoclast activity (Figure 3.11c). Additionally, scaffold mineral density remained unchanged (Figure 3.11d). These findings indicate that 4-OH diclofenac has no impact on bone cell homeostasis. *The data has already been published in the article* (Chen *et al.* 2024).

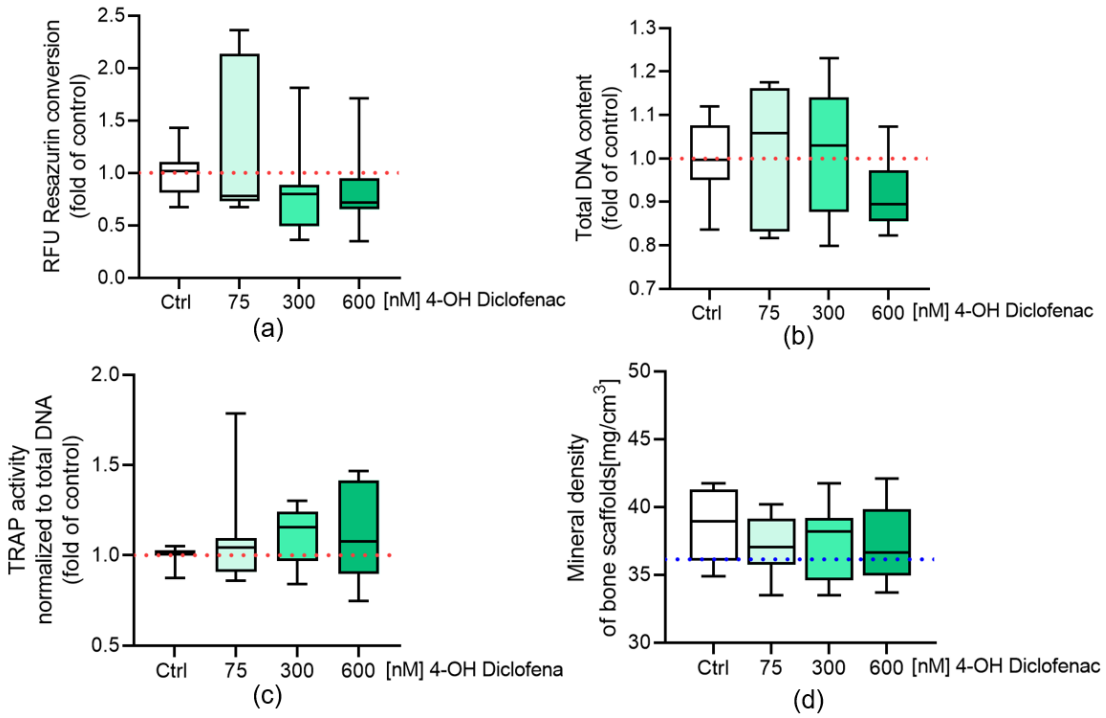

Figure 3.11 The osteoblast-osteoclast co-culture system was exposed to varying concentrations (75, 300, and 600 nM) of 4-OH diclofenac. On day 21, cell viability was determined through (a) mitochondrial activity and (b) DNA content analysis. Additionally, (c) osteoclast activity was evaluated by measuring TRAP levels, normalized to DNA content. (d) Scaffold mineralization was quantified *via* CT on 28 days, with the blue line indicates the mineral content of cell-free scaffolds. Statistical differences were assessed using a two-way ANOVA followed by Dunnett's

multiple comparisons test. The data are presented using box plots, illustrating the median, minimum, maximum, and interquartile range (25^{th} to 75^{th} percentile). N = 3, n ≥ 2.

3. 12. Diclofenac exposure increased ROS and IL-6 levels, and decreased the GSH: GSSG ratio in the liver system

In our system, diclofenac and 4-OH diclofenac did not have a direct impact on bone cells. Thus, we propose that prolonged diclofenac exposure elevates osteoclastic activity by inducing inflammation and oxidative stress, leading to cytokine dysregulation. A single exposure to 3–6 μM diclofenac led to increased ROS levels in the liver system by day 7 (3 μM group: p = 0.67; 6 μM group: p = 0.32; Figure 3.12a). Additionally, the ratio of GSH to GSSG exhibited a decreasing trend after single exposure (3 μM group p = 0.026, 6 μM group p = 0.08; Figure 3.12b). Moreover, continuous diclofenac administration markedly increased IL-6 protein levels, an inflammatory mediator secreted by hepatocytes (Guo *et al.* 2022b), in the supernatant of the L-B system on 7days. (Figure 3.12c). The reduced GSH: GSSG, combined with increased ROS and IL-6, plays a significant role in oxidative stress and inflammatory responses, which are essential in controlling bone metabolism. *The data has already been published in the article* (Chen *et al.* 2024).

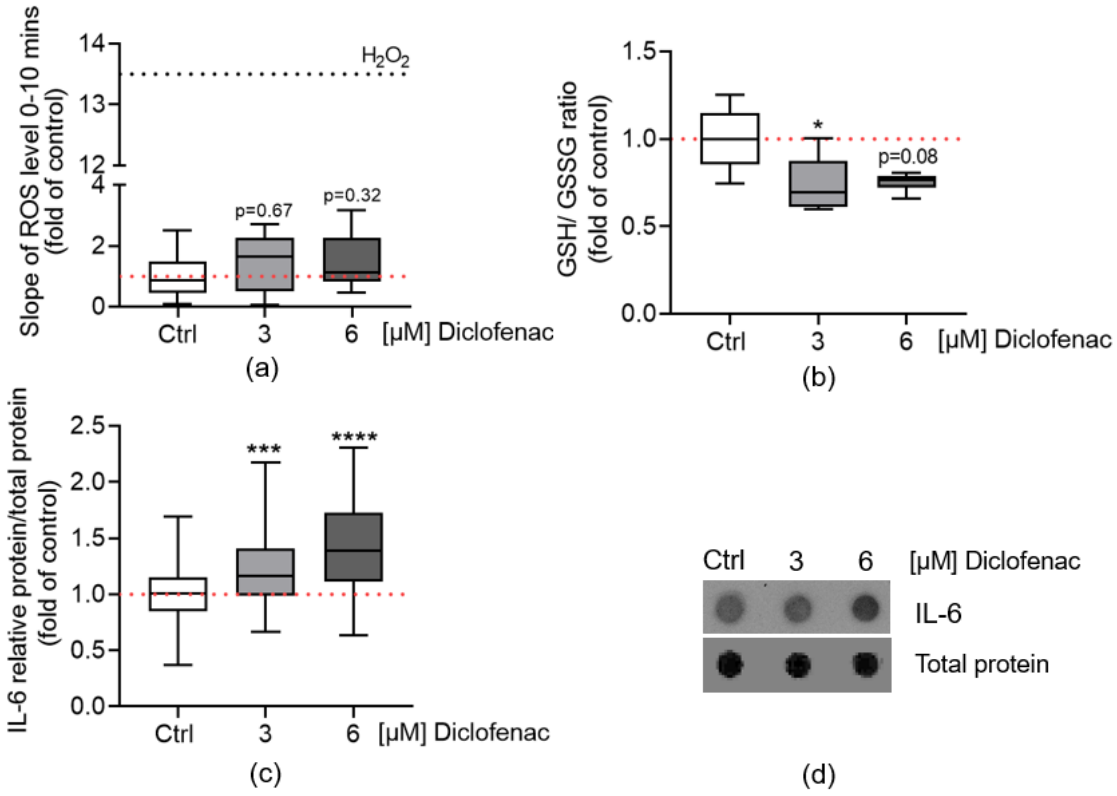

Figure 3.12 ROS levels in HepaRG spheroids were measured using the DCFH-DA assay, while the GSH:GSSG ratio was determined *via* the Ellman assay. The presence of IL-6 in the supernatant of the L-B system was analyzed using dot blot to assess its secretion levels. Following a single diclofenac treatment, the following assessments were conducted on day 7: (a) ROS levels in HepaRG spheroids, with H_2O_2 stimulation serving as a positive control, and (b) the GSH:GSSG ratio in HepaRG spheroids. (c) Under daily exposure to 3–6 µM diclofenac, the secretion of IL-6 protein was analyzed. (d) The image shows the representative of secreted IL-6 protein by dot blot. Statistical differences were assessed using a two-way ANOVA followed by Dunnett's multiple comparisons test. The data are presented using box plots, illustrating the median, minimum, maximum, and interquartile range (25^{th} to 75^{th} percentile), and the significances are shown as * $p < 0.05$, *** $p < 0.001$, and **** $p < 0.0001$ relative to the control group. $N \geq 3$, $n \geq 3$.

3. 13. IL-6 exposure upregulates the osteoclast cells' function in the osteoblast-osteoclast co-culture system

Analysis of the L-B system revealed significantly increased secreted IL-6 levels in the diclofenac-treated group. To assess its potential impact on bone homeostasis, IL-6 was added daily into the bone co-culture system. After 21 days exposure, no significant alterations were observed in mitochondrial activity or DNA content, indicating stable bone cell viability (Figure 3.13a-b). Notable, a significant enhancement in osteoclast activity was observed following 21 days of IL-6 exposure (Figure 3.13c). In addition, *via* dot blot, the secretion of sRANKL (osteoclast activator) protein was significantly upregulated with the daily stimulation of the IL-6 on day 7 (Figure 3.13d). On the contrary, OPG protein levels remained unchanged in the IL-6 group (Figure 3. 13e). Consequently, relative to the control, the RANKL to OPG ratio was marked elevated with the IL-6 stimulation (Figure 3.13f). These findings suggest that chronic IL-6 exposure facilitates bone-resorbing cell activity. *The data has already been published in the article* (Chen *et al.* 2024).

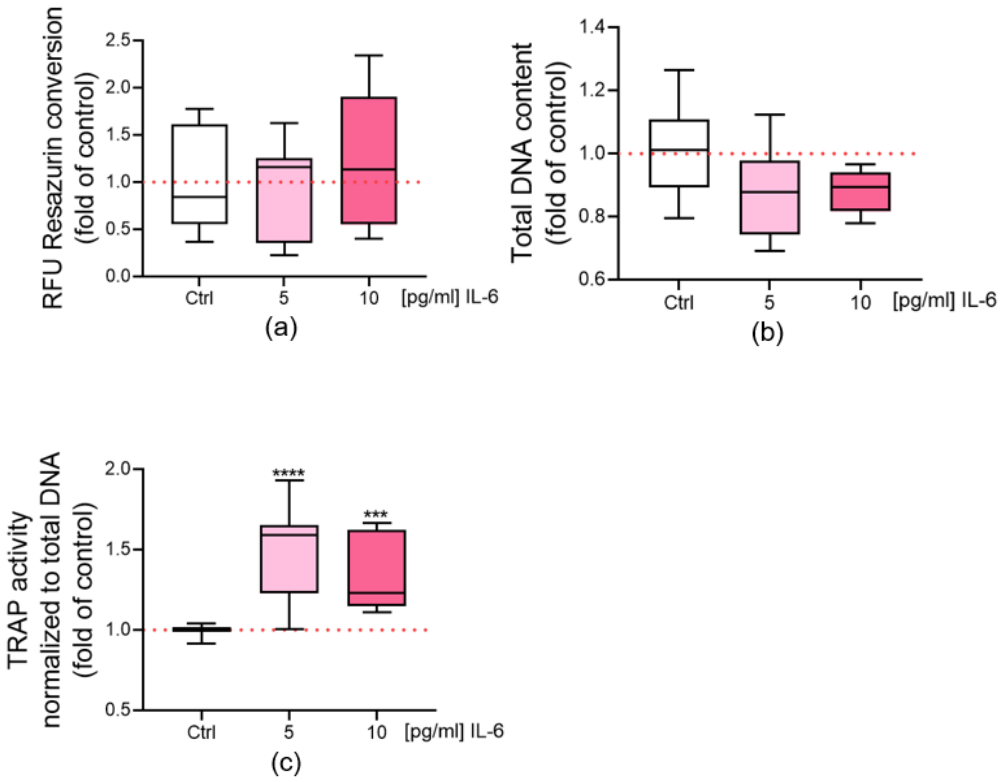

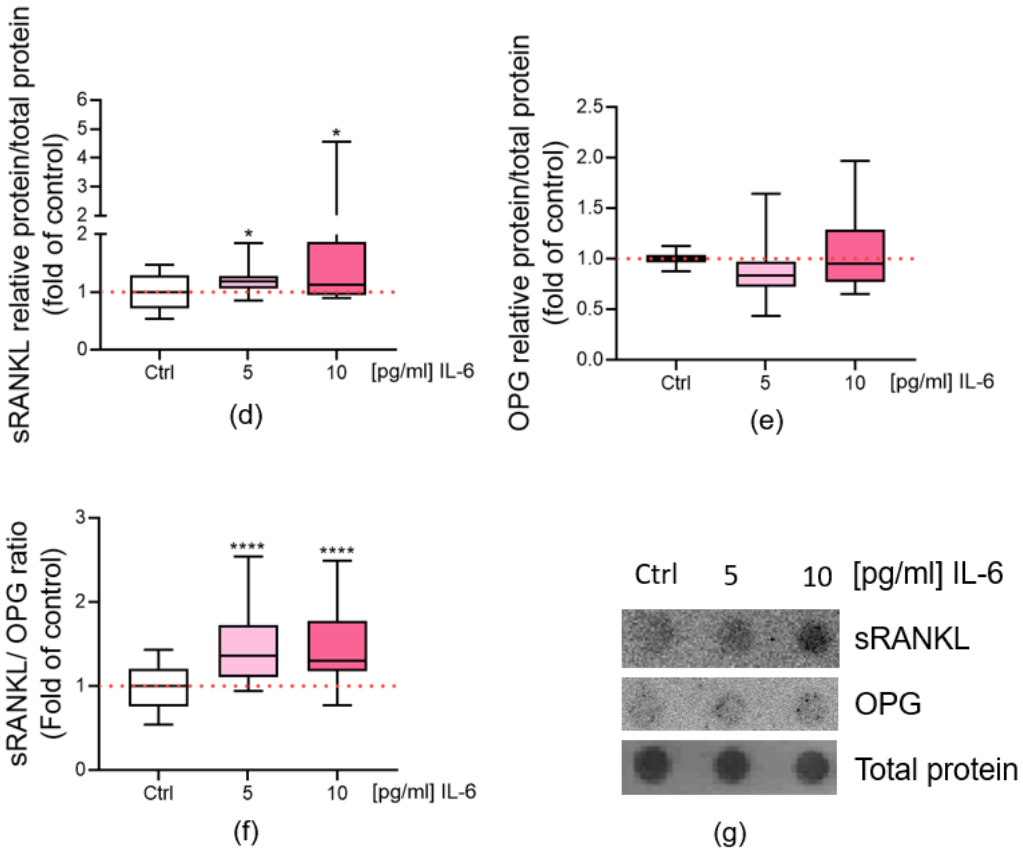

Figure 3.13 IL-6 at concentrations of 5-10 pg/ml was administered to the 3D osteoblast-osteoclast co-culture system for 21 days. Cells viability was determined by assessing (a) mitochondrial activity and (b) DNA content. (c) To assess osteoclast function, TRAP activity was quantified and normalized to DNA content. On 7 days, (d) secreted sRANKL and (e) OPG protein levels was quantified using dot blot. (f) The sRANKL: OPG ratio in the L-B system. (g) The image presents representative results of secreted protein levels (sRANKL, OPG, and total protein) in the supernatant, detected using dot blot analysis. The data are presented using box plots, illustrating the median, minimum, maximum, and interquartile range (25^{th} to 75^{th} percentile), and the significances are shown as * $p < 0.05$, *** $p < 0.001$, and **** $p < 0.0001$ relative to the control group. $N = 3$, $n \geq 2$.

Chapter 4

4. Discussion

The liver plays a central role in the metabolism of most drugs. When liver toxicity from drugs occurs, it can disturb the regulation of bone health, contributing to osteoporosis and a greater risk of bone fractures. Research has shown that about 75% of patients with liver injury may experience disturbances in bone health troubles (Angulo *et al.* 2011; Ehnert *et al.* 2020; Sriuttha *et al.* 2018). The pathological mechanisms behind drug-induced osteoporosis are complex because both medications and their metabolites can have a direct effect on bone balance and may also indirectly affect bones by impairing liver function. This impairment can lead to vitamin D and hormone metabolism imbalances, trigger immune responses or inflammation, potentially progressing to HOD (Ehnert *et al.* 2019). Various studies have used animal models to explore and understand the mechanisms underlying HOD (Hochrath *et al.* 2013; Nussler *et al.* 2014; Sens *et al.* 2017; Spirlandeli *et al.* 2017). Nevertheless, animal models present certain restrictions: they are expensive, require significant time, and raise ethical concerns, with potential difficulties in replicating human biology or disease conditions. Due to these limitations, the findings of the researches might not be entirely translatable to humans (Bracken 2009). Differences in drug metabolism, toxicity tolerance, and bone strength between species highlight the importance of developing a human *in vitro* liver-bone (L-B) model. Although 2D *in vitro* models are widely used, they cannot replicate complex 3D structures. In 2D culture, cells grow on a plastic surface, which can affect metabolic pathways, leading to changes in the cytoskeleton, loss of cell polarity, altered cell-cell and cell-environment interactions, and reduced enzyme activity (Brooks *et al.* 2021). Research indicates that primary human hepatocytes cultured in 3D exhibit metabolic functions that are closer to those in the human body than in 2D culture models (Schyschka *et al.* 2013). These limitations prevent 2D models from accurately predicting drug toxicity. To address these limitations, a stable long-term *in vitro* 3D L-B co-culture model that accurately represents tissue interactions is essential for studying drug toxicity effects on bone

homeostasis and for gaining insights into HOD mechanisms in humans.

To date, no *in vitro* co-culture model has successfully captured the interactions between liver and bone tissues. As previously noted, hPRP scaffolds are well-suited for cultivating osteoblast- and osteoclast-like cells because of their optimal stiffness and pore size enabling the detection of alteration in stiffness and content. Thus, to model bone tissue, THP-1 and SCP-1 cell lines were cultured on human platelet-rich plasma scaffolds (Haussling *et al.* 2019; Weng *et al.* 2020). For the liver, HepaRG cell line were selected because of their high basal CYP activity, closely resembling that of freshly isolated human hepatocytes and surpassing the activity levels of other hepatic cell lines such as HepG2 and Huh-7 (Dean and Kane 2012; Lin *et al.* 2012). The target of our study was to create an *in vitro* 3D liver-bone co-culture model that closely mimics human physiology, providing a valuable tool for drug toxicity screening and investigating the underlying mechanisms of interactions within the L-B axis.

Because the liver cell and bone cell differentiation mediums are distinct, the components in these mediums may affect the other cell types' viability and functionality. Therefore, our initial step was to evaluate the influence of these differentiation supplements on both liver and bone cells. Our findings revealed that HepaRG cell function and growth were adversely affected by 200 μM L-ascorbic acid. Interestingly, prior research indicated that mesenchymal cell proliferation was promoted by L-ascorbic acid (Mekala *et al.* 2013). This dual function possibly due to L-ascorbic acid's dual pro-oxidant and antioxidant properties (Dhage and Sharbidre 2022). Additionally, our data demonstrated that AP activity was marked upregulated by 50 μM hydrocortisone, consistent with the results of Griffin and Ber and Bazzell *et al.*, who reported hydrocortisone or cortisol could increase AP activity in HeLa cells (Bazzell *et al.* 1976; Griffin and Ber 1969). Nevertheless, Bazzell *et al.* clarified that the observed rise in AP activity was not linked to elevated enzyme protein levels but is rather attributed to cortisol's enhanced catalytic. Therefore, we suppose that the elevated AP activity in bone cells treated with hydrocortisone may not correlate with an enhanced differentiation of bone-forming cells. Moreover, our

findings indicated that hepatic factors adversely affected the osteoblast-osteoclast system, especially 1.7% dimethyl sulfoxide causing significantly reduced cell matrix mineralization and viability. While we observed a rise in CAII activity exposed to 1.7% dimethyl sulfoxide, prior studies have suggested that dimethyl sulfoxide actually inhibits osteoclast differentiation (Lemieux *et al.* 2011; Yang *et al.* 2015). Because we used the total DNA content of bone cells to normalize our data, which includes both osteoblast cells and osteoclast cells, the observed rise in CAII activity could be linked to the role of 1.7% dimethyl sulfoxide in affecting bone cell viability. Researches have demonstrated that HepaRG cells can undergo differentiation in the absence of dimethyl sulfoxide (Rose *et al.* 2022), however, a lower dimethyl sulfoxide concentration (0.85%) was still utilized in our L-B co-culture system to maintain hepatic function over extended periods.

Our findings indicate that whether for liver or bone cells, adding the other's mixed supplements to their differentiation medium could affect their own viability and/or function. To identify a more suitable differentiation medium for the L-B co-culture system, we evaluated the effects of different L-B medium ratios on 3D liver and bone models independently. The results from the liver cell revealed a reduction in activity of mitochondria in the group treated with 25:75 L-B medium after 21 days. However, DNA content in this group remained relatively stable, indicating that the 25:75 L-B ratio adversely affected the viability of HepaRG spheroids. For the osteoblast-osteoclast system, raising the amount of HepaRG cell differentiation medium resulted in a steady decrease in cell viability and function, likely due to the higher DMSO concentration. Our findings indicated that a 50:50 L-B medium is optimal for maintaining bone and liver cells viability and function in the co-culture model, preserving them for at least 21 days.

Diclofenac, a widely used NSAID, works by blocking the transformation of arachidonic acid into prostaglandins, offering relief from pain and inflammation (Gunaydin and Bilge 2018), and it is commonly prescribed for a range of orthopedic conditions involving various inflammations (Al-Waeli *et al.* 2021; Altman *et al.* 2015; Ku *et al.* 1986). After entering the body, diclofenac undergoes significant first-pass metabolism, with 40%

processed by hepatocyte enzymes, including UGT, CYP3A4, and CYP2C9. The metabolism produces 4-OH diclofenac and 5-OH diclofenac, and together with the unmetabolized diclofenac, flows in the blood to mediate therapeutic effects (Dean and Kane 2012; Tateishi *et al.* 2020; Todd and Sorkin 1988). Nevertheless, evidence from animal studies suggests that diclofenac negatively impacts bone dynamic balance and slows down the fracture healing process (Cottrell and O'Connor 2010; Karanikola *et al.* 2022; Menger *et al.* 2023). Apart from its direct influence on bone cells, diclofenac-induced liver damage has the potential to alter bone homeostasis through indirect mechanisms. Changes in hepatocyte cytokine production, like bone morphogenetic protein 9 (BMP-9), IGF-1, TGF-β, IL-6, IL-11, and sclerostin could contribute to affecting bone forming and resorbing balance (Ehnert *et al.* 2019). The precise mechanisms by which diclofenac influences bone homeostasis are still not fully understood, as most researches rely on animal models or the exclusion of the liver system (Karanikola *et al.* 2022; Menger *et al.* 2023). Given the crucial role of the liver in drug metabolism, a human *in vitro* L-B cell co-culture model is necessary to explore these interactions further.

This research aimed to test the availability of our L-B co-culture system by using diclofenac, while also exploring diclofenac potential toxicity on bone forming and resorbing balance. Initially, we applied diclofenac three times weekly to avoid impairing hepatocyte function. Our findings indicate that three times weekly diclofenac exposure did not impair hepatocyte's function. However, osteoclast function was reduced in the diclofenac-treated group on day 21. This may be related to diclofenac's inhibition of prostaglandin synthesis, as prostaglandins, especially prostaglandin E2 (PGE2), play a positive role in osteoclast genesis (Kobayashi *et al.* 2005) (Take *et al.* 2005). PGE2 can be produced by various cells, including hepatocytes and osteocytes (Kalinski 2012; Qiang and Xu 2024). PGE2 can promote stromal cells and osteoblasts to release more RANKL, which indirectly promotes osteoclast differentiation (Fujita *et al.* 2003). The direct effect of PGE2 on osteoclast differentiation is still controversial. Some researchers believe that

PGE2 can directly act on osteoclast precursors, promoting their proliferation and transformation into mature osteoclasts (Kobayashi *et al.* 2005), while others indicate that PGE2 inhibits osteoclast formation (Mano *et al.* 2000). Diclofenac has been reported that it can reduce prostaglandin synthesis by inhibiting the activity of cyclooxygenase (COX) in the liver and bone cells (Gan 2010; Hasan *et al.* 2023). This may explain why we observed a decrease in osteoclast function with three times a week stimulation of diclofenac in our L-B system.

To better simulate human diclofenac intake, we increased the frequency of diclofenac exposure, specifically administering it to our models daily. Our findings showed that daily diclofenac stimulation, whether applied to liver spheroids or the L-B system, did not markedly alter the CYP2C9 and UGT enzyme activities in hepatocytes, both of which are essential for diclofenac metabolism (Knospel *et al.* 2016). These findings indicate that in the co-culture system, the hepatocytes were still active and able to metabolize diclofenac over time. Interestingly, in contrast to the three times weekly exposure, daily administration of diclofenac to the L-B system resulted in a marked enhancement of osteoclast function on day 21. Further results showed that bone scaffold mineral density and stiffness showed a significant decline with the daily administration of diclofenac. These results are consistent with prior preclinical and clinical researches that have reported decreased bone quality with diclofenac treatment in orthopedic patients and animal models (Cottrell and O'Connor 2010; Dodwell *et al.* 2010; Gaston and Simpson 2007; Hatipoglu *et al.* 2015; Hernandez *et al.* 2012; Krischak *et al.* 2007a). Additionally, our results revealed that RANKL levels in the supernatant were elevated in the diclofenac-treated group. We also assessed OPG, a decoy receptor for RANKL (Lacey *et al.* 1998), using dot blot analysis. Our findings indicated a rising trend in OPG levels in the supernatant, suggesting that OPG might increase as a compensatory mechanism. Despite this rise in OPG, the RANKL: OPG ratio was elevated, which promotes osteoclast differentiation and activity (Boyce and Xing 2008; Udagawa *et al.* 2021a).

When daily diclofenac was applied exclusively to the 3D osteoblast-osteoclast co-culture

model, the results showed no significant effect on osteoclast or osteoblast function. The differing effects between daily and three times weekly diclofenac stimulation may be related to cytokines secreted by hepatocyte spheroids in our L-B system. Diclofenac has been shown to inhibit PGE2 synthesis (Kondo *et al.* 2015; Ku *et al.* 1975), and the reduced PGE2 released by hepatocytes may explain the decreased osteoclast activity observed with three times weekly diclofenac stimulation. In contrast, daily diclofenac enhanced osteoclast function in our L-B system, which may be due to sustained stimulation of hepatocytes by diclofenac. Continuous stimulation increases metabolite production, meanwhile, the effect of 4-OH diclofenac on bone cells remains unclear. Additionally, continuous diclofenac exposure may induce stronger oxidative stress responses in hepatocytes, prompting the release of inflammatory factor. Although PGE2 synthesis depends directly on COX enzymes and can be inhibited by diclofenac, studies show that inflammatory factors and oxidative stress can also modulate COX enzymes and PGE synthase (Lu and Wahl 2005) (Kulesza *et al.* 2023). We hypothesize that sustained daily diclofenac stimulation could lead to hepatocyte oxidative stress, increasing the release of inflammatory factors that may subsequently upregulate osteoclast function.

Initially, we focused on diclofenac metabolites. Diclofenac has a reported half-life of about 2 hours, but studies by Todd and Sorkin indicate that its metabolites extend this to 25.8–33 hours (Todd and Sorkin 1988). This led us to hypothesize that 4-OH diclofenac, which is the main metabolite of diclofenac (Bouju *et al.* 2016), might play a role in enhancing osteoclast function and differentiation, potentially impacting bone cell balance. Nevertheless, contrary to the hypothesis, our data indicated that 4-OH diclofenac had no effect on the osteoclast function within the osteoblast-osteoclast model. Consequently, it was concluded that the upregulated osteoclast function in the L-B system was not due to direct effects of diclofenac or its metabolite, 4-OH diclofenac, on osteocytes. According to these results, we further proposed that diclofenac-induced oxidative stress and inflammation in hepatocytes may influence the secretion of factors that could, in turn, improve osteoclast differentiation and function.

Upon reaching the liver, medications undergo metabolic changes that render them less harmful or non-toxic and water-soluble for excretion. This process involves liver enzymes, primarily the family of cytochrome P450 (Zhao *et al.* 2021), and often generates ROS, particularly when drugs or their metabolites induce the oxidative stress of cell (Allameh *et al.* 2023). ROS are a class of highly reactive oxygen-containing molecules, including various types such as superoxide anion, hydrogen peroxide, and hydroxyl radical (Agidigbi and Kim 2019). In addition to being produced during the metabolism of exogenous substances by cytochrome P450 enzymes, the primary source of ROS is the leakage of electrons from the respiratory chain complexes during normal cellular respiration, where part of the oxygen is reduced to form superoxide anion (Zangar *et al.* 2004). Low ROS levels play positive roles in supporting signal transduction and immune defense (Schieber and Chandel 2014), but excessive ROS triggers oxidative stress, damaging cellular components and releasing inflammatory factors (Hong *et al.* 2024). Glutathione (GSH), a critical antioxidant in the liver, neutralizes ROS by interacting with them through its thiol group, converting them into non-toxic compounds. GSH could be converted to oxidized glutathione (GSSG) in the process, and the GSH-to-GSSG ratio typically used to evaluate cells' antioxidant defense capacity (Vairetti *et al.* 2021). Generally, oxidative stress occurs when the production of ROS exceeds the cell's ability to counteract them with antioxidants (Lee *et al.* 2022). It could trigger the release of inflammatory factors into the extracellular space, impacting both liver cells and bone cell function *via* the L-B axis. Consistent with previous *in vitro* and *in vivo* research (Ahmad *et al.* 2013; Alabi *et al.* 2017; Thai *et al.* 2023), the findings of our research demonstrate that diclofenac administration lowers GSH levels and elevates oxidative stress in hepatocytes. In addition to processing ROS generated during metabolism, GSH also binds to diclofenac and its metabolites, promoting the detoxification of diclofenac (Sousa *et al.* 2021), which leads to high consumption of GSH. Consequently, low levels of total GSH results in liver cell damage after chronic diclofenac exposure (Mechcatie 2010).

Under oxidative stress, ROS can induce the expression of inflammatory factors such as

interleukins, TNF-α, and chemokines (Hong *et al.* 2024). The overexpression of inflammatory genes can trigger intracellular signaling cascades that generate more ROS, thereby creating a vicious cycle (Hulsmans and Holvoet 2010). Among these inflammatory factors, IL-6 was included in our study because the hepatocytes in our L-B system can secrete it. IL-6 is a versatile cytokine essential to osteoclasts differentiation, binding with its receptor to form a complex that communication with the gp130 signal transducer on osteoclast precursors, improving the mature osteoclasts formation (Feng *et al.* 2017; Mihara *et al.* 2012). In addition to its direct effects, IL-6 also acts on osteoblasts, stimulating them to produce more receptor activator of RANKL *via* the JAK/STAT3 signaling pathway, thereby further promoting osteoclast differentiation and activity (Harmer *et al.* 2019; Wu *et al.* 2017b). To determine the appropriate dosage of IL-6, we referred to its reported serum concentration in humans, which is typically below 5 pg/ml in healthy individuals (Singh *et al.* 2015). In our osteoblast-osteoclast co-culture system, we exposed the cells to IL-6 at concentrations of 5-10 pg/ml to mimic inflammatory conditions. As expected, our findings confirmed that IL-6 enhanced TRAP activity in osteoclasts. Additionally, we observed an increase in RANKL expression and a higher RANKL: OPG ratio following IL-6 stimulation. Our findings indicate that chronic diclofenac-treated hepatocytes release increased levels of IL-6, which contributes to the disruption of bone homeostasis.

In addition to inducing the liver to release inflammatory factors that affect bone cells, the direct effects of ROS on bone cells cannot be overlooked. For osteoblasts, low ROS levels can activate signaling pathways to promote proliferation and differentiation (Riegger *et al.* 2023). However, high ROS levels oxidize Runx2, inhibit osteogenic differentiation (Hu *et al.* 2023), and induce the mesenchymal stem cell adipogenic differentiation by activating adipogenic genes like peroxisome proliferator-activated receptor γ (PPARγ) and CCAAT enhancer binding protein α (C/EBPα) (Atashi *et al.* 2015; de Villiers *et al.* 2018; Lee *et al.* 2009). In our experiments, osteogenic differentiation was marked by AP activity. However, research has shown that preadipocytes also express AP (Ali *et al.* 2006),

indicating that the AP detected in bone scaffolds could originate from both osteoblasts and preadipocytes. In addition to affecting osteoblast differentiation, ROS also impact osteoblast lifespan (Linares *et al.* 2009). For osteoclasts, ROS can directly enhance RANKL-RANK signaling and activate nuclear factor kappa B, promoting osteoclast function and differentiation (Agidigbi and Kim 2019; Ren *et al.* 2021; Wang *et al.* 2018).

Our research suggests that diclofenac affects bone cell homeostasis through oxidative stress and inflammatory responses initially induced in liver cells. Potential therapeutic approaches could target diclofenac-induced liver oxidative stress. Elbaz et al. showed that diclofenac upregulates microRNA 144 (miR-144), decreases nuclear factor erythroid 2-related factor 2 (Nrf2) levels and GSH levels, and induces liver inflammation and apoptosis. Notably, resveratrol can significantly alleviate diclofenac toxicity when used preventatively or therapeutically. Resveratrol is a naturally occurring polyphenolic compound found in various plants, particularly in red wine, grape skins, blueberries, peanuts, and certain medicinal plants. It has potential therapeutic effects on diclofenac-induced liver and kidney damage by regulating the miR-144/Nrf2/GSH axis (Elbaz *et al.* 2022). Kolaviron, a plant compound from Garcinia kola (bitter kola) used in African traditional medicine, has antioxidant and anti-inflammatory properties. Alabi et al. found that Kolaviron administration before diclofenac significantly reduced diclofenac's adverse effects (Alabi and Akomolafe 2020). Yulangsan, a traditional Chinese medicinal herb for acute and chronic hepatitis, protects against diclofenac-induced liver damage *via* free radical scavenging, antioxidant activity, and apoptosis inhibition, as confirmed by Huang *et al.* (Huang *et al.* 2016). These studies provide potential therapeutic avenues for addressing delayed fracture healing and hepatic bone disease related to diclofenac use.

However, the presented study has also some limitations. In addition to IL-6, various other cytokines, including TNF-α and various interleukins, may undergo significant changes when liver cells are exposed to oxidative stress or if there themselves produce some of the mediators. These altered cytokines could disrupt bone cell homeostasis, highlighting the need for further investigation. The complexities of the human physiological

environment are difficult to fully replicate because of the constraints of *in vitro* cellular experiments. Our model did not include several cell types essential for maintaining bone tissue homeostasis, such as chondrocytes, endothelial cells, immune cells, and bone lining cells. Furthermore, the liver model used in this study included only cholangiocytes and hepatocytes, excluding other important types of cells, like hepatic stellate cells, endothelial cells, and Kupffer cells which may influence hepatocyte function and contribute to liver damage. To more accurately mimic the inflammatory response in drug-induced liver injury, future studies should consider incorporating Kupffer cells into the model. Beyond drug toxicity assessment, our system could also serve as a tool to investigate interactions within the L-B axis. The liver not only plays a pivotal role in drug detoxification but also produces various substances that impact bone homeostasis, including those involved in parathyroid hormone metabolism (Duarte *et al.* 2001), vitamin D metabolism (Savic *et al.* 2014), IGF-1 (Liu *et al.* 2017), TGF-β (Lian *et al.* 2012), IL-11 (Kespohl *et al.* 2021), and BMP-9 (Um *et al.* 2022). Consequently, liver dysfunction may positively correlate with disruptions in bone homeostasis, and our L-B *in vitro* system can be utilized to explore the molecular mechanisms underlying this connection. For example, liver fibrosis has been associated with increased TGF-β1 levels (Fabregat *et al.* 2016), and pro-inflammatory cytokines, along with reduced production of IGF (Liu *et al.* 2018), and LCAT (Lu *et al.* 2022), as well as disturbances in parathyroid hormone and vitamin D metabolism. These factors are essential for sustaining bone health, and any imbalances may have both direct and indirect effects. In our study, a fibrosis model was developed by co-culturing HepaRG cells alongside LX-2 hepatic stellate cells that had been activated by TGF-β1 (Zahmatkesh *et al.* 2022). After combined with bone system, this model enables further investigation into the link between liver fibrosis and bone health. *Part of this chapter has been used in the article* (Chen *et al.* 2024).

Chapter 5

5. Summary

This research introduced a novel *in vitro* L-B co-culture model, incorporating human hepatocyte (HepaRG) spheroids with scaffolds embedded with human monocytic cell line (THP-1) and mesenchymal stem cells (SCP-1) on an agarose plate. We investigated how bone and liver differentiation medium supplements affected both bone and liver cells. The findings indicated that 1.7% Dimethyl Sulfoxide markedly influenced bone cell function and viability. Consequently, we optimized the medium in our model, enabling the liver-bone system to maintain stable activity and function for at least 21 days.

Clinical and animal studies have shown that diclofenac can affect fracture healing, although the underlying mechanism remains unclear. We used our liver-bone model to assess the effects of diclofenac administered three times weekly or daily. Our findings indicate that when diclofenac and 4-OH diclofenac come into directly contact with bone cells, they do not impact bone cell differentiation or function. Interestingly, three times weekly diclofenac exposure in our L-B system resulted in reduced osteoclast differentiation and function. In contrast, daily diclofenac exposure enhanced osteoclast differentiation and activity *via* affecting the balance of the RANKL-OPG axis. We hypothesize that continuous diclofenac exposure may induce oxidative stress in hepatocytes, leading to an inflammatory response that impacts bone dynamic balance and impairs fracture healing. Our findings suggest that diclofenac exposure prompts hepatocytes to release more ROS, affecting the antioxidant system by depleting GSH. This triggers an inflammatory response, releasing more of the cytokine IL-6. Additionally, our findings showed that IL-6 upregulates osteoclast differentiation and function by increasing RANKL secretion in bone cells. Our findings provide a potential explanation for diclofenac-induced delayed fracture healing and point toward possible clinical treatment approaches.

Moreover, our study highlights the critical role of the liver in mediating the toxic effects of drugs on bone cells. This 3D *in vitro* liver–bone system presents a promising model for

drug toxicity testing and studying bone metabolism impairment associated with liver dysfunction.

Chapter 6

6. Zusammenfassung

In dieser Studie entwickelten wir ein neuartiges *in vitro* Leber-Knochen-Kokultursystem, das menschliche Hepatozyten (HepaRG)-Sphäroide mit Gerüsten enthält, die humane mesenchymale Stammzellen (SCP-1) und eine humane Monozyten-Zelllinie (THP-1) auf einer Agarose-Plattform beinhalten. Wir untersuchten die Auswirkungen von Leber- und Knochen-Differenzierungsmedium-Zusätzen auf Knochen- und Leberzellen. Unsere Ergebnisse zeigten, dass 1.7 % DMSO die Lebensfähigkeit und Funktion von Knochenzellen signifikant beeinflusst. Folglich optimierten wir das Leber-Knochen-Medium in unserem System, sodass das Leber-Knochen-System für mindestens 21 Tage eine stabile Aktivität und Funktion aufrechterhalten kann.

Klinische und tierexperimentelle Studien haben gezeigt, dass Diclofenac den Heilungsprozess von Knochenfrakturen beeinflussen kann, obwohl der zugrunde liegende Mechanismus unklar bleibt. Wir nutzten unser Leber-Knochen-System, um die Auswirkungen von Diclofenac zu bewerten, das entweder dreimal wöchentlich oder täglich verabreicht wurde. Unsere Ergebnisse zeigen, dass Diclofenac und sein Metabolit, 4-OH-Diclofenac, bei direkter Exposition gegenüber Knochenzellen keinen Einfluss auf deren Differenzierung oder Funktion haben. Interessanterweise führte eine dreimal wöchentliche Diclofenac-Exposition in unserem Leber-Knochen-System zu einer Abnahme der Differenzierung und Funktion von Osteoklasten. Im Gegensatz dazu erhöhte eine tägliche Diclofenac-Exposition in unserem Leber-Knochen-System die Differenzierung und Funktion von Osteoklasten, indem sie die RANKL-OPG-Achse beeinflusste. Wir vermuten, dass eine kontinuierliche Diclofenac-Exposition oxidativen Stress in Hepatozyten auslösen könnte, was zu einer entzündlichen Reaktion führt, die das Knochenhomöostase beeinflusst und die Frakturheilung beeinträchtigt. Unsere Ergebnisse deuten darauf hin, dass Diclofenac Hepatozyten zur Freisetzung von mehr reaktiven Sauerstoffspezies anregt, wodurch das antioxidative System durch die Verringerung des Glutathions beeinträchtigt wird. Dies löst eine entzündliche Reaktion

aus, die zur Freisetzung von mehr IL-6-Zytokinen führt. Darüber hinaus zeigten unsere Ergebnisse, dass IL-6 die Differenzierung und Funktion von Osteoklasten durch eine erhöhte RANKL-Sekretion in Knochenzellen hochreguliert. Unsere Ergebnisse liefern eine potenzielle Erklärung für die durch Diclofenac verursachte verzögerte Frakturheilung und weisen auf mögliche klinische Behandlungsansätze hin.

Unsere Studie hebt außerdem die entscheidende Rolle der Leber bei der Vermittlung der toxischen Wirkungen von Medikamenten auf Knochenzellen hervor. Dieses 3D *in vitro* Leber-Knochen-System stellt ein vielversprechendes Modell für die Prüfung der Medikamententoxizität und das Studium von Knochenstoffwechselstörungen im Zusammenhang mit Leberfunktionsstörungen dar.

7. Bibliography

Adnan Memic TC, Loek J. Eggermont, Mahboobeh Rezaeeyazdi,, Joseph Steingold ZJR, Kasturi Joshi Navare, Halimatu S. Mohammed, and Sidi A. Bencherif (2019) Latest Advances in Cryogel Technology for Biomedical Applications. ADVANCED THERAPEUTICS 2(4):1800114. http://doi.org/10.1002/adtp.201800114

Agidigbi TS, Kim C (2019) Reactive Oxygen Species in Osteoclast Differentiation and Possible Pharmaceutical Targets of ROS-Mediated Osteoclast Diseases. Int J Mol Sci 20(14). http://doi.org/10.3390/ijms20143576

Ahmad I, Shukla S, Kumar A*, et al.* (2013) Biochemical and molecular mechanisms of N-acetyl cysteine and silymarin-mediated protection against maneb- and paraquat-induced hepatotoxicity in rats. Chem Biol Interact 201(1-3):9-18. http://doi.org/10.1016/j.cbi.2012.10.027

Al-Waeli H, Reboucas AP, Mansour A, Morris M, Tamimi F, Nicolau B (2021) Non-steroidal anti-inflammatory drugs and bone healing in animal models-a systematic review and meta-analysis. Syst Rev 10(1):201. http://doi.org/10.1186/s13643-021-01690-w

Alabi QK, Akomolafe RO (2020) Kolaviron Diminishes Diclofenac-Induced Liver and Kidney Toxicity in Wistar Rats Via Suppressing Inflammatory Events, Upregulating Antioxidant Defenses, and Improving Hematological Indices. Dose Response 18(1):1559325819899256. http://doi.org/10.1177/1559325819899256

Alabi QK, Akomolafe RO, Olukiran OS*, et al.* (2017) The Garcinia kola biflavonoid kolaviron attenuates experimental hepatotoxicity induced by diclofenac. Pathophysiology 24(4):281-290. http://doi.org/10.1016/j.pathophys.2017.07.003

Ali AT, Penny CB, Paiker JE, Psaras G, Ikram F, Crowther NJ (2006) The relationship between alkaline phosphatase activity and intracellular lipid accumulation in murine 3T3-L1 cells and human preadipocytes. Analytical Biochemistry 354(2):247-254. http://doi.org/10.1016/j.ab.2006.04.028

Allameh A, Niayesh-Mehr R, Aliarab A, Sebastiani G, Pantopoulos K (2023) Oxidative Stress in Liver Pathophysiology and Disease. Antioxidants (Basel) 12(9). http://doi.org/10.3390/antiox12091653

Almazroo OA, Miah MK, Venkataramanan R (2017) Drug Metabolism in the Liver. Clin Liver Dis 21(1):1-20. http://doi.org/10.1016/j.cld.2016.08.001

Altman R, Bosch B, Brune K, Patrignani P, Young C (2015) Advances in NSAID development: evolution of diclofenac products using pharmaceutical technology. Drugs

75(8):859-77. http://doi.org/10.1007/s40265-015-0392-z

Angulo P, Grandison GA, Fong DG, *et al.* (2011) Bone disease in patients with primary sclerosing cholangitis. Gastroenterology 140(1):180-8. http://doi.org/10.1053/j.gastro.2010.10.014

Aninat C, Piton A, Glaise D, *et al.* (2006) Expression of cytochromes P450, conjugating enzymes and nuclear receptors in human hepatoma HepaRG cells. Drug Metab Dispos 34(1):75-83. http://doi.org/10.1124/dmd.105.006759

Arfeen M, Srivastava A, Srivastava N, Khan RA, Almahmoud SA, Mohammed HA (2024) Design, classification, and adverse effects of NSAIDs: A review on recent advancements. Bioorg Med Chem 112:117899. http://doi.org/10.1016/j.bmc.2024.117899

Arnett TR (2008) Extracellular pH regulates bone cell function. J Nutr 138(2):415S-418S. http://doi.org/10.1093/jn/138.2.415S

Aspera-Werz RH, Chen G, Schilonka L, *et al.* (2024) Impact of Particle Size and Sintering Temperature on Calcium Phosphate Gyroid Structure Scaffolds for Bone Tissue Engineering. J Funct Biomater 15(12). http://doi.org/10.3390/jfb15120355

Aspera-Werz RH, Ehnert S, Heid D, *et al.* (2018) Nicotine and Cotinine Inhibit Catalase and Glutathione Reductase Activity Contributing to the Impaired Osteogenesis of SCP-1 Cells Exposed to Cigarette Smoke. Oxid Med Cell Longev 2018:3172480. http://doi.org/10.1155/2018/3172480

Atashi F, Modarressi A, Pepper MS (2015) The Role of Reactive Oxygen Species in Mesenchymal Stem Cell Adipogenic and Osteogenic Differentiation: A Review. Stem Cells and Development 24(10):1150-1163. http://doi.org/10.1089/scd.2014.0484

Barbu EC, Chitu-Tisu CE, Lazar M, *et al.* (2017) Hepatic Osteodystrophy: A Global (Re)View of the Problem. Acta Clin Croat 56(3):512-525. http://doi.org/10.20471/acc.2017.56.03.19

Bazzell KL, Price G, Tu S, Griffin M (1976) Cortisol modification of HeLa 65 alkaline phosphatase. Decreased phosphate content of the induced enzyme. Eur J Biochem 61(2):493-9. http://doi.org/10.1111/j.1432-1033.1976.tb10044.x

Ben-Moshe S, Itzkovitz S (2019) Spatial heterogeneity in the mammalian liver. Nat Rev Gastroenterol Hepatol 16(7):395-410. http://doi.org/10.1038/s41575-019-0134-x

Bikle DD (2012) Vitamin D and bone. Curr Osteoporos Rep 10(2):151-9. http://doi.org/10.1007/s11914-012-0098-z

Bocker W, Yin Z, Drosse I, *et al.* (2008) Introducing a single-cell-derived human

mesenchymal stem cell line expressing hTERT after lentiviral gene transfer. J Cell Mol Med 12(4):1347-59. http://doi.org/10.1111/j.1582-4934.2008.00299.x

Boelsterli UA (2003) Diclofenac-induced liver injury: a paradigm of idiosyncratic drug toxicity. Toxicol Appl Pharmacol 192(3):307-22. http://doi.org/10.1016/s0041-008x(03)00368-5

Borciani G, Montalbano G, Baldini N, Cerqueni G, Vitale-Brovarone C, Ciapetti G (2020) Co-culture systems of osteoblasts and osteoclasts: Simulating in vitro bone remodeling in regenerative approaches. Acta Biomater 108:22-45. http://doi.org/10.1016/j.actbio.2020.03.043

Boskey AL, Coleman R (2010) Aging and bone. J Dent Res 89(12):1333-48. http://doi.org/10.1177/0022034510377791

Bouju H, Nastold P, Beck B, Hollender J, Corvini PF, Wintgens T (2016) Elucidation of biotransformation of diclofenac and 4'hydroxydiclofenac during biological wastewater treatment. J Hazard Mater 301:443-52. http://doi.org/10.1016/j.jhazmat.2015.08.054

Boyce BF, Xing LP (2008) Functions of RANKL/RANK/OPG in bone modeling and remodeling. Archives of Biochemistry and Biophysics 473(2):139-146. http://doi.org/10.1016/j.abb.2008.03.018

Bracken MB (2009) Why animal studies are often poor predictors of human reactions to exposure. J R Soc Med 102(3):120-2. http://doi.org/10.1258/jrsm.2008.08k033

Brooks A, Liang X, Zhang Y*, et al.* (2021) Liver organoid as a 3D in vitro model for drug validation and toxicity assessment. Pharmacological Research 169:105608. http://doi.org/10.1016/j.phrs.2021.105608

Callaway DA, Jiang JX (2015) Reactive oxygen species and oxidative stress in osteoclastogenesis, skeletal aging and bone diseases. J Bone Miner Metab 33(4):359-70. http://doi.org/10.1007/s00774-015-0656-4

Calzadilla Bertot L, Adams LA (2016) The Natural Course of Non-Alcoholic Fatty Liver Disease. Int J Mol Sci 17(5). http://doi.org/10.3390/ijms17050774

Chen CC, Hsu LW, Chen KD, Chiu KW, Chen CL, Huang KT (2021) Emerging Roles of Calcium Signaling in the Development of Non-Alcoholic Fatty Liver Disease. Int J Mol Sci 23(1). http://doi.org/10.3390/ijms23010256

Chen G, Xin Y, Hammour MM*, et al.* (2024) Establishment of a human 3D in vitro liver-bone model as a potential system for drug toxicity screening. Arch Toxicol. http://doi.org/10.1007/s00204-024-03899-9

Chen X, Wang Z, Duan N, Zhu G, Schwarz EM, Xie C (2018) Osteoblast-osteoclast interactions. Connect Tissue Res 59(2):99-107. http://doi.org/10.1080/03008207.2017.1290085

Chung RT, Stravitz RT, Fontana RJ, *et al.* (2012) Pathogenesis of liver injury in acute liver failure. Gastroenterology 143(3):e1-e7. http://doi.org/10.1053/j.gastro.2012.07.011

Cottrell J, O'Connor JP (2010) Effect of Non-Steroidal Anti-Inflammatory Drugs on Bone Healing. Pharmaceuticals (Basel) 3(5):1668-1693. http://doi.org/10.3390/ph3051668

Cuklev F, Kristiansson E, Fick J, Asker N, Forlin L, Larsson DG (2011) Diclofenac in fish: blood plasma levels similar to human therapeutic levels affect global hepatic gene expression. Environ Toxicol Chem 30(9):2126-34. http://doi.org/10.1002/etc.599

Czekanska EM, Stoddart MJ, Ralphs JR, Richards RG, Hayes JS (2014) A phenotypic comparison of osteoblast cell lines versus human primary osteoblasts for biomaterials testing. J Biomed Mater Res A 102(8):2636-43. http://doi.org/10.1002/jbm.a.34937

de Villiers D, Potgieter M, Ambele MA, Adam L, Durandt C, Pepper MS (2018) The Role of Reactive Oxygen Species in Adipogenic Differentiation. Adv Exp Med Biol 1083:125-144. http://doi.org/10.1007/5584_2017_119

Dean L, Kane M (2012) Celecoxib Therapy and CYP2C9 Genotype. In: Pratt VM, Scott SA, Pirmohamed M, Esquivel B, Kattman BL, Malheiro AJ (eds) Medical Genetics Summaries. Bethesda (MD). https://www.ncbi.nlm.nih.gov/books/NBK379478/

Degen PH, Dieterle W, Schneider W, Theobald W, Sinterhauf U (1988) Pharmacokinetics of diclofenac and five metabolites after single doses in healthy volunteers and after repeated doses in patients. Xenobiotica 18(12):1449-55. http://doi.org/10.3109/00498258809042267

Dhage PA, Sharbidre AA (2022) Bimodal Behavior of Ascorbic Acid in Musca domestica Larvae. Biointerface Research in Applied Chemistry 12(4):5199-5216. http://doi.org/10.33263/BRIAC124.51995216

Díaz-González F, Sánchez-Madrid F (2015) NSAIDs: Learning new tricks from old drugs. European Journal of Immunology 45(3):679-686. http://doi.org/10.1002/eji.201445222

Dodwell ER, Latorre JG, Parisini E, *et al.* (2010) NSAID exposure and risk of nonunion: a meta-analysis of case-control and cohort studies. Calcif Tissue Int 87(3):193-202. http://doi.org/10.1007/s00223-010-9379-7

Doke SK, Dhawale SC (2015) Alternatives to animal testing: A review. Saudi Pharm J 23(3):223-229. http://doi.org/10.1016/j.jsps.2013.11.002

Donato MT, Tolosa L, Gomez-Lechon MJ (2015) Culture and Functional Characterization of Human Hepatoma HepG2 Cells. Methods Mol Biol 1250:77-93. http://doi.org/10.1007/978-1-4939-2074-7_5

Donohue TM, Jr. (2007) Alcohol-induced steatosis in liver cells. World J Gastroenterol 13(37):4974-8. http://doi.org/10.3748/wjg.v13.i37.4974

Dorado P, Berecz R, Cáceres MC, Llerena A (2003) Analysis of diclofenac and its metabolites by high-performance liquid chromatography: relevance of CYP2C9 genotypes in diclofenac urinary metabolic ratios. Journal of Chromatography B 789(2):437-442. http://doi.org/10.1016/S1570-0232(03)00137-5

Duarte MP, Farias ML, Coelho HS, *et al.* (2001) Calcium-parathyroid hormone-vitamin D axis and metabolic bone disease in chronic viral liver disease. J Gastroenterol Hepatol 16(9):1022-7. http://doi.org/10.1046/j.1440-1746.2001.02561.x

Ehnert S, Aspera-Werz RH, Ruoss M, *et al.* (2019) Hepatic Osteodystrophy-Molecular Mechanisms Proposed to Favor Its Development. Int J Mol Sci 20(10):2555. http://doi.org/10.3390/ijms20102555

Ehnert S, Rinderknecht H, Aspera-Werz RH, Haussling V, Nussler AK (2020) Use of in vitro bone models to screen for altered bone metabolism, osteopathies, and fracture healing: challenges of complex models. Arch Toxicol 94(12):3937-3958. http://doi.org/10.1007/s00204-020-02906-z

Ehnert S, van Griensven M, Unger M, *et al.* (2018) Co-Culture with Human Osteoblasts and Exposure to Extremely Low Frequency Pulsed Electromagnetic Fields Improve Osteogenic Differentiation of Human Adipose-Derived Mesenchymal Stem Cells. Int J Mol Sci 19(4):994. http://doi.org/10.3390/ijms19040994

Elbaz EM, Ahmed KA, Abdelmonem M (2022) Resveratrol mitigates diclofenac-induced hepatorenal toxicity in rats via modulation of miR-144/Nrf2/GSH axis. J Biochem Mol Toxicol 36(9):e23129. http://doi.org/10.1002/jbt.23129

Fabregat I, Moreno-Caceres J, Sanchez A, *et al.* (2016) TGF-beta signalling and liver disease. FEBS J 283(12):2219-32. http://doi.org/10.1111/febs.13665

Feng W, Liu HR, Luo TT, *et al.* (2017) Combination of IL-6 and sIL-6R differentially regulate varying levels of RANKL-induced osteoclastogenesis through NF-κB, ERK and JNK signaling pathways. Scientific Reports 7. http://doi.org/10.1038/srep41411

Fisher K, Vuppalanchi R, Saxena R (2015) Drug-Induced Liver Injury. Arch Pathol Lab Med 139(7):876-87. http://doi.org/10.5858/arpa.2014-0214-RA

Foglietta F, Canaparo R, Muccioli G, Terreno E, Serpe L (2020) Methodological aspects

and pharmacological applications of three-dimensional cancer cell cultures and organoids. Life Sciences 254:117784. http://doi.org/10.1016/j.lfs.2020.117784

Fontana RJ (2014) Pathogenesis of idiosyncratic drug-induced liver injury and clinical perspectives. Gastroenterology 146(4):914-28. http://doi.org/10.1053/j.gastro.2013.12.032

Fujita D, Yamashita N, Iita S, Amano H, Yamada S, Sakamoto K (2003) Prostaglandin E2 induced the differentiation of osteoclasts in mouse osteoblast-depleted bone marrow cells. Prostaglandins, Leukotrienes and Essential Fatty Acids 68(5):351-358. http://doi.org/10.1016/S0952-3278(03)00027-9

Gan TJ (2010) Diclofenac: an update on its mechanism of action and safety profile. Curr Med Res Opin 26(7):1715-31. http://doi.org/10.1185/03007995.2010.486301

Gaston MS, Simpson AH (2007) Inhibition of fracture healing. J Bone Joint Surg Br 89(12):1553-60. http://doi.org/10.1302/0301-620X.89B12.19671

Gatta A, Verardo A, Di Pascoli M, Giannini S, Bolognesi M (2014) Hepatic osteodystrophy. Clin Cases Miner Bone Metab 11(3):185-91. http://pmc.ncbi.nlm.nih.gov/articles/PMC4269141/

Gerstenfeld LC, Cullinane DM, Barnes GL, Graves DT, Einhorn TA (2003) Fracture healing as a post-natal developmental process: molecular, spatial, and temporal aspects of its regulation. J Cell Biochem 88(5):873-84. http://doi.org/10.1002/jcb.10435

Gerussi A, Natalini A, Antonangeli F*, et al.* (2021) Immune-Mediated Drug-Induced Liver Injury: Immunogenetics and Experimental Models. Int J Mol Sci 22(9). http://doi.org/10.3390/ijms22094557

Geusens P, Emans PJ, de Jong JJ, van den Bergh J (2013) NSAIDs and fracture healing. Curr Opin Rheumatol 25(4):524-31. http://doi.org/10.1097/BOR.0b013e32836200b8

Ghezelayagh Z, Zabihi M, Zarkesh I*, et al.* (2022) Improved Differentiation of hESC-Derived Pancreatic Progenitors by Using Human Fetal Pancreatic Mesenchymal Cells in a Micro-scalable Three-Dimensional Co-culture System. Stem Cell Rev Rep 18(1):360-377. http://doi.org/10.1007/s12015-021-10266-z

Giustarini G, Vrisekoop N, Kruijssen L*, et al.* (2018) Trovafloxacin-Induced Liver Injury: Lack in Regulation of Inflammation by Inhibition of Nucleotide Release and Neutrophil Movement. Toxicological Sciences 167(2):385-396. http://doi.org/10.1093/toxsci/kfy244

Gomez-Lechon MJ, Ponsoda X, O'Connor E, Donato T, Jover R, Castell JV (2003) Diclofenac induces apoptosis in hepatocytes. Toxicol In Vitro 17(5-6):675-80. http://doi.org/10.1016/s0887-2333(03)00105-x

Gong J, Tu W, Liu J, Tian D (2022) Hepatocytes: A key role in liver inflammation. Front Immunol 13:1083780. http://doi.org/10.3389/fimmu.2022.1083780

Griffin MJ, Ber R (1969) Cell cycle events in the hydrocortisone regulation of alkaline phosphatase in HeLa S3 cells. J Cell Biol 40(2):297-304. http://doi.org/10.1083/jcb.40.2.297

Gunaydin C, Bilge SS (2018) Effects of Nonsteroidal Anti-Inflammatory Drugs at the Molecular Level. Eurasian J Med 50(2):116-121. http://doi.org/10.5152/eurasianjmed.2018.0010

Guo H, Weng W, Zhang S, *et al.* (2022a) Maqui Berry and Ginseng Extracts Reduce Cigarette Smoke-Induced Cell Injury in a 3D Bone Co-Culture Model. Antioxidants (Basel) 11(12):2460. http://doi.org/10.3390/antiox11122460

Guo R, Jiang M, Wang G, *et al.* (2022b) IL6 supports long-term expansion of hepatocytes in vitro. Nat Commun 13(1):7345. http://doi.org/10.1038/s41467-022-35167-8

Hadjidakis DJ, Androulakis, II (2006) Bone remodeling. Ann N Y Acad Sci 1092:385-96. http://doi.org/10.1196/annals.1365.035

Hammour MM, Othman A, Aspera-Werz R, *et al.* (2022) Optimisation of the HepaRG cell line model for drug toxicity studies using two different cultivation conditions: advantages and limitations. Arch Toxicol 96(9):2511-2521. http://doi.org/10.1007/s00204-022-03329-8

Hardy R, Cooper MS (2009) Bone loss in inflammatory disorders. J Endocrinol 201(3):309-20. http://doi.org/10.1677/JOE-08-0568

Harmer D, Falank C, Reagan MR (2019) Interleukin-6 Interweaves the Bone Marrow Microenvironment, Bone Loss, and Multiple Myeloma. Frontiers in Endocrinology 9. http://doi.org/10.3389/fendo.2018.00788

Hasan MK, Akhter S, Fatema K, Hossain MR, Sultana T, Uzzaman M (2023) Selective modification of diclofenac to reduce the adverse effects; A computer-aided drug design approach. Informatics in Medicine Unlocked 36:101159. http://doi.org/10.1016/j.imu.2023.101159

Hatipoglu MG, Inal S, Kabay S, *et al.* (2015) The Influence of Different Nonsteroidal Anti-Inflammatory Drugs on Alveolar Bone in Rats: An Experimental Study. Acta Stomatol Croat 49(4):325-30. http://doi.org/10.15644/asc49/4/8

Haussling V, Deninger S, Vidoni L, *et al.* (2019) Impact of Four Protein Additives in Cryogels on Osteogenic Differentiation of Adipose-Derived Mesenchymal Stem Cells. Bioengineering (Basel) 6(3):67. http://doi.org/10.3390/bioengineering6030067

Häussling V, Deninger S, Vidoni L, *et al.* (2019) Impact of Four Protein Additives in Cryogels on Osteogenic Differentiation of Adipose-Derived Mesenchymal Stem Cells. Bioengineering 6(3):67. http://doi.org/10.3390/bioengineering6030067

Heidelbaugh JJ, Bruderly M (2006) Cirrhosis and chronic liver failure: part I. Diagnosis and evaluation. Am Fam Physician 74(5):756-62. http://www.aafp.org/pubs/afp/issues/2006/0901/p756.html

Hernandez RK, Do TP, Critchlow CW, Dent RE, Jick SS (2012) Patient-related risk factors for fracture-healing complications in the United Kingdom General Practice Research Database. Acta Orthop 83(6):653-60. http://doi.org/10.3109/17453674.2012.747054

Hochrath K, Ehnert S, Ackert-Bicknell CL, *et al.* (2013) Modeling hepatic osteodystrophy in Abcb4 deficient mice. Bone 55(2):501-11. http://doi.org/10.1016/j.bone.2013.03.012

Hoffmann SA, Muller-Vieira U, Biemel K, *et al.* (2012) Analysis of drug metabolism activities in a miniaturized liver cell bioreactor for use in pharmacological studies. Biotechnol Bioeng 109(12):3172-81. http://doi.org/10.1002/bit.24573

Hong Y, Boiti A, Vallone D, Foulkes NS (2024) Reactive Oxygen Species Signaling and Oxidative Stress: Transcriptional Regulation and Evolution. Antioxidants 13(3):312. http://doi.org/10.3390/antiox13030312

Hu G, Yu Y, Sharma D, *et al.* (2023) Glutathione limits RUNX2 oxidation and degradation to regulate bone formation. JCI Insight 8(16). http://doi.org/10.1172/jci.insight.166888

Huang J, Nguyen V, Tang X, *et al.* (2016) Protection from diclofenac-induced liver injury by Yulangsan polysaccharide in a mouse model. Journal of Ethnopharmacology 193:207-213. http://doi.org/10.1016/j.jep.2016.08.012

Hulsmans M, Holvoet P (2010) The vicious circle between oxidative stress and inflammation in atherosclerosis. J Cell Mol Med 14(1-2):70-8. http://doi.org/10.1111/j.1582-4934.2009.00978.x

Jaeschke H (2007) Troglitazone Hepatotoxicity: Are We Getting Closer to Understanding Idiosyncratic Liver Injury? Toxicological Sciences 97(1):1-3. http://doi.org/10.1093/toxsci/kfm021

Jenne CN, Kubes P (2013) Immune surveillance by the liver. Nat Immunol 14(10):996-1006. http://doi.org/10.1038/ni.2691

Jensen C, Teng Y (2020) Is It Time to Start Transitioning From 2D to 3D Cell Culture? Front Mol Biosci 7:33. http://doi.org/10.3389/fmolb.2020.00033

Jurado S, Garcia-Giralt N, Diez-Perez A, *et al.* (2010) Effect of IL-1beta, PGE(2), and TGF-beta1 on the expression of OPG and RANKL in normal and osteoporotic primary human osteoblasts. J Cell Biochem 110(2):304-10. http://doi.org/10.1002/jcb.22538

Kalinski P (2012) Regulation of immune responses by prostaglandin E2. J Immunol 188(1):21-8. http://doi.org/10.4049/jimmunol.1101029

Karanikola T, Cheva A, Sarafidou K, *et al.* (2022) Effect of Diclofenac and Simvastatin on Bone Defect Healing-An In Vivo Animal Study. Biomimetics (Basel) 7(4):143. http://doi.org/10.3390/biomimetics7040143

Kespohl B, Schumertl T, Bertrand J, Lokau J, Garbers C (2021) The cytokine interleukin-11 crucially links bone formation, remodeling and resorption. Cytokine Growth Factor Rev 60:18-27. http://doi.org/10.1016/j.cytogfr.2021.04.002

Khotib J, Marhaeny HD, Miatmoko A, *et al.* (2023) Differentiation of osteoblasts: the links between essential transcription factors. J Biomol Struct Dyn 41(19):10257-10276. http://doi.org/10.1080/07391102.2022.2148749

Khundmiri SJ, Murray RD, Lederer E (2016) PTH and Vitamin D. Compr Physiol 6(2):561-601. http://doi.org/10.1002/cphy.c140071

Kim JM, Lin C, Stavre Z, Greenblatt MB, Shim JH (2020) Osteoblast-Osteoclast Communication and Bone Homeostasis. Cells 9(9). http://doi.org/10.3390/cells9092073

Knospel F, Jacobs F, Freyer N, *et al.* (2016) In Vitro Model for Hepatotoxicity Studies Based on Primary Human Hepatocyte Cultivation in a Perfused 3D Bioreactor System. Int J Mol Sci 17(4):584. http://doi.org/10.3390/ijms17040584

Kobayashi Y, Mizoguchi T, Take I, Kurihara S, Udagawa N, Takahashi N (2005) Prostaglandin E2 enhances osteoclastic differentiation of precursor cells through protein kinase A-dependent phosphorylation of TAK1. J Biol Chem 280(12):11395-403. http://doi.org/10.1074/jbc.M411189200

Kondo T, Oshima T, Tomita T, *et al.* (2015) The Nonsteroidal Anti-inflammatory Drug Diclofenac Reduces Acid-Induced Heartburn Symptoms in Healthy Volunteers. Clin Gastroenterol Hepatol 13(7):1249-1255.e1. http://doi.org/10.1016/j.cgh.2015.01.014

Krischak GD, Augat P, Blakytny R, Claes L, Kinzl L, Beck A (2007a) The non-steroidal anti-inflammatory drug diclofenac reduces appearance of osteoblasts in bone defect healing in rats. Arch Orthop Trauma Surg 127(6):453-8. http://doi.org/10.1007/s00402-007-0288-9

Krischak GD, Augat P, Sorg T, *et al.* (2007b) Effects of diclofenac on periosteal callus maturation in osteotomy healing in an animal model. Arch Orthop Trauma Surg 127(1):3-

9. http://doi.org/10.1007/s00402-006-0202-x

Ku EC, Lee W, Kothari HV, Scholer DW (1986) Effect of diclofenac sodium on the arachidonic acid cascade. Am J Med 80(4B):18-23. http://doi.org/10.1016/0002-9343(86)90074-4

Ku EC, Wsvary JM, Cash WD (1975) Diclofenac sodium (GP 45840, voltaren), a potent inhibitor of prostaglandin synthetase. Biochemical Pharmacology 24(5):641-643. http://doi.org/10.1016/0006-2952(75)90186-0

Kulesza A, Paczek L, Burdzinska A (2023) The Role of COX-2 and PGE2 in the Regulation of Immunomodulation and Other Functions of Mesenchymal Stromal Cells. Biomedicines 11(2). http://doi.org/10.3390/biomedicines11020445

Kuna L, Bozic I, Kizivat T*, et al.* (2018) Models of Drug Induced Liver Injury (DILI) - Current Issues and Future Perspectives. Curr Drug Metab 19(10):830-838. http://doi.org/10.2174/1389200219666180523095355

Lacey DL, Timms E, Tan HL*, et al.* (1998) Osteoprotegerin ligand is a cytokine that regulates osteoclast differentiation and activation. Cell 93(2):165-176. http://doi.org/10.1016/S0092-8674(00)81569-X

Lambertini E, Penolazzi L, Pandolfi A, Mandatori D, Sollazzo V, Piva R (2021) Human osteoclasts/osteoblasts 3D dynamic co-culture system to study the beneficial effects of glucosamine on bone microenvironment. Int J Mol Med 47(4). http://doi.org/10.3892/ijmm.2021.4890

Lee H, Lee YJ, Choi H, Ko EH, Kim JW (2009) Reactive oxygen species facilitate adipocyte differentiation by accelerating mitotic clonal expansion. J Biol Chem 284(16):10601-9. http://doi.org/10.1074/jbc.M808742200

Lee J, Kim J, Lee R*, et al.* (2022) Therapeutic strategies for liver diseases based on redox control systems. Biomedicine & Pharmacotherapy 156. http://doi.org/10.1016/j.biopha.2022.113764

Lemieux JM, Wu G, Morgan JA, Kacena MA (2011) DMSO regulates osteoclast development in vitro. In Vitro Cell Dev Biol Anim 47(3):260-7. http://doi.org/10.1007/s11626-011-9385-8

Levrero M (2006) Viral hepatitis and liver cancer: the case of hepatitis C. Oncogene 25(27):3834-3847. http://doi.org/10.1038/sj.onc.1209562

Lian N, Lin T, Liu W*, et al.* (2012) Transforming Growth Factor β Suppresses Osteoblast Differentiation via the Vimentin Activating Transcription Factor 4 (ATF4) Axis *. Journal of Biological Chemistry 287(43):35975-35984.

http://doi.org/10.1074/jbc.M112.372458

Lin J, Schyschka L, Muhl-Benninghaus R, *et al.* (2012) Comparative analysis of phase I and II enzyme activities in 5 hepatic cell lines identifies Huh-7 and HCC-T cells with the highest potential to study drug metabolism. Arch Toxicol 86(1):87-95. http://doi.org/10.1007/s00204-011-0733-y

Linares GR, Xing W, Govoni KE, Chen ST, Mohan S (2009) Glutaredoxin 5 regulates osteoblast apoptosis by protecting against oxidative stress. Bone 44(5):795-804. http://doi.org/10.1016/j.bone.2009.01.003

Liu Z, Han T, Werner H, Rosen CJ, Schaffler MB, Yakar S (2017) Reduced Serum IGF-1 Associated With Hepatic Osteodystrophy Is a Main Determinant of Low Cortical but Not Trabecular Bone Mass. Journal of Bone and Mineral Research 33(1):123-136. http://doi.org/10.1002/jbmr.3290

Liu Z, Han T, Werner H, Rosen CJ, Schaffler MB, Yakar S (2018) Reduced Serum IGF-1 Associated With Hepatic Osteodystrophy Is a Main Determinant of Low Cortical but Not Trabecular Bone Mass. J Bone Miner Res 33(1):123-136. http://doi.org/10.1002/jbmr.3290

Lu K, Shi TS, Shen SY, *et al.* (2022) Defects in a liver-bone axis contribute to hepatic osteodystrophy disease progression. Cell Metab 34(3):441-457 e7. http://doi.org/10.1016/j.cmet.2022.02.006

Lu Y, Wahl LM (2005) Oxidative Stress Augments the Production of Matrix Metalloproteinase-1, Cyclooxygenase-2, and Prostaglandin E2 through Enhancement of NF-κB Activity in Lipopolysaccharide-Activated Human Primary Monocytes1. The Journal of Immunology 175(8):5423-5429. http://doi.org/10.4049/jimmunol.175.8.5423

Lubberstedt M, Muller-Vieira U, Mayer M, *et al.* (2011) HepaRG human hepatic cell line utility as a surrogate for primary human hepatocytes in drug metabolism assessment in vitro. J Pharmacol Toxicol Methods 63(1):59-68. http://doi.org/10.1016/j.vascn.2010.04.013

Mano M, Arakawa T, Mano H, *et al.* (2000) Prostaglandin E2 directly inhibits bone-resorbing activity of isolated mature osteoclasts mainly through the EP4 receptor. Calcif Tissue Int 67(1):85-92. http://doi.org/10.1007/s00223001102

Marahleh A, Kitaura H, Ohori F, *et al.* (2019) TNF-alpha Directly Enhances Osteocyte RANKL Expression and Promotes Osteoclast Formation. Front Immunol 10:2925. http://doi.org/10.3389/fimmu.2019.02925

Maruyama M, Rhee C, Utsunomiya T, *et al.* (2020) Modulation of the Inflammatory Response and Bone Healing. Front Endocrinol (Lausanne) 11:386.

http://doi.org/10.3389/fendo.2020.00386

McGonigle P, Ruggeri B (2014) Animal models of human disease: challenges in enabling translation. Biochem Pharmacol 87(1):162-71. http://doi.org/10.1016/j.bcp.2013.08.006

McMillian MK, Li L, Parker JB, *et al.* (2002) An improved resazurin-based cytotoxicity assay for hepatic cells. Cell Biol Toxicol 18(3):157-73. http://doi.org/10.1023/a:1015559603643

Mechcatie E (2010) FDA Highlights Liver Risks With Diclofenac. Caring for the Ages 11(4):23. http://doi.org/10.1016/S1526-4114(10)60108-4

Mekala NK, Baadhe RR, Rao Parcha S, Prameela Devi Y (2013) Enhanced proliferation and osteogenic differentiation of human umbilical cord blood stem cells by L-ascorbic acid, in vitro. Curr Stem Cell Res Ther 8(2):156-62. http://doi.org/10.2174/1574888x11308020006

Menger MM, Stief M, Scheuer C, *et al.* (2023) Diclofenac, a NSAID, delays fracture healing in aged mice. Exp Gerontol 178:112201. http://doi.org/10.1016/j.exger.2023.112201

Mihara M, Hashizume M, Yoshida H, Suzuki M, Shiina M (2012) IL-6/IL-6 receptor system and its role in physiological and pathological conditions. Clinical Science 122(3-4):143-159. http://doi.org/10.1042/Cs20110340

Miyatake S, Ichiyama H, Kondo E, Yasuda K (2009) Randomized clinical comparisons of diclofenac concentration in the soft tissues and blood plasma between topical and oral applications. Br J Clin Pharmacol 67(1):125-9. http://doi.org/10.1111/j.1365-2125.2008.03333.x

Moon AM, Singal AG, Tapper EB (2020) Contemporary Epidemiology of Chronic Liver Disease and Cirrhosis. Clin Gastroenterol Hepatol 18(12):2650-2666. http://doi.org/10.1016/j.cgh.2019.07.060

Nakchbandi IA, van der Merwe SW (2009) Current understanding of osteoporosis associated with liver disease. Nat Rev Gastroenterol Hepatol 6(11):660-70. http://doi.org/10.1038/nrgastro.2009.166

Nussler AK, Wildemann B, Freude T, *et al.* (2014) Chronic CCl4 intoxication causes liver and bone damage similar to the human pathology of hepatic osteodystrophy: a mouse model to analyse the liver-bone axis. Arch Toxicol 88(4):997-1006. http://doi.org/10.1007/s00204-013-1191-5

Osna NA, Donohue TM, Jr., Kharbanda KK (2017) Alcoholic Liver Disease: Pathogenesis and Current Management. Alcohol Res 38(2):147-161.

http://arcr.niaaa.nih.gov/alcohol-organ-interactions-injury-and-repair/alcoholic-liver-disease-pathogenesis-and-current-management

Park G, Rim YA, Sohn Y, Nam Y, Ju JH (2024) Replacing Animal Testing with Stem Cell-Organoids : Advantages and Limitations. Stem Cell Rev Rep 20(6):1375-1386. http://doi.org/10.1007/s12015-024-10723-5

Piwocka O, Musielak M, Ampuła K, *et al.* (2024) Navigating challenges: optimising methods for primary cell culture isolation. Cancer Cell Int 24(1):28. http://doi.org/10.1186/s12935-023-03190-4

Qiang E, Xu H (2024) PGE2 synthesis and signaling in the liver physiology and pathophysiology: An update. Prostaglandins & Other Lipid Mediators 174:106875. http://doi.org/10.1016/j.prostaglandins.2024.106875

Raina DB, Isaksson H, Teotia AK, Lidgren L, Tägil M, Kumar A (2016) Biocomposite macroporous cryogels as potential carrier scaffolds for bone active agents augmenting bone regeneration. Journal of Controlled Release 235:365-378. http://doi.org/10.1016/j.jconrel.2016.05.061

Ren X, Liu H, Wu X, Weng W, Wang X, Su J (2021) Reactive Oxygen Species (ROS)-Responsive Biomaterials for the Treatment of Bone-Related Diseases. Front Bioeng Biotechnol 9:820468. http://doi.org/10.3389/fbioe.2021.820468

Riegger J, Schoppa A, Ruths L, Haffner-Luntzer M, Ignatius A (2023) Oxidative stress as a key modulator of cell fate decision in osteoarthritis and osteoporosis: a narrative review. Cellular & Molecular Biology Letters 28(1):76. http://doi.org/10.1186/s11658-023-00489-y

Rose S, Cuvellier M, Ezan F, *et al.* (2022) DMSO-free highly differentiated HepaRG spheroids for chronic toxicity, liver functions and genotoxicity studies. Arch Toxicol 96(1):243-258. http://doi.org/10.1007/s00204-021-03178-x

Ruoss M, Damm G, Vosough M, *et al.* (2019) Epigenetic Modifications of the Liver Tumor Cell Line HepG2 Increase Their Drug Metabolic Capacity. Int J Mol Sci 20(2):347. http://doi.org/10.3390/ijms20020347

Ruoß M, Vosough M, Königsrainer A, *et al.* (2020) Towards improved hepatocyte cultures: Progress and limitations. Food and Chemical Toxicology 138:111188. http://doi.org/10.1016/j.fct.2020.111188

Saeki C, Saito M, Tsubota A (2024) Association of chronic liver disease with bone diseases and muscle weakness. Journal of Bone and Mineral Metabolism 42(4):399-412. http://doi.org/10.1007/s00774-023-01488-x

Savic Z, Damjanov D, Curic N, *et al.* (2014) Vitamin D status, bone metabolism and bone mass in patients with alcoholic liver cirrhosis. Bratisl Lek Listy 115(9):573-578. http://doi.org/10.4149/bll_2014_111

Scallion R, Moore KA (2009) Effects of food intake on the pharmacokinetics of diclofenac potassium soft gelatin capsules: a single-dose, randomized, two-way crossover study. Clin Ther 31(10):2233-41. http://doi.org/10.1016/j.clinthera.2009.10.001

Schieber M, Chandel NS (2014) ROS function in redox signaling and oxidative stress. Curr Biol 24(10):R453-62. http://doi.org/10.1016/j.cub.2014.03.034

Schyschka L, Sanchez JJ, Wang Z, *et al.* (2013) Hepatic 3D cultures but not 2D cultures preserve specific transporter activity for acetaminophen-induced hepatotoxicity. Arch Toxicol 87(8):1581-93. http://doi.org/10.1007/s00204-013-1080-y

Sens C, Altrock E, Rau K, *et al.* (2017) An O-Glycosylation of Fibronectin Mediates Hepatic Osteodystrophy Through alpha4beta1 Integrin. J Bone Miner Res 32(1):70-81. http://doi.org/10.1002/jbmr.2916

Shergill R, Syed W, Rizvi SA, Singh I (2018) Nutritional support in chronic liver disease and cirrhotics. World J Hepatol 10(10):685-694. http://doi.org/10.4254/wjh.v10.i10.685

Shin JY, Kim MJ, Kim ES, *et al.* (2015) Association between serum calcium and phosphorus concentrations with non-alcoholic fatty liver disease in Korean population. J Gastroenterol Hepatol 30(4):733-41. http://doi.org/10.1111/jgh.12832

Singh P, Rastogi S, Bansal M, *et al.* (2015) A prospective study to assess the levels of interleukin-6 following administration of diclofenac, ketorolac and tramadol after surgical removal of lower third molars. J Maxillofac Oral Surg 14(2):219-25. http://doi.org/10.1007/s12663-013-0609-1

Sousa B, Lopes J, Leal A, *et al.* (2021) Specific glutathione-S-transferases ensure an efficient detoxification of diclofenac in Solanum lycopersicum L. plants. Plant Physiol Biochem 168:263-271. http://doi.org/10.1016/j.plaphy.2021.10.019

Spirlandeli AL, Dick-de-Paula I, Zamarioli A, *et al.* (2017) Hepatic Osteodystrophy: The Mechanism of Bone Loss in Hepatocellular Disease and the Effects of Pamidronate Treatment. Clinics (Sao Paulo) 72(4):231-237. http://doi.org/10.6061/clinics/2017(04)07

Sriuttha P, Sirichanchuen B, Permsuwan U (2018) Hepatotoxicity of Nonsteroidal Anti-Inflammatory Drugs: A Systematic Review of Randomized Controlled Trials. Int J Hepatol 2018:5253623. http://doi.org/10.1155/2018/5253623

Stewart DE (2002) Hepatic adverse reactions associated with nefazodone. Can J Psychiatry 47(4):375-7. http://doi.org/10.1177/070674370204700409

Stokes CS, Volmer DA, Grunhage F, Lammert F (2013) Vitamin D in chronic liver disease. Liver Int 33(3):338-52. http://doi.org/10.1111/liv.12106

Stravitz RT, Lee WM (2019) Acute liver failure. Lancet 394(10201):869-881. http://doi.org/10.1016/s0140-6736(19)31894-x

Sun M, Liu A, Yang X, *et al.* (2021) 3D Cell Culture—Can It Be As Popular as 2D Cell Culture? Advanced NanoBiomed Research 1(5):2000066. http://doi.org/10.1002/anbr.202000066

Suriawinata AA, Thung SN (2006) Acute and chronic hepatitis. Semin Diagn Pathol 23(3-4):132-48. http://doi.org/10.1053/j.semdp.2006.11.001

Take I, Kobayashi Y, Yamamoto Y, *et al.* (2005) Prostaglandin E2 Strongly Inhibits Human Osteoclast Formation. Endocrinology 146(12):5204-5214. http://doi.org/10.1210/en.2005-0451

Tang Y, Wu X, Lei W, *et al.* (2009) TGF-beta1-induced migration of bone mesenchymal stem cells couples bone resorption with formation. Nat Med 15(7):757-65. http://doi.org/10.1038/nm.1979

Tarasov AI, Griffiths EJ, Rutter GA (2012) Regulation of ATP production by mitochondrial Ca(2+). Cell Calcium 52(1):28-35. http://doi.org/10.1016/j.ceca.2012.03.003

Tateishi Y, Ohe T, Ogawa M, Takahashi K, Nakamura S, Mashino T (2020) Development of Novel Diclofenac Analogs Designed to Avoid Metabolic Activation and Hepatocyte Toxicity. ACS Omega 5(50):32608-32616. http://doi.org/10.1021/acsomega.0c04942

Taylor JG, Bushinsky DA (2009) Calcium and phosphorus homeostasis. Blood Purif 27(4):387-94. http://doi.org/10.1159/000209740

Taylor K, Alvarez LR (2019) An Estimate of the Number of Animals Used for Scientific Purposes Worldwide in 2015. Alternatives to Laboratory Animals 47(5-6):196-213. http://doi.org/10.1177/0261192919899853

Thai PN, Ren L, Xu W, *et al.* (2023) Chronic Diclofenac Exposure Increases Mitochondrial Oxidative Stress, Inflammatory Mediators, and Cardiac Dysfunction. Cardiovasc Drugs Ther 37(1):25-37. http://doi.org/10.1007/s10557-021-07253-4

Todd PA, Sorkin EM (1988) Diclofenac sodium. A reappraisal of its pharmacodynamic and pharmacokinetic properties, and therapeutic efficacy. Drugs 35(3):244-85. http://doi.org/10.2165/00003495-198835030-00004

Trefts E, Gannon M, Wasserman DH (2017) The liver. Curr Biol 27(21):R1147-R1151.

http://doi.org/10.1016/j.cub.2017.09.019

Udagawa N, Koide M, Nakamura M*, et al.* (2021a) Osteoclast differentiation by RANKL and OPG signaling pathways. Journal of Bone and Mineral Metabolism 39(1):19-26. http://doi.org/10.1007/s00774-020-01162-6

Udagawa N, Koide M, Nakamura M*, et al.* (2021b) Osteoclast differentiation by RANKL and OPG signaling pathways. J Bone Miner Metab 39(1):19-26. http://doi.org/10.1007/s00774-020-01162-6

Um J-H, Park S-Y, Hur JH*, et al.* (2022) Bone morphogenic protein 9 is a novel thermogenic hepatokine secreted in response to cold exposure. Metabolism 129:155139. http://doi.org/10.1016/j.metabol.2022.155139

Usuda D, Kaneoka Y, Ono R*, et al.* (2024) Current perspectives of viral hepatitis. World J Gastroenterol 30(18):2402-2417. http://doi.org/10.3748/wjg.v30.i18.2402

Vairetti M, Di Pasqua LG, Cagna M, Richelmi P, Ferrigno A, Berardo C (2021) Changes in Glutathione Content in Liver Diseases: An Update. Antioxidants (Basel) 10(3). http://doi.org/10.3390/antiox10030364

Wang X, Chen B, Sun J*, et al.* (2018) Iron-induced oxidative stress stimulates osteoclast differentiation via NF-κB signaling pathway in mouse model. Metabolism 83:167-176. http://doi.org/10.1016/j.metabol.2018.01.005

Weng W, Bovard D, Zanetti F*, et al.* (2023) Tobacco heating system has less impact on bone metabolism than cigarette smoke. Food Chem Toxicol 173:113637. http://doi.org/10.1016/j.fct.2023.113637

Weng W, Haussling V, Aspera-Werz RH*, et al.* (2020) Material-Dependent Formation and Degradation of Bone Matrix-Comparison of Two Cryogels. Bioengineering (Basel) 7(2):52. http://doi.org/10.3390/bioengineering7020052

Weng W, Zanetti F, Bovard D*, et al.* (2021) A simple method for decellularizing a cell-derived matrix for bone cell cultivation and differentiation. J Mater Sci Mater Med 32(9):124. http://doi.org/10.1007/s10856-021-06601-y

Wheatley BM, Nappo KE, Christensen DL, Holman AM, Brooks DI, Potter BK (2019) Effect of NSAIDs on Bone Healing Rates: A Meta-analysis. J Am Acad Orthop Surg 27(7):e330-e336. http://doi.org/10.5435/jaaos-d-17-00727

Wu Q, Zhou X, Huang D, Ji Y, Kang F (2017a) IL-6 Enhances Osteocyte-Mediated Osteoclastogenesis by Promoting JAK2 and RANKL Activity In Vitro. Cell Physiol Biochem 41(4):1360-1369. http://doi.org/10.1159/000465455

Wu Q, Zhou XK, Huang DQ, Ji YC, Kang FW (2017b) IL-6 Enhances Osteocyte-Mediated Osteoclastogenesis by Promoting JAK2 and RANKL Activity. Cellular Physiology and Biochemistry 41(4):1360-1369. http://doi.org/10.1159/000465455

Xian L, Wu X, Pang L, *et al.* (2012) Matrix IGF-1 maintains bone mass by activation of mTOR in mesenchymal stem cells. Nat Med 18(7):1095-101. http://doi.org/10.1038/nm.2793

Yang C, Madhu V, Thomas C, *et al.* (2015) Inhibition of differentiation and function of osteoclasts by dimethyl sulfoxide (DMSO). Cell Tissue Res 362(3):577-85. http://doi.org/10.1007/s00441-015-2245-1

Yasar U, Eliasson E, Forslund-Bergengren C, *et al.* (2001) The role of CYP2C9 genotype in the metabolism of diclofenac in vivo and in vitro. Eur J Clin Pharmacol 57(10):729-35. http://doi.org/10.1007/s00228-001-0376-7

Yuste I, Luciano FC, González-Burgos E, Lalatsa A, Serrano DR (2021) Mimicking bone microenvironment: 2D and 3D in vitro models of human osteoblasts. Pharmacological Research 169:105626. http://doi.org/10.1016/j.phrs.2021.105626

Zahmatkesh E, Othman A, Braun B, *et al.* (2022) In vitro modeling of liver fibrosis in 3D microtissues using scalable micropatterning system. Arch Toxicol 96(6):1799-1813. http://doi.org/10.1007/s00204-022-03265-7

Zangar RC, Davydov DR, Verma S (2004) Mechanisms that regulate production of reactive oxygen species by cytochrome P450. Toxicology and applied pharmacology 199(3):316-331. http://doi.org/10.1016/j.taap.2004.01.018

Zhao MZ, Ma JS, Li M, *et al.* (2021) Cytochrome P450 Enzymes and Drug Metabolism in Humans. International Journal of Molecular Sciences 22(23). http://doi.org/10.3390/ijms222312808

Zhen R, Yang J, Wang Y, *et al.* (2018) Hepatocyte growth factor improves bone regeneration via the bone morphogenetic protein-2-mediated NF-kappaB signaling pathway. Mol Med Rep 17(4):6045-6053. http://doi.org/10.3892/mmr.2018.8559

Zhu S, Haussling V, Aspera-Werz RH, *et al.* (2020) Bisphosphonates Reduce Smoking-Induced Osteoporotic-Like Alterations by Regulating RANKL/OPG in an Osteoblast and Osteoclast Co-Culture Model. Int J Mol Sci 22(1):53. http://doi.org/10.3390/ijms22010053

Chapter 8

8. Declaration

The research was entirely conducted in Siegfried Weller Institute for Trauma Research, Eberhard Karls Universität Tübingen, Tübingen.

Prof. Dr. rer. nat. Andreas K. Nüssler, Dr. sc. hum. Romina H. Aspera-Werz and I conceptualized the study. Dr. sc. hum. Romina H. Aspera-Werz and I designed the experiments. All experiments were carried out and analyzed by myself.

I declare that all relevant data are our original work, except for the quoted references and figures.

I hereby declare that the submitted thesis entitled: “Diclofenac affects the bone and liver negatively: Establishment of an *in vitro* 3D liver-bone culture system” has been written by myself. This work has not been submitted for any other degree. This thesis was linguistically edited by a commercial Professional English Proofreading Service (Proof-Reading-Service.com; Proof reading for language errors in spelling, grammar and word choice).

_____

Place/date/signature of doctoral candidate

Chapter 9

9.Publication

Results of this thesis were partially used for publication:

- *Title:*

Establishment of a human 3D *in vitro* liver-bone model as a potential system for drug toxicity screening (Chen *et al.* 2024)

Author:

Guanqiao Chen, Yuxuan Xin, Mohammad Majd Hammour, Bianca Braun, Sabrina Ehnert, Fabian Springer, Massoud Vosough, Maximilian M. Menger, Ashok Kumar, Andreas K. Nüssler and Romina H. Aspera-Werz

Journal:

Archives of Toxicology. Impact score 4.8

Chapter 10

10. Acknowledgements

I would like to express my heartfelt gratitude to all those who have supported me throughout the process of writing this dissertation.

My deepest gratitude goes to my supervisor, Prof. Dr. rer. nat. Andreas K. Nüssler, for providing me with the chance to undertake my doctoral studies at the Siegfried Weller Institute (SWI) and for his invaluable guidance throughout the writing of this dissertation. Prof. Nüssler has imparted to me a wealth of knowledge, and his enthusiasm and drive for scientific exploration, which have been a profound inspiration to me. This dissertation's accomplishments would not have been possible without his helpful suggestions and generous guidance.

Furthermore, I wish to express my heartfelt gratitude to Dr. sc. hum. Romina H. Aspera-Werz for her kind support. She has an infectious passion and enthusiasm for science, and she has given me invaluable academic assistance. She has always encouraged me, shown genuine care, and provided me with tremendous moral support. Her encouragement, patience, and professional guidance have helped me overcome numerous challenges throughout my studies.

I am deeply appreciative of all my colleagues at SWI: Sabrina, Svetlana, Bianca, Kevin, Majd, Engin, Filiz, Maximilian, and Melike, for their valuable assistance in my research. I am also grateful to my Chinese colleagues—Yuxuan Xin, Xiang Gao, Ruizhuo Zhang, Sanhuan Yuan, and Pengcheng Zhou—for the wonderful memories they helped create in Tübingen.

Finally, I would like to thank my family. I am especially grateful to my parents, Yang Chen and Yanmei Wei, for their unwavering support, without which none of my accomplishments would have been possible. My deepest thanks go to my wife, Ying Sun, for her companionship and devotion, providing me with a strong source of support and a warm and loving home in Tübingen.